For Reference

NOT TO BE TAKEN FROM THIS ROOM

Ex libris
universitatis
albertaensis

QUAECUMQUE VERA

The University of Alberta
Edmonton, Alberta
Printing Department

THE UNIVERSITY OF ALBERTA

PHYSICAL TAPERING OF LARGE ANTENNA ARRAYS

by

© DESMOND ANTHONY WYNNE

A THESIS

SUBMITTED TO THE FACULTY OF GRADUATE STUDIES AND RESEARCH

IN PARTIAL FULFILMENT OF THE REQUIRMENTS FOR THE DEGREE

OF MASTER OF SCIENCE

IN

ELECTRICAL ENGINEERING

DEPARTMENT OF ELECTRICAL ENGINEERING

EDMONTON, ALBERTA

FALL, 1973

DEDICATION

To my Parents

Digitized by the Internet Archive
in 2023 with funding from
University of Alberta Library

https://archive.org/details/Wynne1973

ABSTRACT

The performance of large fan beam arrays (160λ by 4λ) for T-type Radio Telescopes is studied using a summation technique that takes advantage of the fast Fourier transform algorithm. The effects, on sidelobe levels and beamwidths, of physical and resistive tapering of the excitation distributions are examined. The effects of random errors in the excitation of the elements are also considered. It is shown that the number of elements required for this type of array system may be substantially reduced, without degrading the performance of the system, by using a combination of both physical and resistive tapering.

ACKNOWLEDGEMENTS

The author wishes to thank Dr. C. R. James and Dr. F. S. Chute for their supervision and encouragement throughout the project.

The financial support provided by the Department of Electrical Engineering is gratefully acknowledged.

The author also wishes to express his thanks to the staff of the Computing Centre for their assistance with the computing problems.

TABLE OF CONTENTS

Page

CHAPTER 1 INTRODUCTION 1

1.1 General 1

1.2 Tapering 2

1.3 Resistive vs Physical Tapering 3

1.4 Purpose of the Thesis 5

CHARTER 2 ANALYSIS OF THE POWER PATTERN 7

2.1 Introduction 7

2.2 Radiation 9

2.3 Radiation from a Y-directed λ/2 Dipole in the X-Y Plane 10

2.4 Effects of a Ground Screen 15

2.5 Radiation from an Array of λ/2 Dipoles in the X-Y Plane 16

2.6 The Array Factor 21

2.7 Calculation of the Array Factor 24

2.8 Beam Steering 29

CHAPTER 3 ANALYSIS OF ONE-DIMENSIONAL ARRAYS 32

3.1 Introduction 32

3.2 Excitation 33

3.3 Main Beam Response 36

3.4 Sidelobe Levels 46

Page

CHAPTER 4 ANALYSIS OF TWO-DIMENSIONAL ARRAYS 54

4.1 Introduction 54

4.2 Excitation 56

4.3 Array Factor in the Principle Planes 60

4.4 Peak Sidelobe Levels 66

4.5 Discussion 74

CHAPTER 5 EFFECTS OF RANDOM ERRORS 76

5.1 Introduction 76

5.2 Generation of the Random Errors 78

5.3 Effects of the Errors on One-Dimensional Arrays 79

5.4 Effects of the Errors on Two-Dimensional Arrays 89

5.5 Discussion 95

CHAPTER 6 SUMMARY AND CONCLUSIONS 97

REFERENCES 101

APPENDIX A 103

APPENDIX B 104

APPENDIX C COMPUTER PROGRAMMS 106

LIST OF TABLES

Page

Table 3.1 Power Patterns for the Arrays. 45

3.2 Average Sidelobe Levels Close to the Main Beam. 53

Table 4.1 Peak Sidelobe Levels in dB Below the Main Beam. Uniform Array. No Errors. 67

4.2 Peak Sidelobe Levels in dB Below the Main Beam. Physically Tapered Array. No Errors. 68

4.3 Peak Sidelobe Levels in dB Below the Main Beam. Combination Array. No Errors. 69

4.4 Peak Sidelobe Levels in dB Below the Main Beam. Gaussian Array. No Errors. 70

Table 5.1 Average Sidelobe Levels Over all the Sidelobes. 89

5.2 Peak Sidelobe Levels in dB Below the Main Beam. Uniform Array. 5° Phase Errors. 90

5.3 Peak Sidelobe Levels in dB Below the Main Beam. Physically Tapered Array. 5° Phase Errors. 91

5.4 Peak Sidelobe Levels in dB Below the Main Beam. Combination Array. 5° Phase Errors. 92

5.5 Peak Sidelobe Levels in dB Below the Main Beam. Gaussian Array. 5° Phase Errors. 93

LIST OF FIGURES

			Page
Figure	1.1	Excitation Distributions for Uniform, Truncated Gaussian and Binomial Arrays.	4
Figure	2.1	Coordinate System.	11
	2.2	Location of the Elements.	11
	2.3	The Parameters of K-space.	12
	2.4	Arrangement of the Elements in an Array.	18
	2.5	Identification of the Elements in an Rectangular Array.	26
	2.6	Identification of the Elements in a Physically Tapered Array.	26
Figure	3.1	Arrangement of the Elements in One-dimensional Arrays.	32
	3.2a	Excitation Data for a Uniform and a Truncated Gaussian Array.	34
	3.2b	Excitation Data for an Array with 2 Stages of Tapering.	34
	3.2c	Excitation Data for an Array with 4 Stages of Tapering.	35
	3.2d	Excitation Data for an Array with 8 Stages of Tapering.	35
	3.3	Main Beam Characteristics of the one-dimensional Arrays.	37
	3.4a	First Sidelobes for the Uniform Array.	39
	3.4b	First Sidelobes for the Array with 2 Stages of Tapering.	40
	3.4c	First Sidelobes for the Array with 4 Stages of Tapering.	41
	3.4d	First Sidelobes for the Array with 8 Stages of Tapering.	42

Page

3.4e First Sidelobes for the Gaussian Array. 43

3.5 Excitation Data for Gaussian Arrays. 44

3.6 Effects of Phasing on the Beam Width. 47

3.7 Peak Sidelobe Levels for the Uniform and the Gaussian Arrays. 48

3.8a Peak Sidelobe Levels Near the Main Beam for the Array with 2 Stages of Tapering. 50

3.8b Peak Sidelobe Levels Near the Main Beam for the Array with 4 Stages of Tapering. 51

3.8c Peak Sidelobe Levels Near the Main Beam for the Array with 8 Stages of Tapering. 52

Figure 4.1a Arrangement of the Elements in the Rectangular Arrays. 55

4.1b Arrangement of the Elements in the Physically Tapered Arrays. 55

4.2 Block Representation of K-space. 57

4.3a Arrangement of the Elements and the Excitation Data for the Uniform Array. 58

4.3b Arrangement of the Elements and the Excitation Data for the Physically Tapered Array. 58

4.3c Arrangement of the Elements and the Excitation Data for the Combination Array. 59

4.3d Arrangement of the Elements and the Excitation Data for the Gaussian Array. 59

4.4a Effective Excitation in the Transverse Plane for the Uniform and the Gaussian Arrays. 62

4.4b Effective Excitation in the Transverse Plane for the Physically Tapered Array. 62

Page

4.4c Effective Excitation in the Transverse Plane for the Combination Array. 62

4.5a Array Factor in the Transverse Plane for the Uniform and Gaussian Arrays. 63

4.5b Array Factor in the Transverse Plane for the Physically Tapered Array. 64

4.5c Array Factor in the Transverse Plane for the Combination Array. 65

Figure 5.1a Effects of Errors on the Array Factor of the Uniform and Gaussian Arrays. 81

5.1b Effects of Errors on the Array Factor Near the Main Beam of the Array with 2 Stages of Tapering. 82

5.1c Effects of Errors on the Array Factor Near the Main Beam of the Array with 4 Stages of Tapering. 83

5.1d Effects of Errors on the Array Factor Near the Main Beam of the Array with 8 Stages of Tapering. 84

5.2a Effects of Errors on the Peak Sidelobe Levels of the Uniform and Gaussian Arrays. 86

5.2b Effects of Errors on the Peak Sidelobe Levels of the Arrays with 2, 4 and 8 Stages of Tapering. 87

CHAPTER 1

INTRODUCTION

1.1 General

In recent years there has been considerable interest in low frequency radio astronomy. Work has been done at 10 MHz and 22 MHz at Penticton in western Canada [1,2]. A broadband system from 10 MHz to 25 MHz is in operation in central Russia [3,4]. The University of Maryland's Clark Lake Radio Observatory has a system presently under construction which will operate between 10 MHz and 110 MHz [5]; however, below 20 MHz its use will be limited as the collecting area of the antenna will be low. In the southern hemisphere work has been done at 3.5 MHz and 19 MHz [6,7].

All of the above radio telescopes use a cross or tee type antenna system first described by Mills and Little [8]. This type of telescope produces two orthogonal fan beams and by the multiplication of these beams a pencil beam is obtained which gives high resolution at low frequencies.

At present there is a need for a new radio telescope that has greater resolution and sensitivity at low frequencies than any of the instruments presently available. A proposal for such an instrument, to be located in Alberta, has been made and site testing is being carried out [9]. The telescope would operate near 12 MHz and would consist of

an array of horizontal antennas arranged in a tee with a north-south arm 2.5km by 100m and an east-west arm 5km by 50m. Such an array would have a collecting area of the order of 100,000m² and a resolving power of about 30 arcmins at the zenith.

The distribution of radio emission in the sky is very complex. Radiation is received from sources of all angular sizes in addition to the general background emission. For this reason a pencil beam antenna system with as low a sidelobe level as possible is most desireable. Sidelobe level reduction is achieved through what is referred to as tapering [10]. Tapering consists of gradually reducing the level of the excitation of the array elements to some small value at the ends of the array.

1.2 Tapering

There are many forms that the excitation distribution may take. A uniform excitation distribution produces a narrow beam but the sidelobe levels are high. For large arrays the level of the first sidelobe is 13.6 dB below the peak of the main beam. A beam with no sidelobes could be produced by using a binomial excitation distribution but this increases the beamwidth and reduces the gain of the array by a large amount. Other excitation distributions such as triangular, cosine or cosine squared produce beams with intermediate characteristics.

In the following chapters, array systems which are 160 wavelengths long, less than 4 wavelengths wide, and that have an excitation distribution approximating a Gaussian will be examined. Such arrays produce fan beams in a direction transverse to the principle axis of the array. A true Gaussian excitation distribution, infinite in extent, would produce a beam with no sidelobes. In practice, the excitation distribution of a finite array can be represented by a truncated Gaussian. Choosing a taper such that the excitation of the elements at the ends of the array is 1/16 that of the centre elements [11] represents a good compromise between the requirements for gain, beamwidth and sidelobe levels of the power pattern. Some typical excitation distributions are illustrated in Figure 1.1 for a linear array 160 wavelengths long. Note that the excitation is assumed to be symmetric about the centre of the array. In each case the excitations of the centre elements have been set to unity.

1.3 Resistive vs Physical Tapering

The most straightforward method of obtaining a specified excitation distribution is to place attenuators in the lead to each antenna element. This approach is known as resistive tapering. Another technique is to completely eliminate some of the elements of the array or to replace a group of elements, in a section of the array where the excitation is low, by a smaller group of elements with modified excitations. This is known as physical tapering.

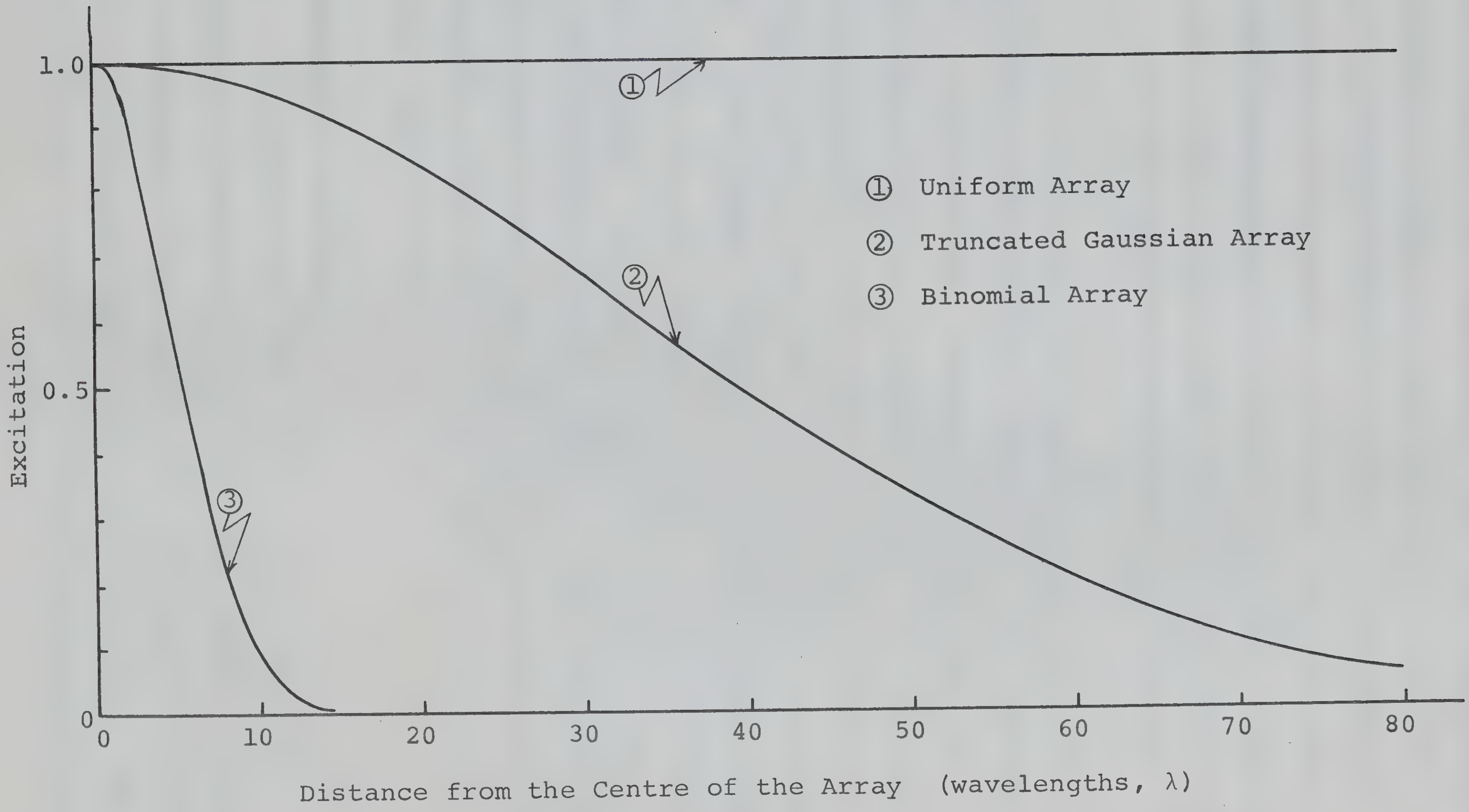

Figure 1.1. Excitation Distributions for Uniform, Truncated Gaussian and Binomial Arrays.

The excitations of the elements in physically tapered arrays may be found by setting the total contribution of the elements in sections of the array equal to the total contribution of the elements in the same sections of a resistively tapered array. It is also possible to use a combination of both physical and resistive tapering in an array to achieve a specified excitation distribution.

In the case of large array systems, physical tapering offers many practical advantages over resistive tapering. The physically tapered arrays discussed in Chapter 4 have 37% fewer elements than the corresponding resistively tapered arrays. This reduction represents a significant saving in the cost of constructing such an array system. If the system requires signal processing at each element there will be a further saving in the processing equipment needed. The time involved in setting up and tuning the array will also be reduced. There will be fewer points at which errors can occur and if everything else is unchanged the effect of the errors should be less on a physically tapered array.

1.4 Purpose of the Thesis

The purpose of this thesis is to compare the performance of resistively and physically tapered arrays in which the widths of the arrays are small compared to their lengths. A technique will be developed in Chapter 2 for finding the power pattern of one and twc-dimensional arrays.

It will be shown that if all the elements in the array are identical then the power pattern can be split into the power pattern of a reference antenna times an array factor which takes into account the location and excitation of every elememt in the array. A comparison between different array systems can then be made on the basis of their array factors. In Chapter 3 the effects of coarse resistive tapering on the gain, beamwidth, average sidelobe level and peak sidelobe levels of one-dimensional arrays will be examined. These results will be extended to two-dimensional arrays, in Chapter 4, and a comparison between resistive and physical tapering will be made. The difference between resistive and physical tapering will be shown to be greatest at points far from the main beam. The effects of random errors in the excitation of the elements of both one and two-dimensional arrays will be studied in Chapter 5. It will be demonstrated that the effects of errors are greatest on the carefully adjusted resistively tapered arrays and not so great on the physically tapered arrays.

CHAPTER 2

ANALYSIS OF THE POWER PATTERN

2.1 Introduction

The power pattern of an array of antennas may be determined by summing the contributions from each element at each angle for which the total field is to be calculated. This method is not practical for large arrays because of the time involved in doing the calculation and the problems encountered in retaining accuracy. Considerable simplification may be achieved by use of the concept of the array factor which is the power pattern of an array of isotropic point sources with the same physical arrangement as the actual array. The following analysis of the power pattern and the array factor for rectangular arrays is directed towards finding the result in a suitable form for calculation using computing facilities such as those provided by the IBM model 360/67 computer.

Throughout the analysis the effect of the mutual impedances between the elements will be neglected and it will be assumed that each of the elements in the array can be excited as specified.

The analysis of the arrays will be performed using Fourier transforms and so the behaviour of the arrays will be examined in the transform space (K-space). The primary advantage of working in K-space is that the fast Fourier

transform algorithm [12], which is both fast and accurate, may be used to compute the array factor. Another advantage is seen when dealing with phased arrays. An unphased arrary is one in which the phases of the excitations of every element are identical. Beam steering in K-space is represented by simple linear shifts as will be shown in Section 2.8. Although the array factor can be transformed back to real-space, the process would involve a lot of computing time and for the purpose of comparisons between different array systems it is not really necessary.

The analysis of arrays with physical tapering will be performed by breaking the arrays up into sub-arrays where each sub-array is of constant width. The total field strength pattern may then be found by summing the field strength patterns of the sub-arrays. For array systems in which the widths of the arrays are very much less than their lengths this technique achieves an additional saving in computational time over a direct application of the fast Fourier transform.

The calculation of the array factors will involve the generation of large tables of data and a repetitive sequence of operations at about 10^6 points in K-space. The computational time can be reduced considerably by efficient coding of the repetitive sequence in assembler language [13].

2.2 Radiation

Radiation in unbounded space from a local source may be described in terms of a magnetic vector potential, $\vec{A}$, which satisfies the Helmholtz equation 2-1 [14].

$$\nabla^2\vec{A} + k^2\vec{A} = -\vec{J} \tag{2-1}$$

$\vec{J}$ is the current density (Amps/m²) and k is the wave number of the medium and is given by

$$k = \frac{2\pi}{\lambda} \tag{2-2}$$

The resulting magnetic and electric fields ($\vec{E}$ and $\vec{H}$) are functions of $\vec{A}$ as indicated in equations 2-3a and 2-3b.

$$\vec{E} = -j\omega\mu\vec{A} + \frac{1}{j\omega\varepsilon}\nabla(\nabla.\vec{A}) \tag{2-3a}$$

$$\vec{H} = \nabla\times\vec{A} \tag{2-3b}$$

$$\vec{A}(\vec{r}) = \frac{1}{4\pi}\int_{-\infty}^{\infty}\int_{-\infty}^{\infty}\int_{-\infty}^{\infty}\vec{J}(\vec{r}')\,\frac{\mathrm{Exp}\{-jk|\vec{r}-\vec{r}'|\}}{|\vec{r}-\vec{r}'|}\,dX'dY'dZ' \tag{2-4}$$

Equation 2-4 is a general solution of equation 2-1 for $\vec{A}$ in an unbounded region. The primed variables represent the source coordinates and the unprimed variables the field coordinates. The integration is carried out over the source coordinates. When the current distribution in some localized area is known, equations 2-3a, 2-3b and 2-4 completely specify the resulting electromagnetic radiation.

2.3 Radiation from a Y-directed $\lambda/2$ Dipole in the X-Y Plane

Consider a Y-directed $\lambda/2$ dipole located at X',Y' in the X-Y plane as indicated in Figure 2.1. Assuming that the dipole is oriented with its axis parallel to the Y-axis, the current distribution and hence the magnetic vector potential of equation 2-4 will have only a Y-component. When only the nature of the field at large distances from the antenna is required, $|\vec{r}-\vec{r}'|$ may be replaced by (Appendix A)

$$|\vec{r}-\vec{r}'| = r\{1-\frac{\text{Sin}\theta}{r}(X'\text{Cos}\phi+Y'\text{Sin}\phi)\} \qquad (2\text{-}5)$$

Thus equation 2-4 becomes

$$A_y(r) = \frac{1}{4\pi}\int_{-\infty}^{\infty}\int_{-\infty}^{\infty}\int_{-\infty}^{\infty} J_y(r')\frac{\text{Exp}\{-jkr+jk\text{Sin}\theta(X'\text{Cos}\phi+Y'\text{Sin}\phi)\}}{r-\text{Sin}\theta(X'\text{Cos}\phi+Y'\text{Sin}\phi)}dX'dY'dZ \qquad (2\text{-}6)$$

In the denominator of equation 2-6 the trigonometric terms are small compared to r and may be neglected. In the exponent they represent phase shifts and since X' and Y' may be comparable to λ they must be retained.

Let

$$K_x = k\text{Sin}\theta\text{Cos}\phi \qquad (2\text{-}7a)$$

$$K_y = k\text{Sin}\theta\text{Sin}\phi \qquad (2\text{-}7b)$$

$$A(r) = \frac{\text{Exp}\{-jkr\}}{4\pi r} \qquad (2\text{-}8)$$

Then equation 2-6 becomes

$$A_y(r) = A(r)\int_{-\infty}^{\infty}\int_{-\infty}^{\infty}\int_{-\infty}^{\infty} J_y(r')\text{Exp}\{jK_xX'+jK_yY'\}dX'dY'dZ' \qquad (2\text{-}9)$$

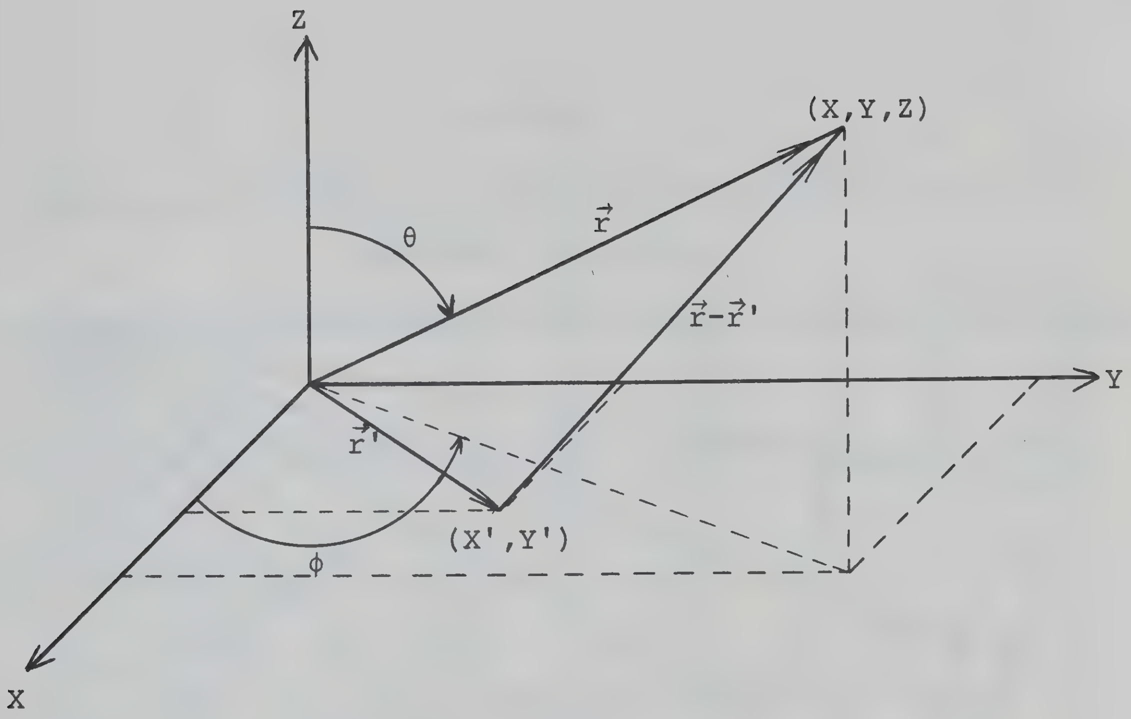

Figure 2.1. Coordinate System.

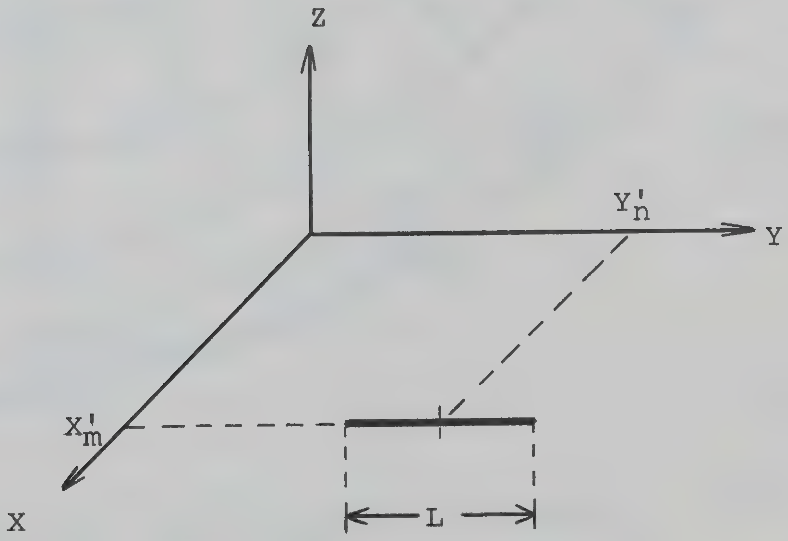

Figure 2.2. Location of the Elements.

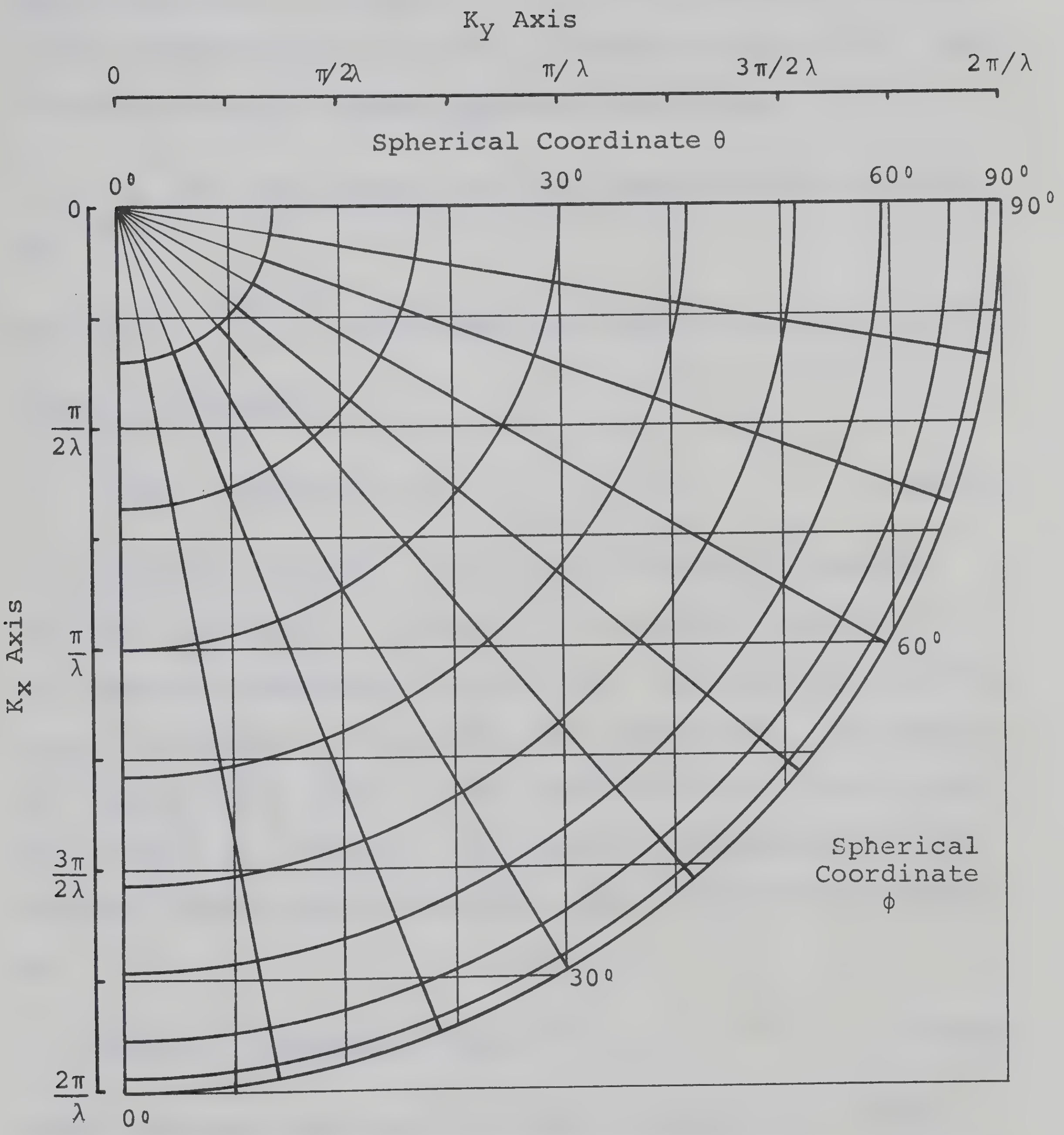

Figure 2.3. The Parameters of K-space.

The relationship between the parameters of K-space and real space are shown in Figure 2.3. K_x and K_y extend to infinity in all directions but, as will be shown in Section 2.6, only a limited area of K-space represents real space.

Let the integral part of equation 2-9 be denoted by

$$A(K_x,K_y) = \int_{-\infty}^{\infty}\int_{-\infty}^{\infty}\int_{-\infty}^{\infty} J_y(r')\,\mathrm{Exp}\{jK_xX'+jK_yY'\}\,dX'dY'dZ' \qquad (2\text{-}10)$$

Then $A_y(r)$ becomes

$$A_y(r) = A(r)A(K_x,K_y) \qquad (2\text{-}11)$$

In equation 2-10 $J_y(r')$ is a current density in Amps/m². Consider the dipole, of length L, located at (X_m',Y_n') in the X-Y plane as indicated in Figure 2.2. The subscripts m and n are introduced at this point for convenience. In Section 2.5 (X_m',Y_n') will refer to the position of the element (m,n) in an array of elements. If $I(X_m',Y_n')$ represents the total current flowing along the dipole then $J_y(r')$ may be written as

$$J_y(r') = I(X_m',Y_n')\delta(X'-X_m')\delta(Z') \qquad (2\text{-}12)$$

where the delta functions have the dimensions of inverse length. It may be assumed that the current at the ends of the dipole is zero and varies sinusoidally over its length. Hence, $J_y(r')$ becomes

$$J_y(r') = I_oC_{mn}\delta(X'-X_m')\overline{U}(Y'-Y_n')\delta(Z')\,\mathrm{Sin}(kY'') \qquad (2\text{-}13)$$

where I_o is the peak current on a hypothetical antenna and where

$$C_{mn} = \frac{\text{the current on a dipole located at } (X'_m, Y'_n)}{I_o} \qquad (2\text{-}14)$$

$$\overline{U}(Y'-Y'_n) = u(Y'-Y'_n-L/2) - u(Y'-Y'_n+L/2) \qquad (2\text{-}15)$$

$$Y'' = L/2-|Y'-Y'_n| \qquad (2\text{-}16)$$

C_{mn} has been introduced at this stage so that in subsequent sections arrays of dipoles with different currents may be discussed directly in terms of the results presented here. For this current element located at X'_m and Y'_n the magnetic vector potential becomes

$$A_{ymn}(r) = A(r)A_{mn}(K_x, K_y) \qquad (2\text{-}17)$$

where $A_{mn}(K_x, K_y)$ is obtained by substituting equation 2-13 into equation 2-10. Thus

$$A_{mn}(K_x, K_y) = \int_{-\infty}^{\infty}\int_{-\infty}^{\infty}\int_{-\infty}^{\infty} [I_o C_{mn} \delta(X'-X'_m) \overline{U}(Y'-Y'_n) \delta(Z') \mathrm{Sin}(kY'') \mathrm{Exp}\{jK_x X' + jK_y Y'\}] dX' dY' dZ' \qquad (2\text{-}18)$$

The indicated integration is carried out in Appendix B where it is shown that

$$A_{mn}(K_x, K_y) = C_{mn} \mathrm{Exp}\{jK_x X'_m + jK_y Y'_n\} A_{yr}(K_x, K_y) \qquad (2\text{-}19)$$

where

$$A_{yr}(K_x, K_y) = 2I_o \frac{[\mathrm{Cos}\{(kL/2)\mathrm{Sin}\theta \mathrm{Sin}\phi\} - \mathrm{Cos}\{kL/2\}]}{1 - \mathrm{Sin}^2\theta\ \mathrm{Sin}^2\phi} \qquad (2\text{-}20)$$

$A_{yr}(K_x,K_y)$ is known as the element pattern. It may be interpreted as the magnetic vector potential that would result if the element at (X'_m,Y'_n) were located at the centre of the coordinate system with its peak current adjusted to a hypothetical reference level, I_o. The exponential factor in equation 2-19 represents the phase shift associated with displacing the element from the origin to (X'_m,Y'_n). The constant C_{mn} accounts for the relative magnitude and phase of the current in the element (m,n) with respect to the reference level, I_o.

2.4 Effects of a Ground Screen

It was assumed in the earlier sections that the dipole was radiating in free space. In practice the dipoles will be placed over a reflecting screen which will modify the fields and power pattern of the antenna. These effects will be considered separately as it will be shown that they are common to all the different array systems to be examined

The effects of the screen may be calculated by considering the antenna as composed of two antennas one above the screen and the other, an image antenna with its current reversed, below the screen. The reversal of the currents is necessary to produce the zero tangential E-field which must occur on the screen.

For the antenna above the plane of the screen the phase of the magnetic vector potential must be advanced by an amount ψ where

$$\psi = kh\text{Cos}\theta \tag{2-21}$$

and h is the height of the antenna above the screen. For the array below the screen the phase must be retarded by the same amount. By combining the two antennas equation 2-17 becomes

$$A_{ymn}(r) = A(r)A_{mn}(K_x,K_y)[\text{Exp}\{jkh\text{Cos}\theta\}-\text{Exp}\{-jkh\text{Cos}\theta] \tag{2-22}$$

This additional factor will be called the screen factor $SF(K_z)$ which may be written as

$$SF(K_z) = 2j\text{Sin}(jhK_z) \qquad \text{where } K_z = k\text{Cos}\theta \tag{2-23}$$

Thus,

$$A_{ymn}(r) = A(r)A_{mn}(K_x,K_y)SF(K_z) \tag{2-24}$$

$SF(K_z)$ depends only on the distance from the reflecting screen to the antenna and not on the shape of the antenna.

2.5 Radiation from an Array of $\lambda/2$ Dipoles in the X-Y Plane

Assume that the array is rectangular and that each position in the array contains a dipole. This assumption produces no loss in generality, since, for a non-rectangular shaped array it is possible to fill out the array to a rectangular shape by including a number of additional elements for which the level of the excitation is set to zero. The resulting fields and power pattern will be

unchanged. Assume also that the numbers of dipoles in the X and Y directions are even. For the case in which the number of dipoles in either direction is odd only a slight modification to the method of analysis described in this section and the following sections is required.

Let the array of dipoles be laid out as shown in Figure 2.4. The spacings between the dipoles in the X and Y directions are D_x and D_y respectively and the numbers of elements in the X and Y directions are N_x and N_y respectively. Let (m,n) be the system used for identifying the element located in column m and row n. (X'_m, Y'_n) is the location of element (m,n).

$A_y(r)$ for the complete array is found by summing $A_{ymn}(r)$ over all m and n. Thus from equation 2-24

$$A_y(r) = \sum_{m=0}^{N_x-1} \sum_{n=0}^{N_y-1} A(r) A_{mn}(K_x, K_y) SF(K_z) \tag{2-25}$$

$$= A(r) SF(K_z) \sum_{m=0}^{N_x-1} \sum_{n=0}^{N_y-1} A_{mn}(K_x, K_y) \tag{2-26}$$

From equation 2-19

$$A_y(r) = A(r) SF(K_z) A_{yr}(K_x, K_y) \sum_{m=0}^{N_x-1} \sum_{n=0}^{N_y-1} C_{mn} \mathrm{Exp}\{jK_x X'_m + jK_y Y'_n\} \tag{2-27}$$

By defining an array facfor $AF(K_x, K_y)$ as

$$AF(K_x, K_y) = \sum_{m=0}^{N_x-1} \sum_{n=0}^{N_y-1} C_{mn} \mathrm{Exp}\{jK_x X'_m + jK_y Y'_n\} \tag{2-28}$$

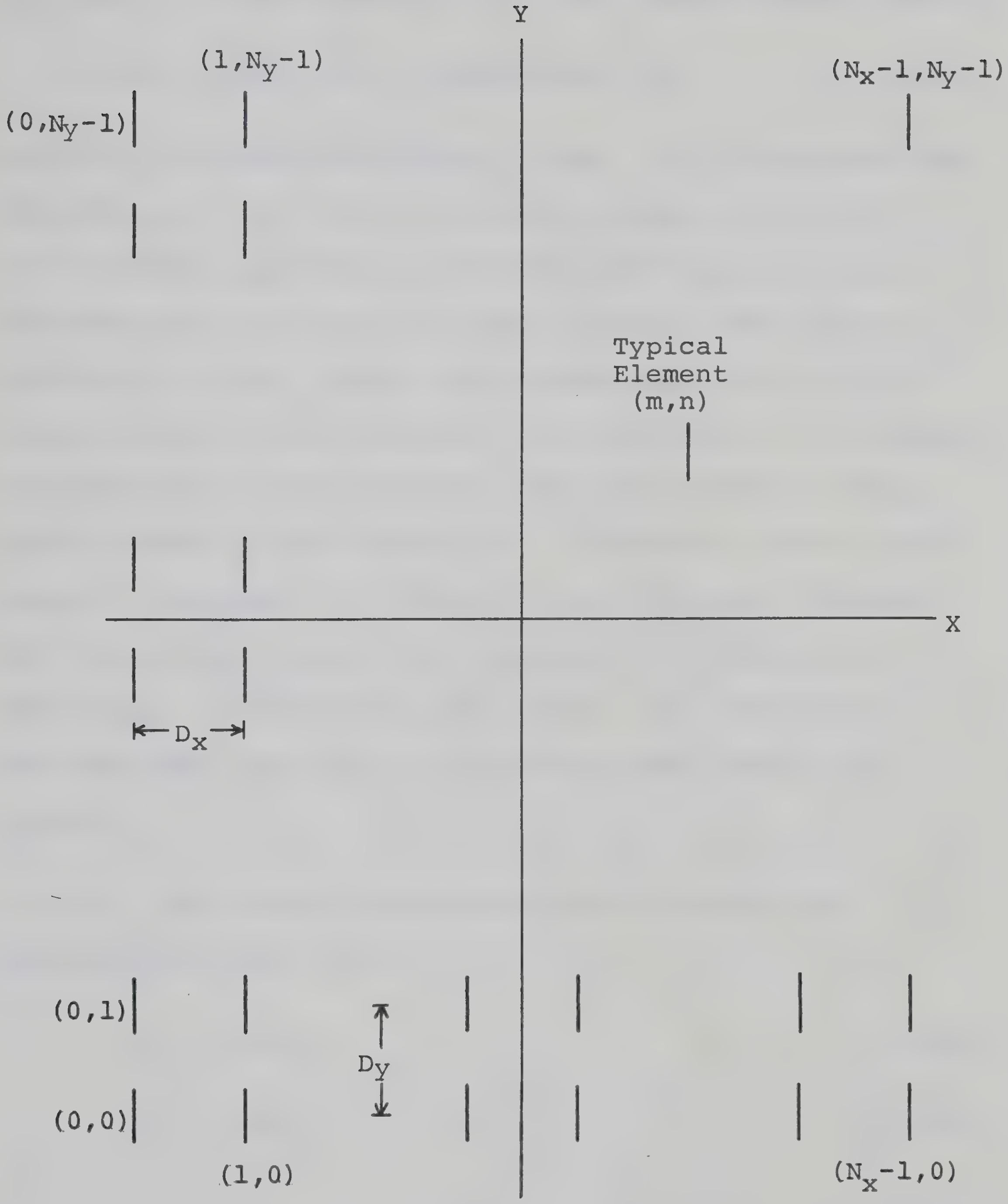

Figure 2.4. Arrangement of the Elements in an Array.

the magnetic vector potential for the complete array becomes

$$A_y(r) = A(r)A_{yr}(K_x,K_y)SF(K_z)AF(K_x,K_y) \tag{2-29}$$

Equation 2-29 has four distinct terms. A(r) represents the dependance on the distance from the antenna to a point in the far field and will not be taken into account in the comparison of the different array systems. The element pattern $A_{yr}(K_x,K_y)$, takes into account the shape of the elements used in the array and the basic form of the current distributions in the elements. The screen factor, $SF(K_z)$, takes account of the effects of a reflecting screen placed below the antenna. The array factor, $AF(K_x,K_y)$, accounts for the physical layout and arrangement of the elements in the array. It also takes into account the differences in the magnitude and phase of the excitations between the elements.

The E and H vectors now can be found from equations 2-3a and 2-3b.

$$E_\theta = -j\omega\mu A_\theta \tag{2-30a}$$

$$E_\phi = -j\omega\mu A_\phi \tag{2-30b}$$

$$H_\theta = jkA_\phi \tag{2-30c}$$

$$H_\phi = -jkA_\theta \tag{2-30d}$$

$$A_\theta = A_y(r)\,\text{Cos}\theta\,\text{Sin}\phi \tag{2-31a}$$

$$A_\phi = A_y(r)\,\text{Cos}\phi \tag{2-31b}$$

$$E_\theta = -j\omega\mu A_y(r)\,\text{Cos}\theta\,\text{Sin}\phi \tag{2-32a}$$

$$E_\phi = -j\omega\mu A_y(r)\,\text{Cos}\phi \tag{2-32b}$$

$$H_\theta = \ jkA_y(r)\,\text{Cos}\phi \tag{2-32c}$$

$$H_\phi = -jkA_y(r)\,\text{Cos}\theta\,\text{Sin}\phi \tag{2-32d}$$

Finally, the power pattern is given by

$$\begin{aligned} Pr &= \frac{1}{2}(E_\theta H_\phi^* - E_\phi H_\theta^*) \\ &= \frac{|A_y(r)|^2}{2}\omega\mu k(\text{Cos}^2\theta\ \text{Sin}^2\phi + \text{Cos}^2\phi) \end{aligned} \tag{2-33}$$

The array factor is the only term which will vary when the arrangement of the array or the excitations of the elements are changed. Hence, comparison between different array systems will be made on the basis of their array factors.

It will not be necessary to refer to the element pattern or the screen factor except when the array factor has large sidelobes near the zeros of the element pattern or the screen factor. Under such circumstances the element pattern or the screen factor may reduce these sidelobes to an acceptable level. Equation 2-33, for the power, contains an additional factor arising from the conversion of the

magnetic vector potential from rectangular to polar coordinates. This factor also contains zeros and if the array factor has large sidelobes at the location of these zeros this term must be taken into account in determining the actual sidelobe levels of the array.

2.6 The Array Factor

The location of the elements shown in Figure 2.4 is given by

$$X'_m = \left(m-\frac{N_x-1}{2}\right) D_x \tag{2-34a}$$

$$Y'_n = \left(n-\frac{N_y-1}{2}\right) D_y \tag{2-34b}$$

By substituting these values for X'_m and Y'_n in equation 2-28 the array factor becomes

$$AF(K_x,K_y) = B(K_x,K_y) \sum_{m=0}^{N_x-1} \sum_{n=0}^{N_y-1} C_{mn} Exp\{jK_x D_x m + jK_y D_y n\} \tag{2-35}$$

Where

$$B(K_x,K_y) = Exp\{-jK_x D_x (N_x-1)/2 - jK_y D_y (N_y-1)/2\} \tag{2-36}$$

Let
$$P_x = \frac{K_x D_x}{2\pi} \tag{2-37a}$$

$$P_y = \frac{K_y D_y}{2\pi} \tag{2-37b}$$

Then,

$$AF(K_x,K_y) = B(K_x,K_y) \sum_{m=0}^{N_x-1} \sum_{n=0}^{N_y-1} C_{mn} Exp\{j2\pi P_x m + j2\pi P_y n\} \tag{2-38}$$

The advantage of expressing the array factor in this way is that the summation part of equation 2-38 is very similar in form to the two-dimensional finite Fourier transform [15] which may be written as

$$X(L_1,L_2) = \sum_{K_1=0}^{N_1-1} \sum_{K_2=0}^{N_2-1} A(K_1,K_2)\,\mathrm{Exp}\{j2\pi K_1 L_1/N_1 + j2\pi K_2 L_2/N_2\} \qquad (2\text{-}39)$$

Where N_1, and N_2 are integer constants and where L_1, L_2, K_1 and K_2 are integer variables defined in the following ranges.

$$0 \le K_1 \le N_1-1 \qquad (2\text{-}40)$$

$$0 \le K_2 \le N_2-1$$

$$0 \le L_1 \le N_1-1$$

$$0 \le L_2 \le N_2-1$$

$X(L_1,L_2)$ and $A(K_1,K_2)$ are complex variables. The summation defined by equation 2-39 may be computed using the techniques of the fast Fourier transform.

Let $N_x = N_1$ (2-41a)

$N_y = N_2$ (2-41b)

$m = K_1$ (2-41c)

$n = K_2$ (2-41d)

$P_x = L_1/N_1$ (2-41e)

$P_y = L_2/N_2$ (2-41f)

$C_{mn} = A(K_1,K_2)$ (2-41g)

By using the substitutions defined by equations 2-41a through 2-41g it is possible to use the finite Fourier transform algorithm to do the summation part of equation 2-38.

It can readily be shown from equations 2-7a, 2-7b, 2-37a and 2-37b that K_x, K_y, P_x and P_y are continuous variables which are defined in the following ranges

$$-\frac{2\pi}{\lambda} \leq K_x \leq \frac{2\pi}{\lambda} \qquad (2\text{-}42)$$

$$-\frac{2\pi}{\lambda} \leq K_y \leq \frac{2\pi}{\lambda}$$

$$-\frac{D_x}{\lambda} \leq P_x \leq \frac{D_x}{\lambda}$$

$$-\frac{D_y}{\lambda} \leq P_y \leq \frac{D_y}{\lambda}$$

It should be noted that although K_x, K_y, P_x and P_y are continuous variables equations 2-41e and 2-41f define values of P_x and P_y which can be expressed only as rational numbers. For this reason it is apparent that the array factor can only be found at discrete points in K-space by using the finite Fourier transform. In addition to these restrictions on K_x, K_y, P_x and P_y only certain values of these variables represent real points in the sky. These values may be found as follows

$$\mathrm{Sin}\theta = \frac{(K_x^2+K_y^2)^{1/2}}{k} \qquad (2\text{-}43)$$

Therefore

$$0 \le (K_x^2+K_y^2) \le k^2 \qquad (2\text{-}44)$$

$$0 \le \left\{\frac{(2\pi P_x)^2}{D_x^2} + \frac{(2\pi P_y)^2}{D_y^2}\right\} \le k^2 \qquad (2\text{-}45)$$

If $$D_x = D_y = \lambda/2 \qquad (2\text{-}46)$$

then $$0 \le (P_x^2+P_y^2) \le 1/4 \qquad (2\text{-}47)$$

The relationship between θ,ϕ and K_x,K_y is shown in Figure 2.3. The sidelobes of the array factor which occur in the regions of K-space outside the region defined by equation 2-43 do not contribute any power to the system. If the array is phased by the introduction of a progressive phase shift in the excitation of the elements, these sidelobes may be shifted into the region of K-space representing real points in the sky and will now contribute power to the system.

2.7 Calculation of the Array Factor

By using the techniques of the fast Fourier transform the array factor can only be found at points in K-space where P_x and P_y are rational numbers as was indicated in the last section. The intervals in P_x and P_y between the points defined by equations 2-41e and 2-41f are $1/N_1$ and $1/N_2$ respectively. Increasing N_1 and N_2 reduces the size of these intervals and increases the resolution since the total range of P_x and P_y is limited by equation

2-47. N_1 and N_2 will both be set to 2048 in the following work. This choice sets the increment in K-space to 0.006136/λ for both K_x and K_y when $D_x=D_y=\lambda/2$. Also, in this case, it sets the overall size of the array to 1024λ by 1024λ which is much larger than any of the arrays to be examined in later chapters. The size of these arrays will be 160λ by 4λ. The array factor of these arrays can be examined with a high degree of resolution in K-space and hence in real space by using the fast Fourier transform on an array 1024λ by 1024λ where the level of excitation outside an area 160λ by 4λ is set to zero.

Figure 2.5 illustrates how an array 320 elements long (160λ) by 8 elements wide (4λ) might be numbered. The excitation of the elements outside the shaded area is set to zero. In other words,

$$C_{mn} = 0 \quad \begin{array}{l} \text{for } m<1020 \text{ and all } n \\ \text{for } m>1027 \text{ and all } n \\ \text{for } n< 864 \text{ and all } m \\ \text{for } n>1183 \text{ and all } m \end{array} \qquad (2\text{-}48)$$

For a physically tapered array the excitation of some of the elements inside the shaded area would also be set to zero as suggested by Figure 2-6. If the excitation of the elements does not change across the width of the array the m-subscript in C_{mn} may be dropped and the array factor may be written as

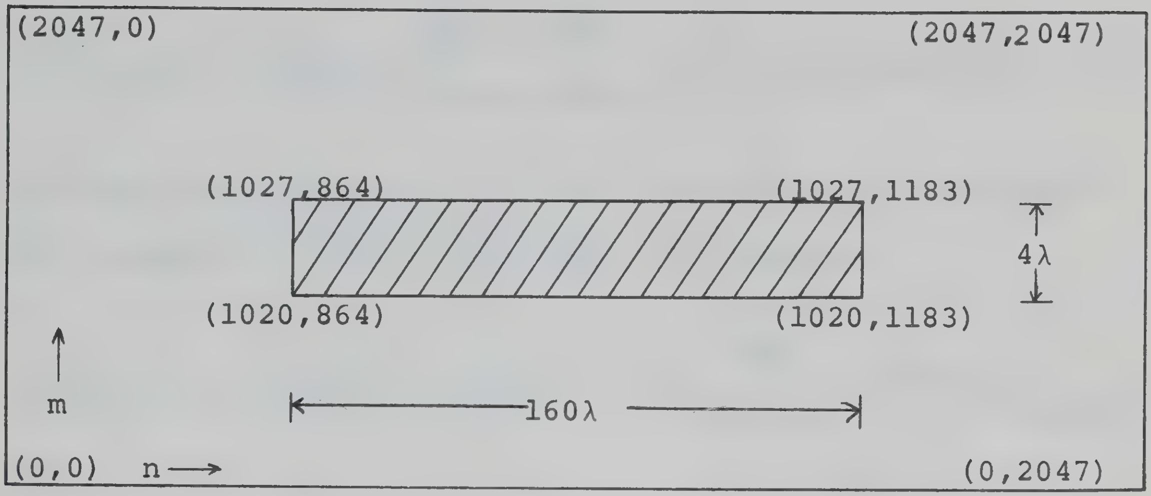

Figure 2.5. Arrangement of the Elements in Resistively Tapered Arrays.

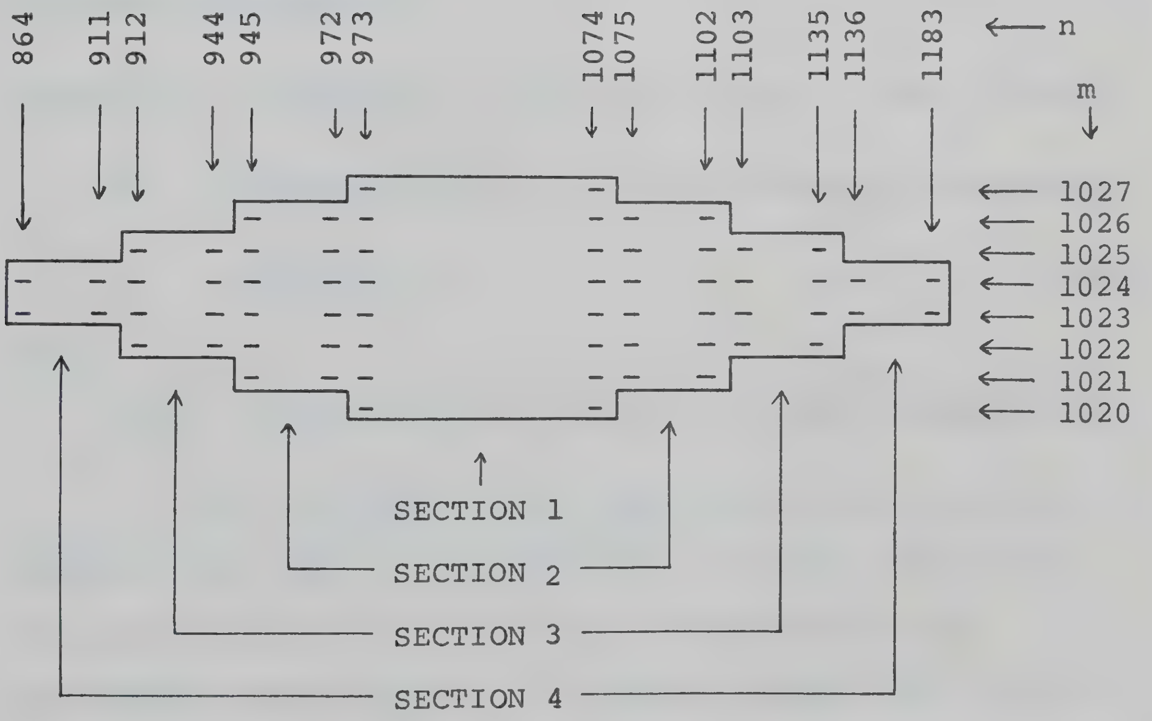

Figure 2.6. Arrangement of the Elements in Physically Tapered Arrays.

$$AF(K_x,K_y) = B(K_x,K_y) \sum_{m=1020}^{1027} \sum_{n=864}^{1183} C_n \mathrm{Exp}\{j2\pi(P_x m+P_y n)\} \quad (2\text{-}49)$$

By substituting for $B(K_x,K_y)$ and separating the summations with respect to m and n equation 2-49 becomes

$$AF(K_x,K_y) = G(P_y)\mathrm{Exp}\{-j2\pi P_x(2047/2)\} \sum_{m=1020}^{1027} \mathrm{Exp}\{j2\pi P_x m\} \quad (2\text{-}50)$$

Where

$$G(P_y) = \mathrm{Exp}\{-j2\pi P_y(2047/2)\} \sum_{n=864}^{1183} C_n \mathrm{Exp}\{j2\pi P_y n\} \quad (2\text{-}51)$$

In the actual running of the fast Fourier transform subroutine n will be incrimented from 0 to 2047, of course, since $C_n=0$ for n<864 and for n>1183 the value of equation 2-49 will be unchanged.

$$\begin{aligned} AF(K_x,K_y) &= G(P_y)[\mathrm{Exp}\{-j7\pi P_x\}+\mathrm{Exp}\{-j5\pi P_x\}\ldots+\mathrm{Exp}\{+j7\pi P_x\}] \\ &= G(P_y)2\{\mathrm{Cos}(7\pi P_x)+\mathrm{Cos}(5\pi P_x)+\mathrm{Cos}(3\pi P_x)+\mathrm{Cos}(\pi P_x)\} \\ &= F(P_x)G(P_y) \quad (2\text{-}52) \end{aligned}$$

where

$$F(P_y) = 2\{\mathrm{Cos}(7\pi P_x)+\mathrm{Cos}(5\pi P_x)+\mathrm{Cos}(3\pi P_x)+\mathrm{Cos}(\pi P_x)\} \quad (2\text{-}53)$$

It is apparent from equation 2-52 that when the width of the array is constant over its whole length the array factor may be expressed as the product of two orthoganal array factors. To find the array factor of an array which is physically tapered the array must be broken up into sub arrays in which the widths of the sub-arrays are

constant over their lengths. In the case of the physically tapered array shown in Figure 2.6 there are four distinct sections so there will be four terms in the array factor. Let the functions $F(P_x)$ and $G(P_y)$ be defined as follows.

$$G_8(P_y) = G(P_y) \quad \text{where} \quad C_n = 0 \quad \text{when} \quad \begin{array}{l} n < 973 \\ \text{or } n > 1074 \end{array} \tag{2-54a}$$

$$G_6(P_y) = G(P_y) \quad \text{where} \quad C_n = 0 \quad \text{when} \quad \begin{array}{l} n < 945 \\ \text{or } n > 1102 \\ \text{or } 973 \le n \le 1074 \end{array} \tag{2-54b}$$

$$G_4(P_y) = G(P_y) \quad \text{where} \quad C_n = 0 \quad \text{when} \quad \begin{array}{l} n < 912 \\ \text{or } n > 1135 \\ \text{or } 945 \le n \le 1102 \end{array} \tag{2-54c}$$

$$G_2(P_y) = G(P_y) \quad \text{where} \quad C_n = 0 \quad \text{when} \quad \begin{array}{l} n < 864 \\ \text{or } n > 1183 \\ \text{or } 912 \le n \le 1135 \end{array} \tag{2-54d}$$

$$F_8(P_x) = F(P_x) \tag{2-55a}$$

$$F_6(P_x) = 2\{\mathrm{Cos}(5\pi P_x) + \mathrm{Cos}(3\pi P_x) + \mathrm{Cos}(\pi P_x)\} \tag{2-55b}$$

$$F_4(P_x) = 2\{\mathrm{Cos}(3\pi P_x) + \mathrm{Cos}(\pi P_x)\} \tag{2-55c}$$

$$F_2(P_x) = 2\{\mathrm{Cos}(\pi P_x)\} \tag{2-55d}$$

The array factor for the array shown in Figure 2.6 can now be written as

$$AF(K_x, K_y) = F_8(P_x)G_8(P_y) + F_6(P_x)G_6(P_y) + F_4(P_x)G_4(P_y) + F_2(P_x)G_2(P_y) \tag{2-56}$$

2.8 Beam Steering

Beam steering may be achieved by progressively delaying (i.e. Phase Shifting) the excitation of the elements towards the desired position of the beam. The effect is to shift the array factor in K-space so that the main beam points in the new direction. To show this effect consider beam steering along the principle axis. In this case ϕ is 90 degrees and equation 2-38 may be re-written as follows.

$$AF(K_y) = Exp\{-jK_yD_y(N_y-1)/2\} \sum_{n=0}^{Ny-1} C_nExp\{jK_yD_yn\} \qquad (2\text{-}57)$$

For the case in which the phase of the excitation is zero set

$$C_n = A_n \qquad (2\text{-}58)$$

$$AF(K_y) = Exp\{-jK_yD_y(N_y-1)/2\} \sum_{n=0}^{Ny-1} A_nExp\{jK_yD_yn\} \qquad (2\text{-}59)$$

For the case in which there is a progressive phase shift in the excitation it is possible to represent C_n as

$$C_n = A_nExp\{-jK_{yo}D_yn\} \qquad (2\text{-}60)$$

where $K_{yo} = kSin\theta_o$

$$AF(K_y) = Exp\{-jK_yD_y(N_y-1)/2\} \sum_{n=0}^{Ny-1} A_nExp\{(K_y-K_{yo})D_yn\} \qquad (2\text{-}61)$$

If the array factor for the array with the progressive phase shift is now evaluated at K_y+K_{yo} instead of at K_y, equation

2-61 becomes

$$AF(K_y+K_{yo}) = Exp\{-j(K_y+K_{yo})D_y(N_y-1)/2\}\sum_{n=0}^{N_y-1} A_n Exp\{jK_yD_yn\} \quad (2\text{-}62)$$

Equation 2-62 may be written as

$$AF(K_y+K_{yo}) = Exp\{jK_{yo}D_y(N_y-1)/2\}Exp\{-jK_yD_y(N_y-1)/2\} \sum_{n=0}^{N_y-1} A_n Exp\{jK_yD_yn\} \quad (2\text{-}63)$$

Except for the first exponential factor equations 2-63 and 2-59 are identical. In other words, when the array factor for the case in which a progressive phase shift is present is evaluated at K_y+K_{yo} and the array factor for the case in which no progressive phase shift is present is evaluated at K_y, the two array factors are identical except for a shift in phase. By taking the magnitude of both equations 2-59 and 2-63 it is apparent that the shape of the array factors for the phased and the unphased arrays are identical and that the effect of introducing a progressive phase shift has been to shift the array factor in K-space by an amount K_{yo}. Hence

$$|AF(K_y+K_{yo})|_{\text{Phased array}} = |AF(K_y)|_{\text{Unphased array}} \quad (2\text{-}64)$$

It should be noted that although the peak levels of the array factor do not change when the array is scanned, the widths of the main beam and the sidelobes do change which may produce changes in the relative power contributed

by the main beam and the sidelobes. The changes in width are due to the way θ and ϕ are related to K_x and K_y. For values of θ close to zero in Figure 2.3 the smallest increment in K_x or K_y represents 0.056 degrees in θ while for θ close to 90 degrees the same increment in K_x or K_y represents 3.532 degrees in θ. It should also be noted that the peak levels of the power pattern may change when the array is phased. If this occurs it is due to the fact that the combined effects of the element pattern, the screen factor and the factor introduced by the change in coordinates from rectangular to polar do not produce an isotropic pattern in the direction in which the main beam is shifted.

CHAPTER 3

ANALYSIS OF ONE-DIMENSIONAL ARRAYS

3.1 Introduction

In this chapter the array factor of five one-dimensional arrays will be examined. In all cases the array will consist of half-wavelength dipoles and their arrangement will be as indicated in Figure 3.1.

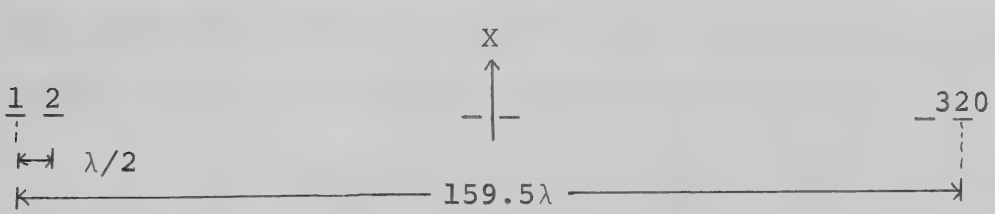

Figure 3.1. Arrangement of the Elements in One-dimensional Arrays.

The tapering will be entirely resistive and the excitation distributions will vary from uniform through four progressively better approximations to a Gaussian. The first three approximations to the Gaussian excitation distribution represent a very coarse taper. This type of taper will necessarily exist along the transverse axis of the physically tapered two-dimensional arrays to be discussed in Chapter 4. Indeed the exact form of the excitation distribution, in this chapter, will be chosen such that the response of these one-dimensional arrays will correspond very closely in their principle plane to the array factor of one of the four arrays to be discussed in Chapter 4. Correspondence is achieved by setting the

excitation at each point along the axis of the one-dimensional array equal to the sum of the excitations across the width of the two-dimensional arrays at the same points along the principle axis of these arrays.

One-dimensional analysis allows the principle features of the array factor to be examined without the necessity of expensive computing. The beam width in the principle plane, the effects of phasing on the beam width, the location of the first zeros and the maximum sidelobe level that may be expected can easily be found.

The analysis was done using an IBM 360 computer. Programs were written to generate the excitation data for the different types of arrays to be examined. The summation part of the calculation was performed using a fast Fourier transform subroutine called HARM which is available in the IBM Scientific Subroutine Package, [16]. Additional programs were written to analyse the results and present the output in a useful form. These programs and the problems encountered in computing are discussed in Appendix C.

3.2 Excitation

The excitation data for the uniform and the truncated Gaussian arrays are shown in Figure 3.2a. The excitation is symmetric so only half has been shown. The shape of the Gaussian distribution is based on a taper of -24.0 dB over a distance of 80 wavelengths. The choice of -24.0 dB for the taper is based on a compromise between the

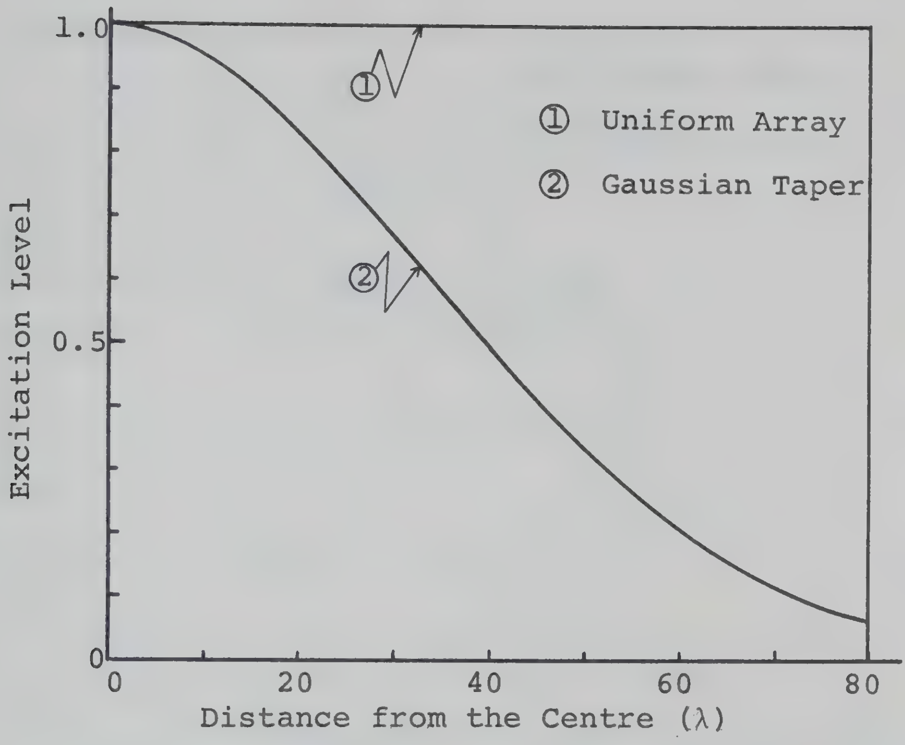

Figure 3.2a. Excitation Data for a Uniform and a Truncated Gaussian Array.

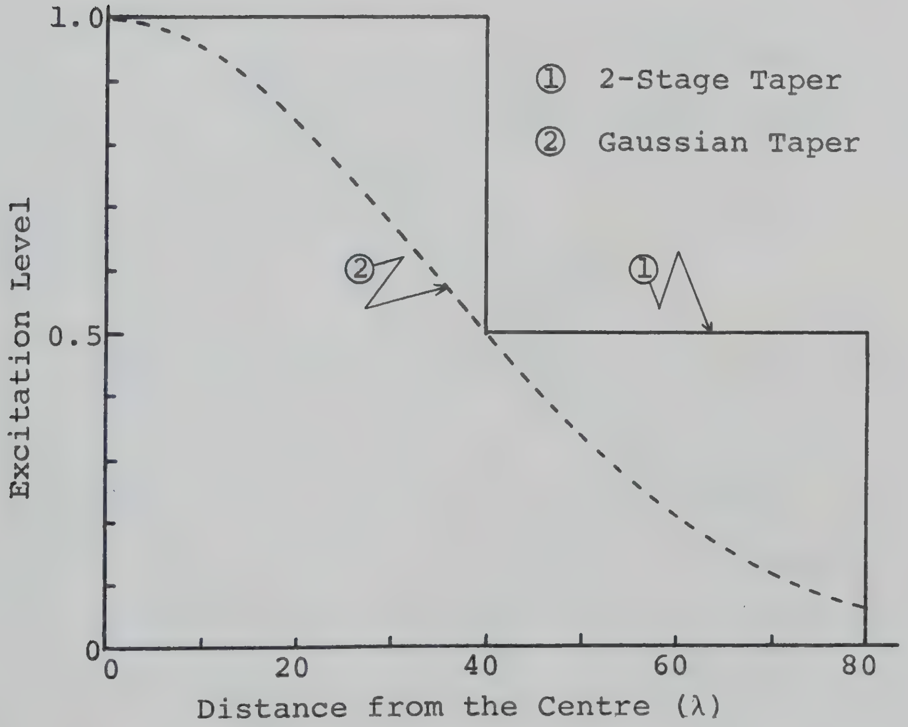

Figure 3.2b. Excitation Data for an Array with 2 Stages of Tapering.

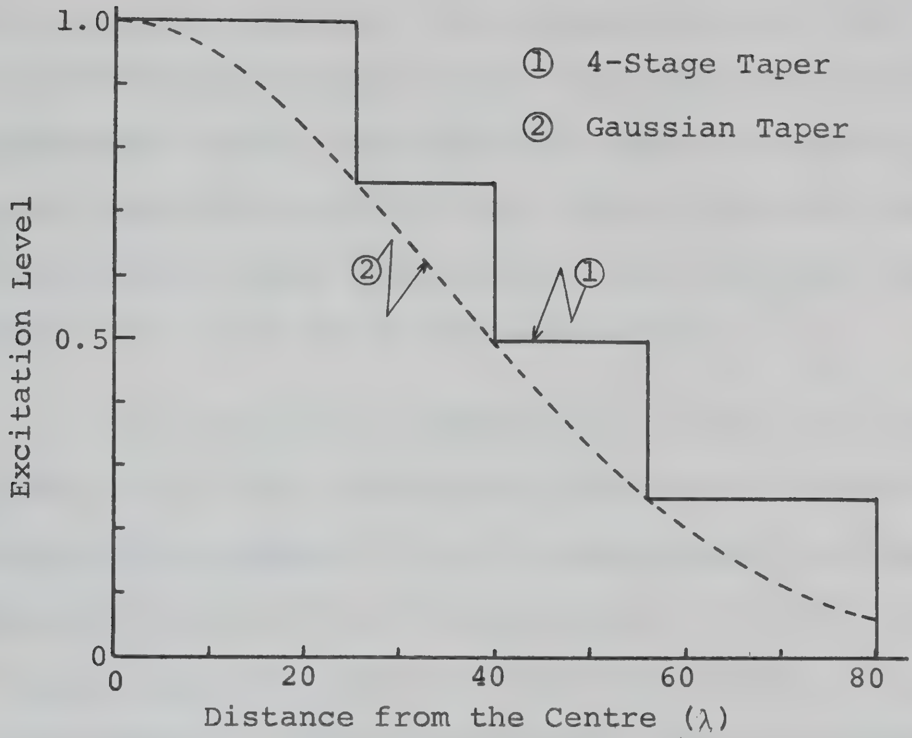

Figure 3.2c. Excitation Data for an Array with 4 Stages of Tapering.

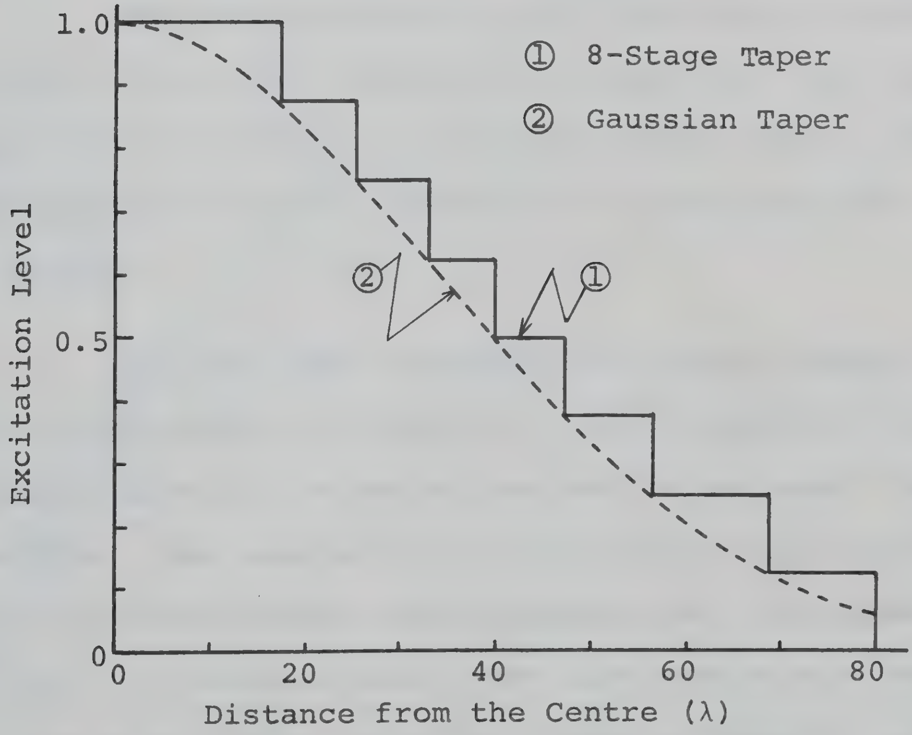

Figure 3.2d. Excitation Data for an Array with 8 Stages of Tapering.

requirements for gain and the maximum sidelobe level that can be tolerated. Figures 3.2b, 3.2c and 3.2d show the progressively better approximations from the uniform to the Gaussian excitation distribution. They represent tapering in two, four and eight stages where the excitation step sizes are 0.5, 0.25 and 0.125 respectively.

In all cases the excitation of the centre elements has been set to unity so that the gain of the different systems may be compared. All the excitations are real. No progressive phase shifts were introduced as it was shown in Section 2.8 that the effects of scanning on the array factor can be examined by shifting the array factor in K-space.

3.3 Main Beam Response

The array factors for the five array systems described in the last section were computed. Each was normalized with respect to its own maximum level. The normalizing factors are related to the relative gain between the systems.

The main beam responses for levels greater than −6.0 dB are shown in Figure 3.3. It is apparent that the principle effect of tapering has been to increase the beamwidth. The response of an array with a true Gaussian excitation distribution was calculated but the response in this part of the main beam is not distinguishable from the response of the array with the truncated Gaussian excitation distribution.

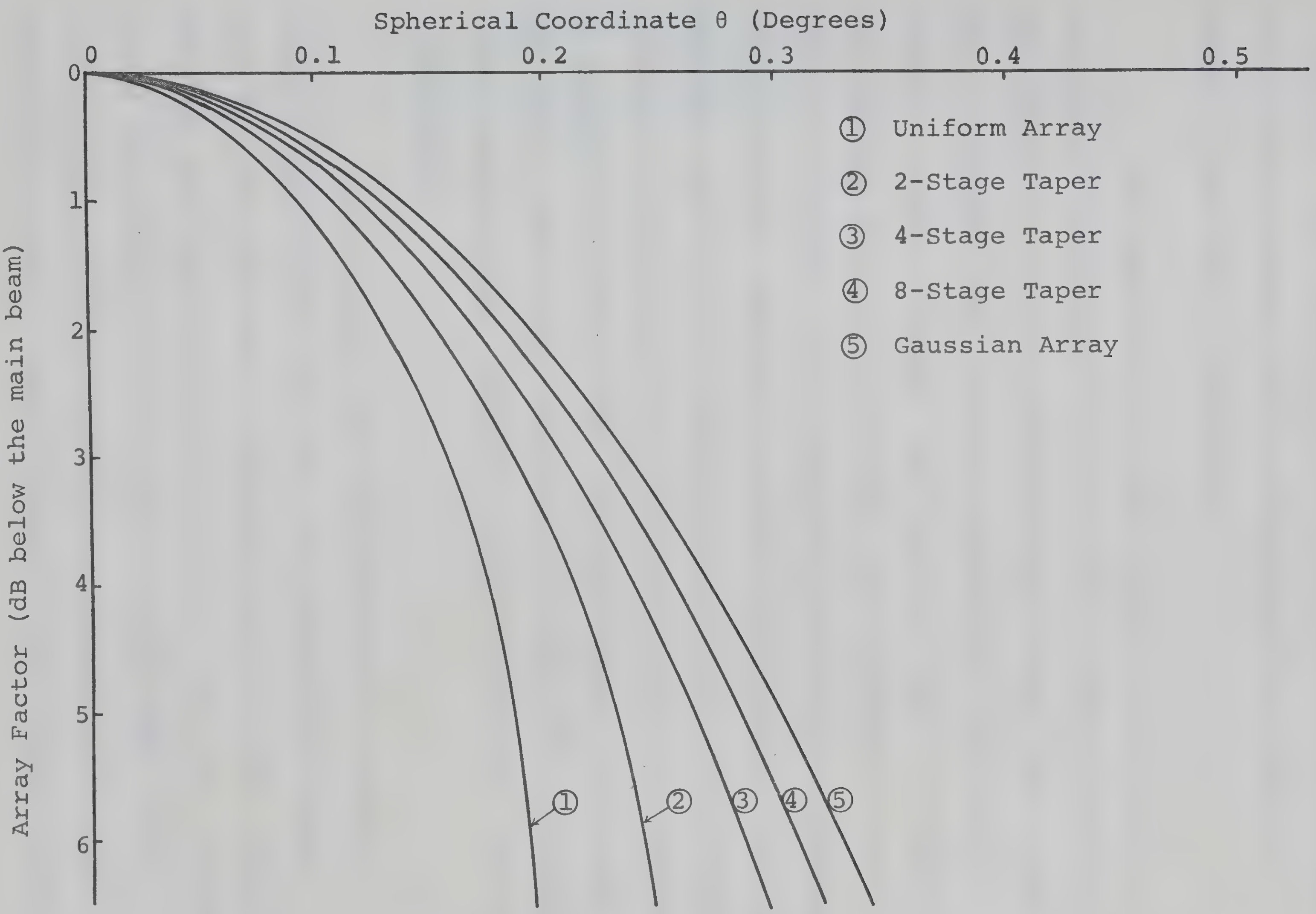

Figure 3.3. Main Beam Characteristics of the One-dimensional Arrays

Figures 3.4a through 3.4e show the first two degrees in the principle plane of each array factor. It can be seen that the beamwidth to the first minimum increases and the peak sidelobe level decreases as the number of stages of tapering is increased.

The response of an array with a true Gaussian excitation distribution is also shown in Figure 3.4e for comparison with the truncated Gaussian array. For θ less than 0.8 degrees the difference between the two array factors is small, however, for θ greater than 0.8 degrees the response of the true Gaussian falls rapidly to zero while the response of the truncated Gaussian has sidelobes. These sidelobes represent the effect of truncating the true Gaussian excitation distribution and could be considered as representing the array factor produced by an error function, as suggested by Figure 3.5. The array factor of an array with type 1 excitation, as shown in Figure 3.5, is identical to the combined array factors of arrays with type 2 and type 3 excitation.

In all cases, for the array factors shown in Figures 3.4b through 3.4d, for the arrays with coarse tapering, the locations of maximum sidelobe levels close to the main beam are not very predictable. The first sidelobe is not the greatest and the relative magnitudes of the sidelobes are not determined by the amount of tapering. There is, however, a general trend in the average sidelobe

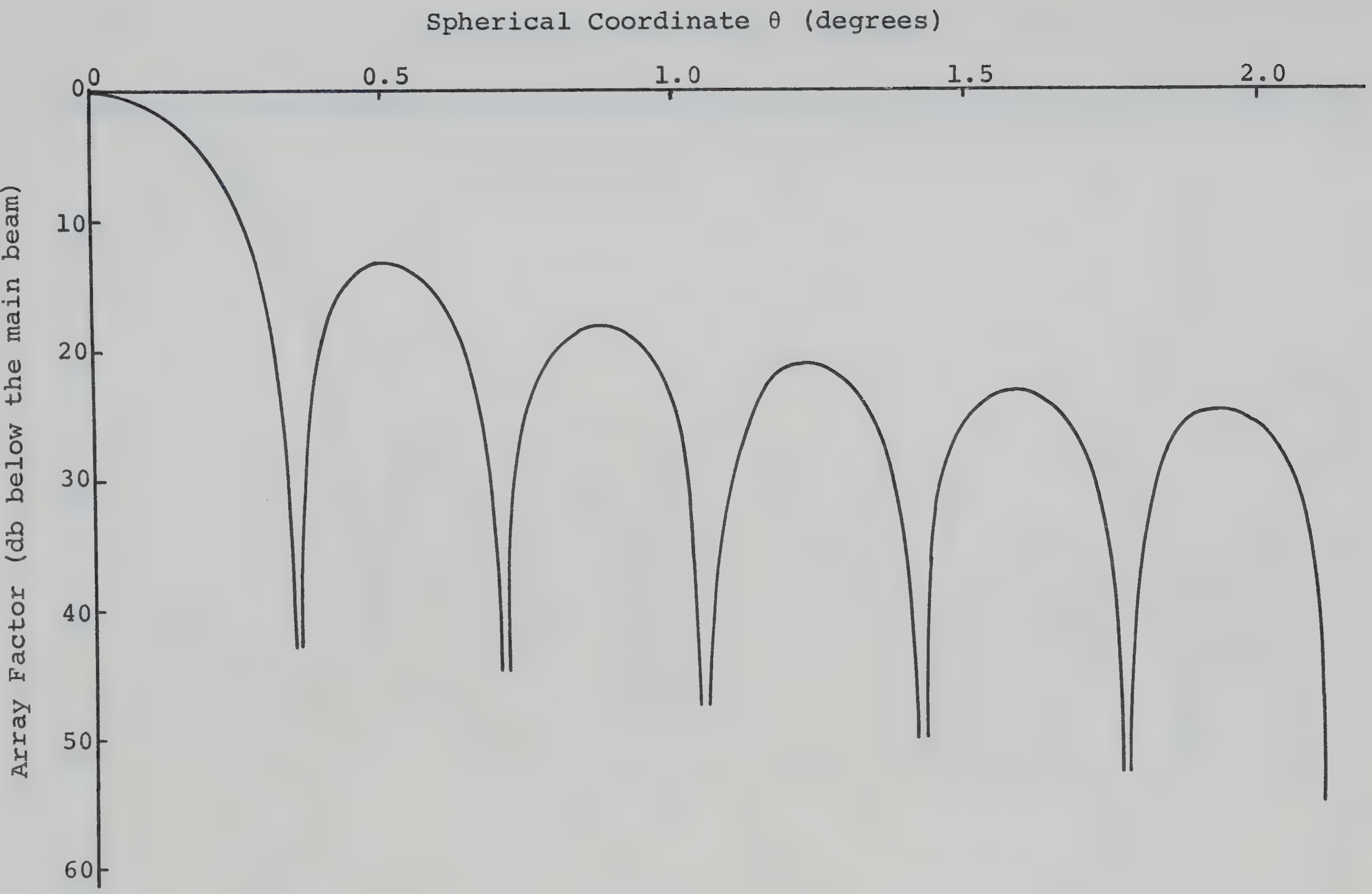

Figure 3.4a. First Sidelobes for the Uniform Array.

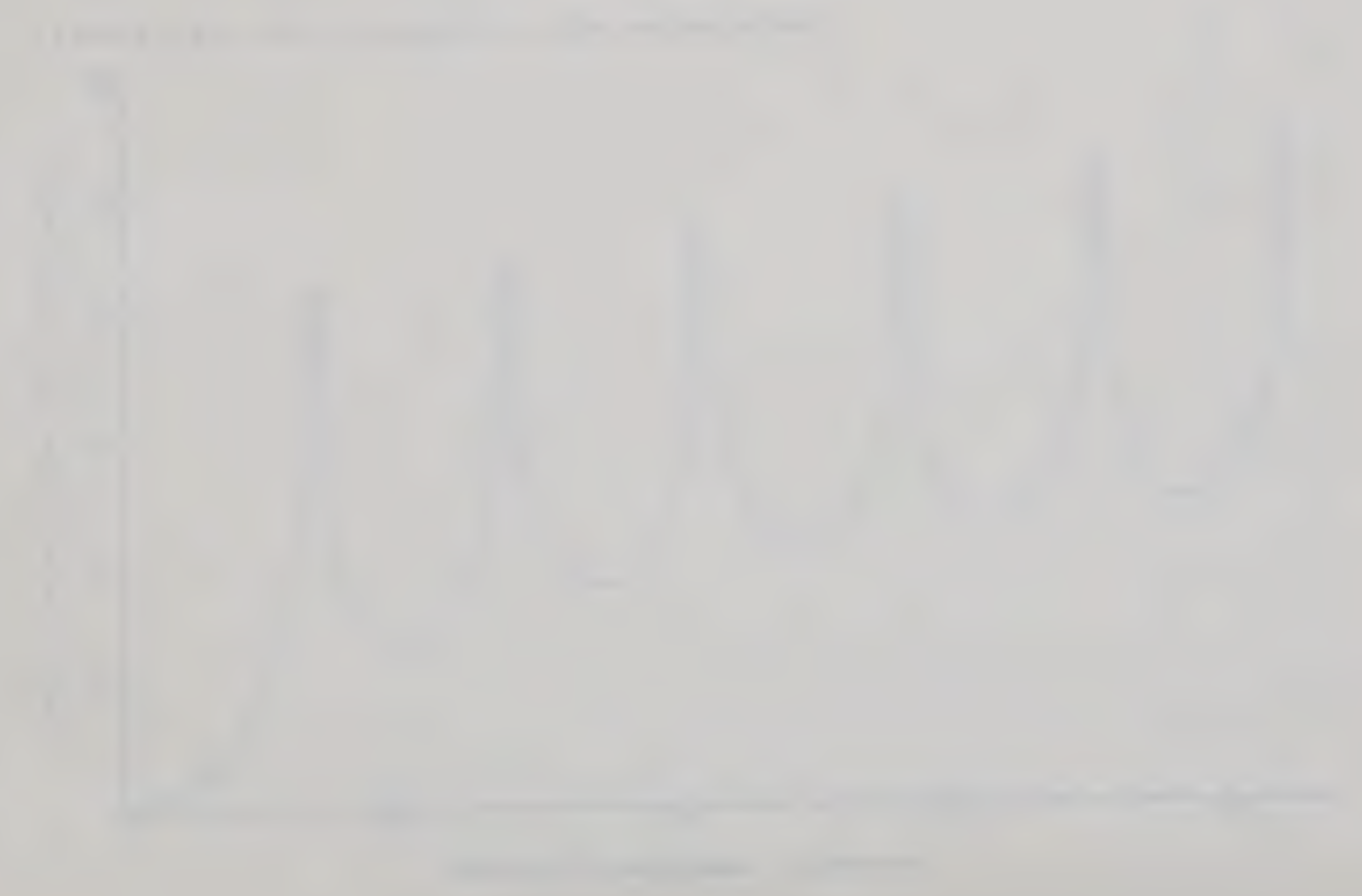

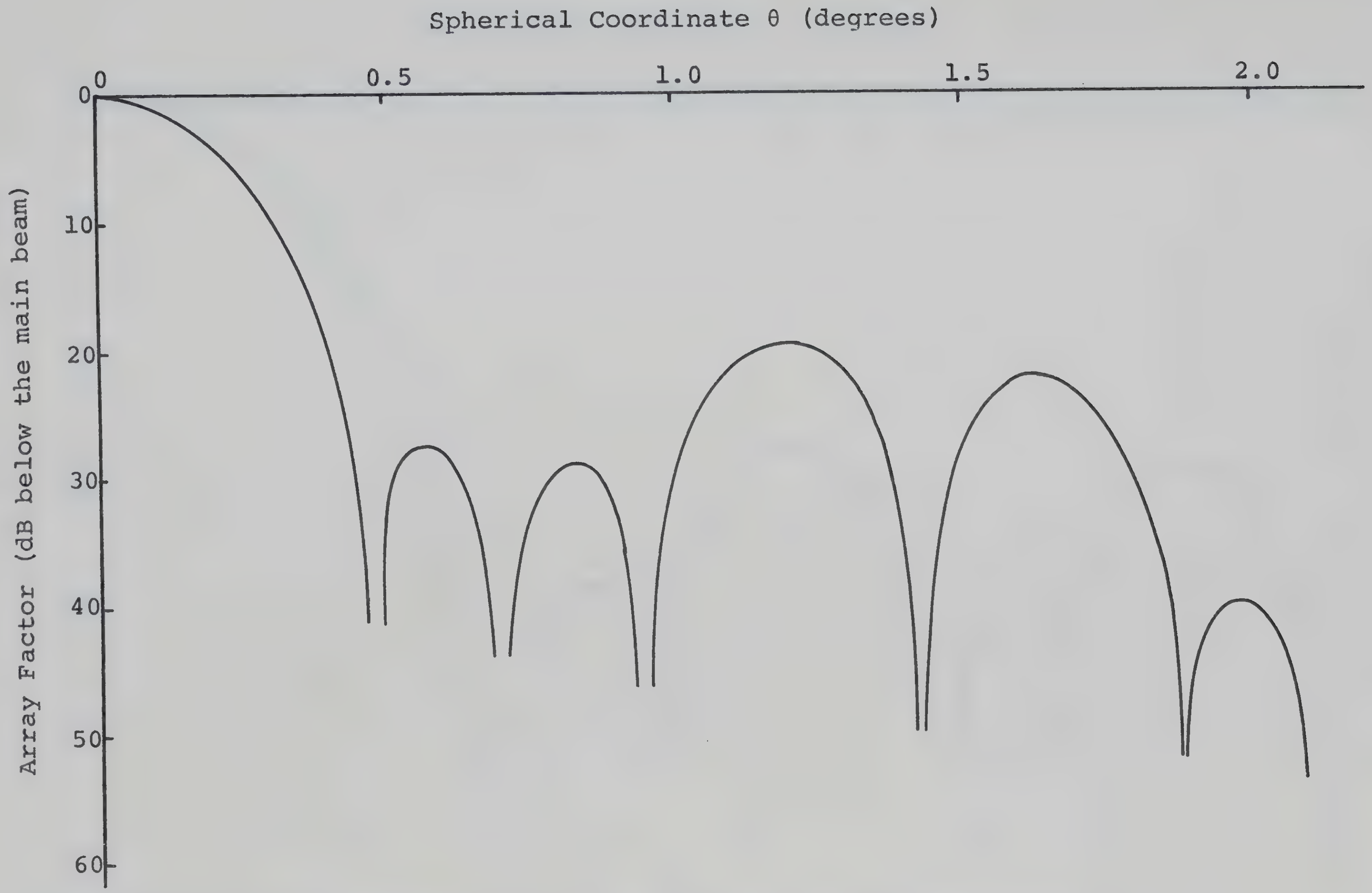

Figure 3.4b. First Sidelobes for the Array with 2 Stages of Tapering.

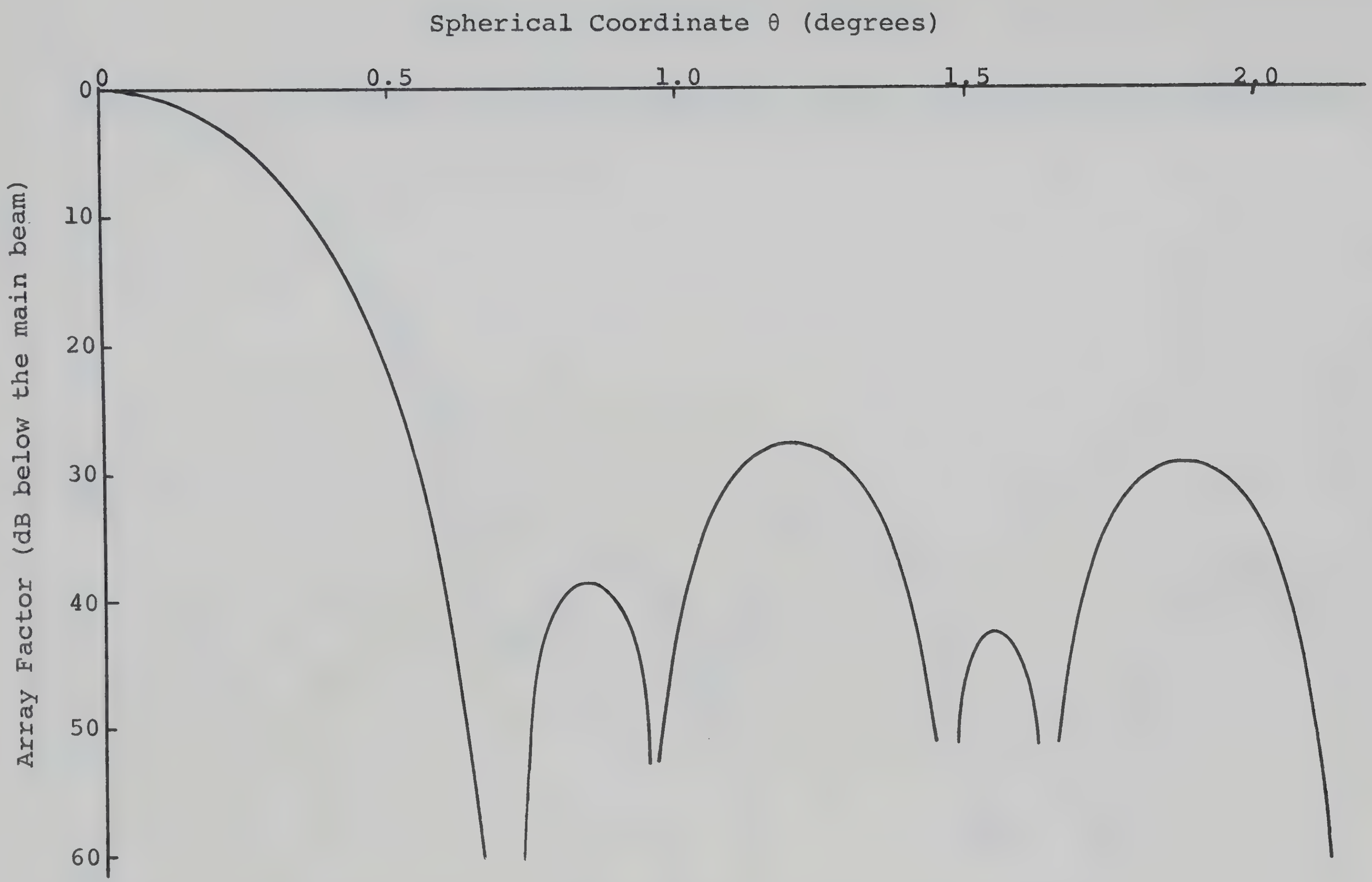

Figure 3.4c. First Sidelobes for the Array with 4 Stages of Tapering.

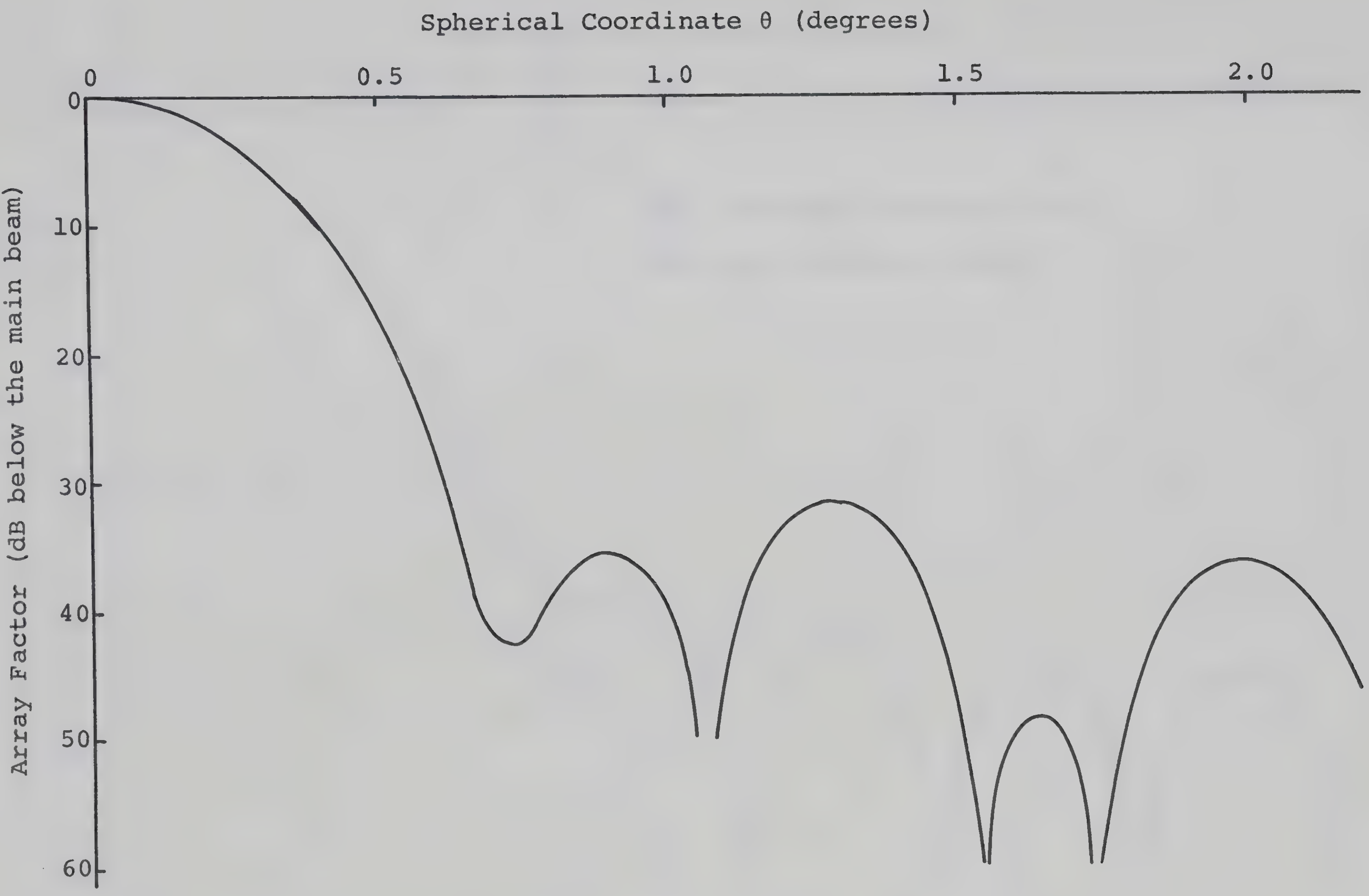

Figure 3.4d. First Sidelobes for the Array with 8 Stages of Tapering.

[illegible]

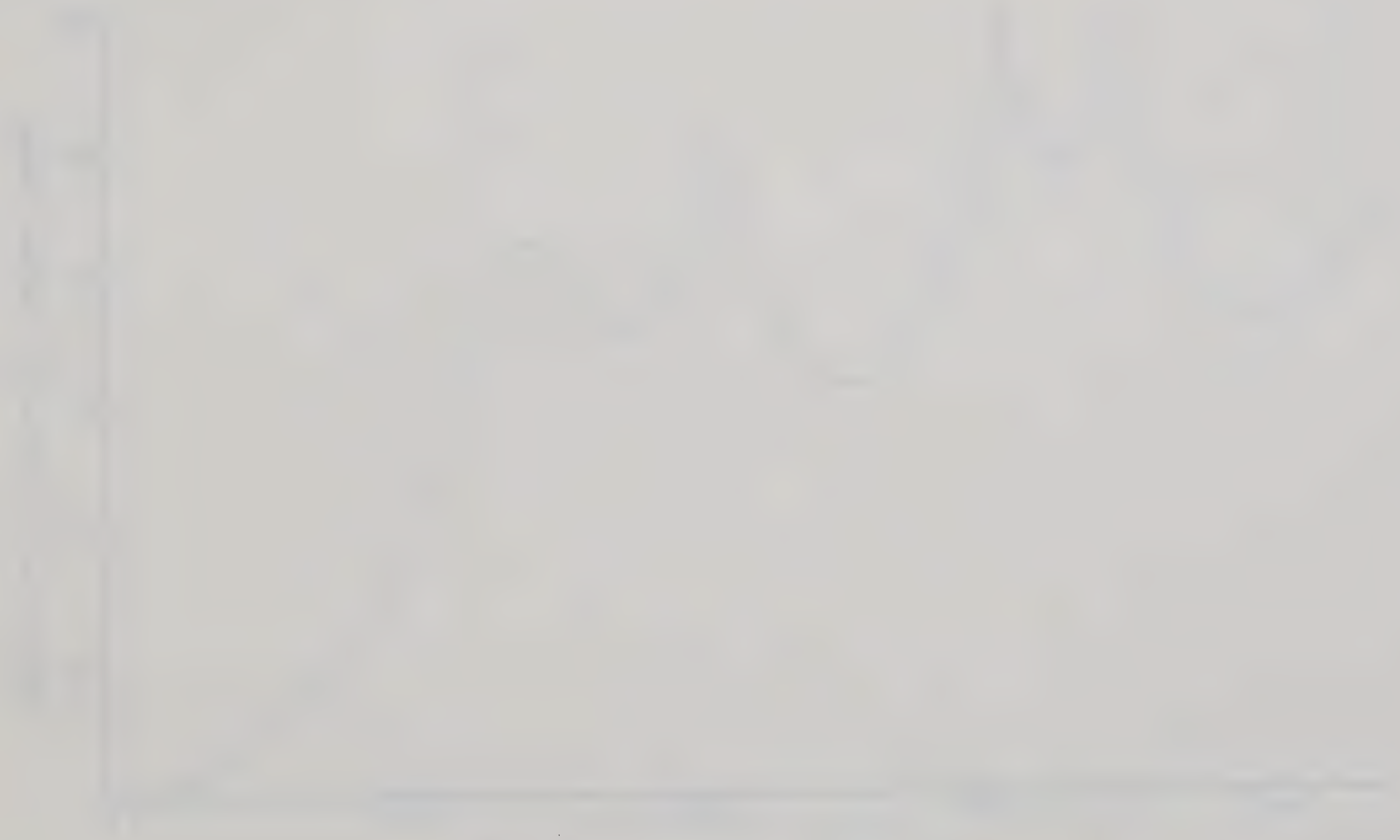

[illegible]

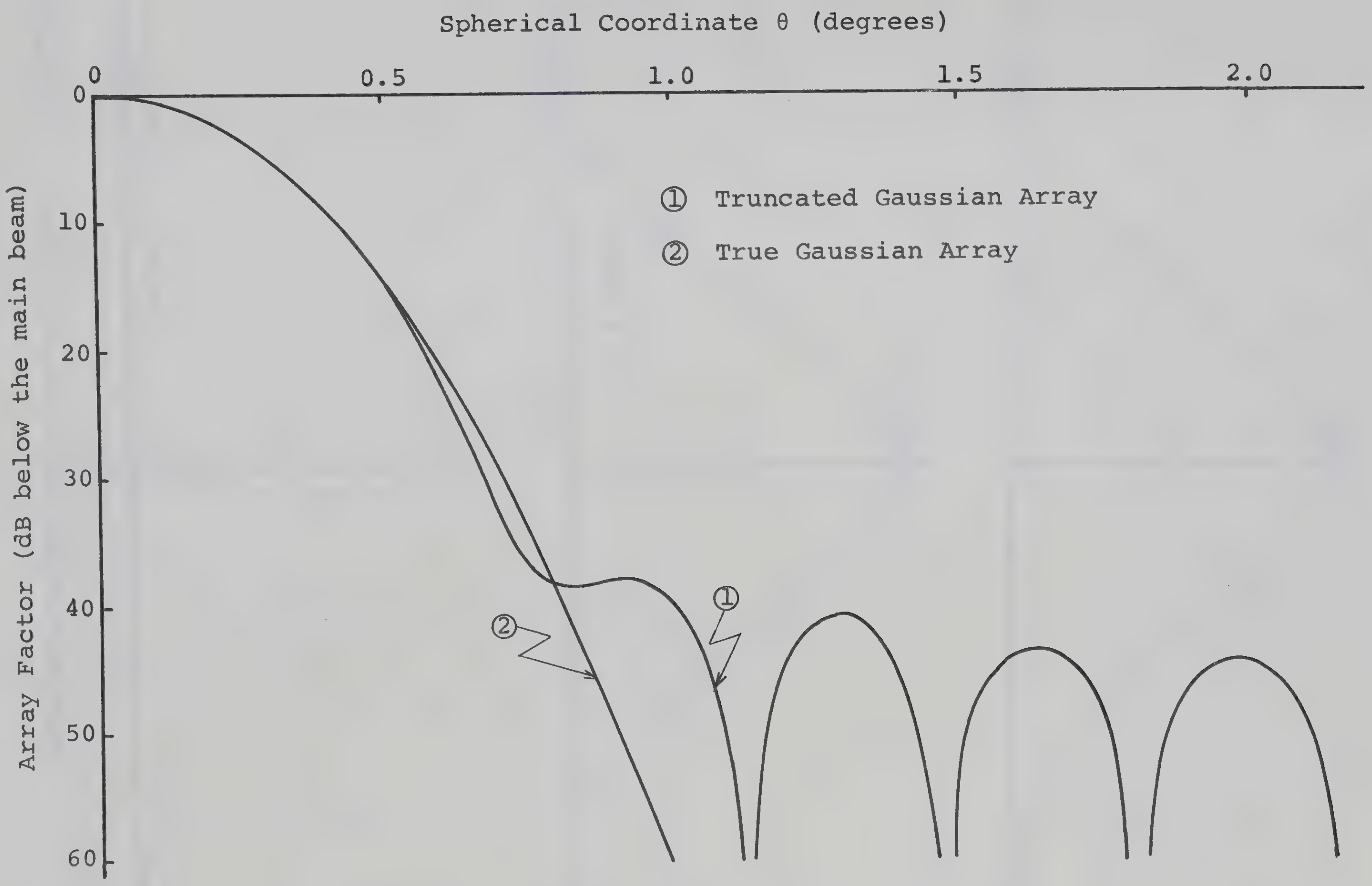

Figure 3.4e. First Sidelobes for the Gaussian Array.

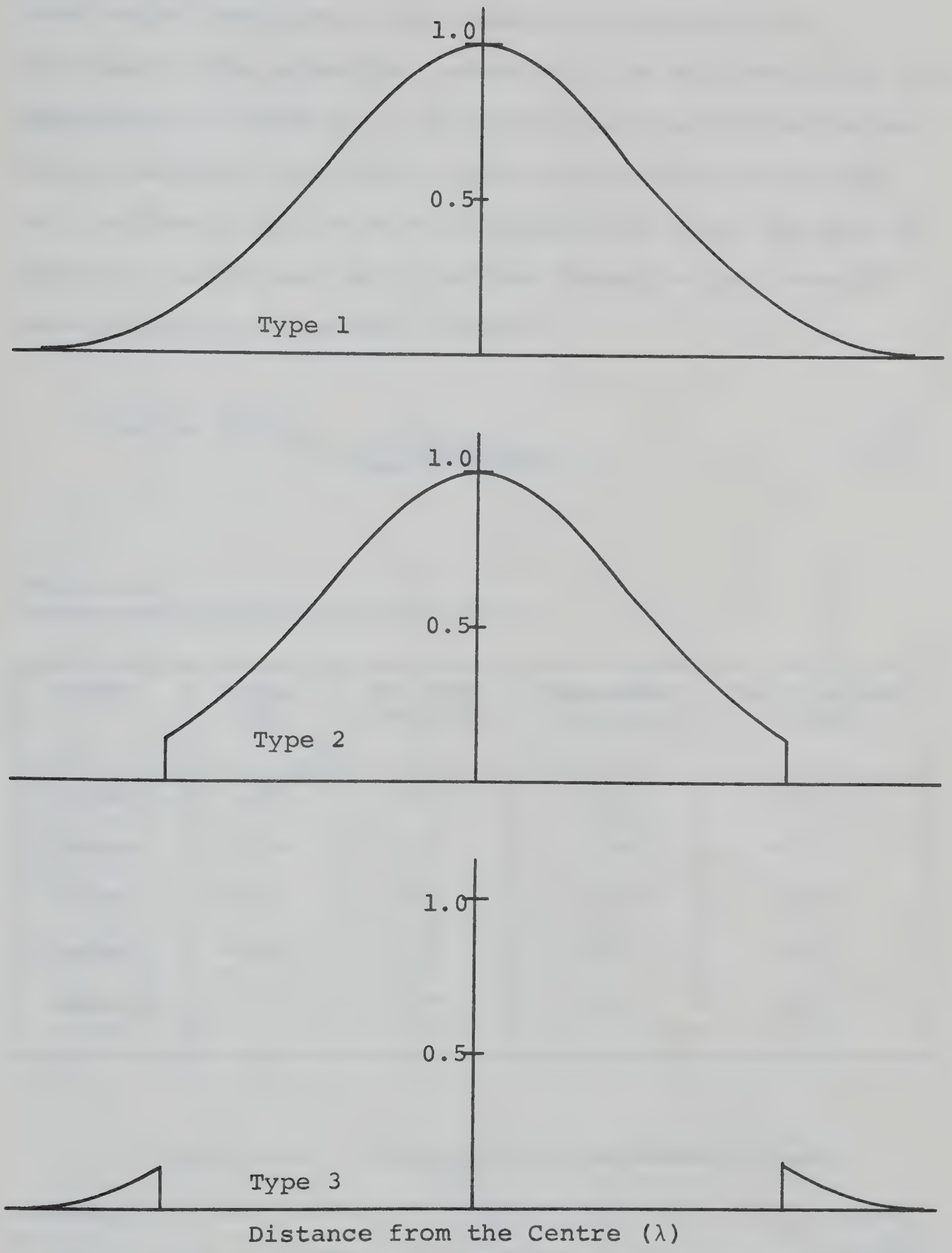

Figure 3.5. Excitation Data for Gaussian Arrays.

level which decreases as the amount of tapering is increased. The principle features of the main beam area are summarized in Table 3.1. It is also instructive to define a 'figure of merit' for each array as indicated in equation 3-1. Although this term will be referred to as the gain it should be noted that it is not the directive gain usually associated with an antenna system.

$$\text{Gain} = 20\log_{10} \frac{AF_{max}}{AF_{max}(\text{Uniform})} \qquad (3\text{-}1)$$

Table 3.1
Characteristics of the Main Beam

Taper	Gain (dB)	1st Min (Degrees)	Beamwidth (Degrees)	Max Sidelobe (dB)
Uniform	0.00	0.34	0.320	-13.3
2-stage	-2.34	0.50	0.360	-19.1
4-stage	-4.24	0.73	0.420	-27.6
8-stage	-4.84	0.73	0.442	-31.9
Gaussian	-5.72	0.84	0.468	-38.0

The effects of phasing on the beamwidth were examined for each system by shifting the main beams, shown in Figure 3.3, to different locations in K-space and finding the new values of θ which correspond to the 3 dB points located in the new diagram. The effects of phasing on the

beamwidth when the main beam is shifted up to 30 degrees from the zenith are shown in Figure 3.6. For θ close to zero the beamwidth of the Gaussian array is 46% greater than the beamwidth of the uniform array and for θ close to 30 degrees it is 50% greater. The percentage increase in beamwidth is 12.8%. For the Gaussian array the percentage increase is 15.2%.

3.4 Sidelobe Levels

The purpose of tapering is to reduce the sidelobe levels of the array factor. Consider first the peak sidelobe levels, as functions of θ, of the uniform array and the truncated Gaussian arrays shown in Figure 3.7. The curves represent the locus of values of the peaks of the sidelobes. It is apparent that for both arrays the sidelobe levels decrease smoothly for increasing θ. In both cases they drop off rapidly from the level of their first sidelobe and then level out as θ approaches 90 degrees. The peak sidelobe levels for small values of θ are about 25 dB lower in the case of the array with the Gaussian taper. But, for θ greater than about 2.5 degrees the difference is about 20dB. It was observed during the study, although it is not shown here, that for large values of θ the location of the sidelobes and the zeros in the array factors for both array systems occur very close together. The spacing between the zeros for both systems for large values of θ is determined by the overall dimensions of the array.

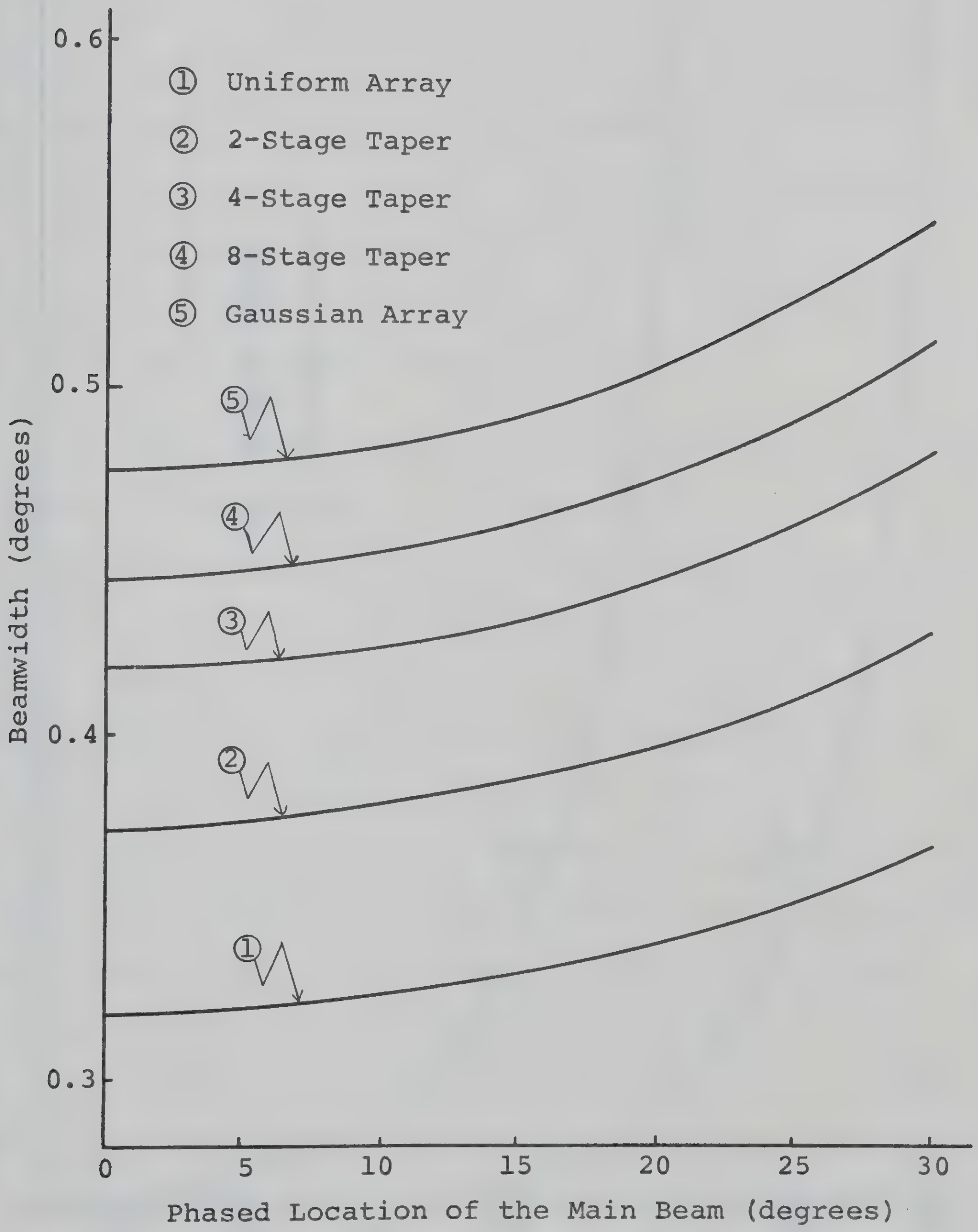

Figure 3.6. Effects of Phasing on the Main Beam.

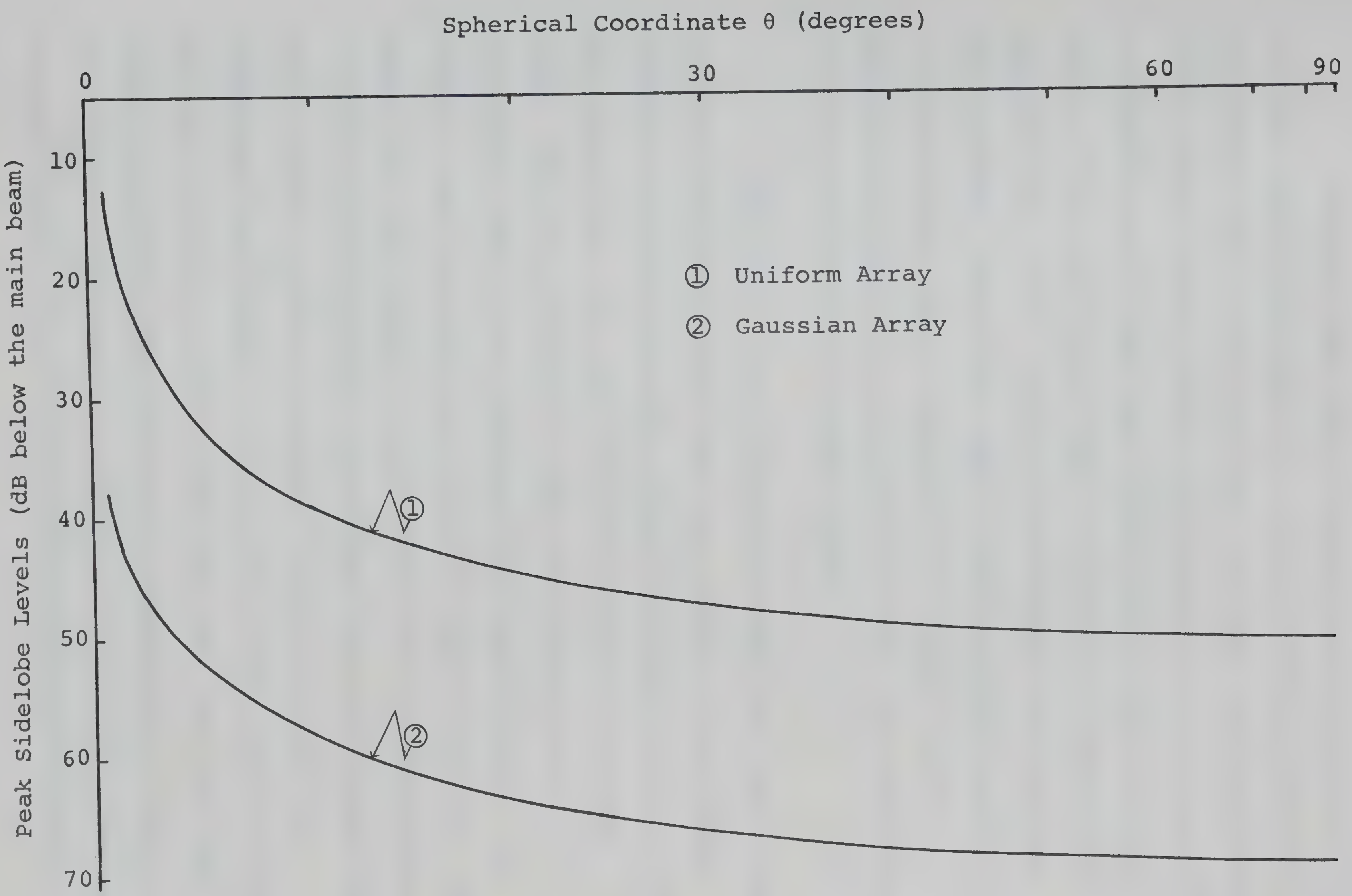

Figure 3.7. Peak Sidelobe Levels for the Uniform and the Gaussian Arrays.

Attempts were made to obtain similar diagrams for the three coarse approximations to the Gaussian excitation distribution but it was found that the peak sidelobe levels do not follow a smooth curve. The scale of θ in Figure 3.7 is insufficient to show these variations in the sidelobe levels. The array factors were then drawn in sections to an expanded scale of θ. Figures 3.8a through 3.8c show the peak sidelobe levels that occur in the first 10 degrees of θ. The sections from 2 degrees to 10 degrees can be considered typical for each system and only the analysis of these sections will be presented here.

One of the most striking features that can be seen on these diagrams is that there are points, in all three systems with course tapering, where the peak sidelobe levels are greater than the peak sidelobe levels of a uniform array. What has happened is that the tapering has eliminated some of the sidelobes and reduced many of the others. Some sidelobes have remained almost unchanged. The reason that they appear to be greater than the sidelobes of a uniform array is because each array factor was normalized with respect to its own maximum. If they had all been normalized with respect to the maximum of the uniform array, the array factors for the arrays with two, four and eight stages of tapering would have to be reduced by 2.3 dB, 4.2 dB and 4.8 dB respectively. If this were done some of the peak sidelobe levels of the arrays with coarse tapering would

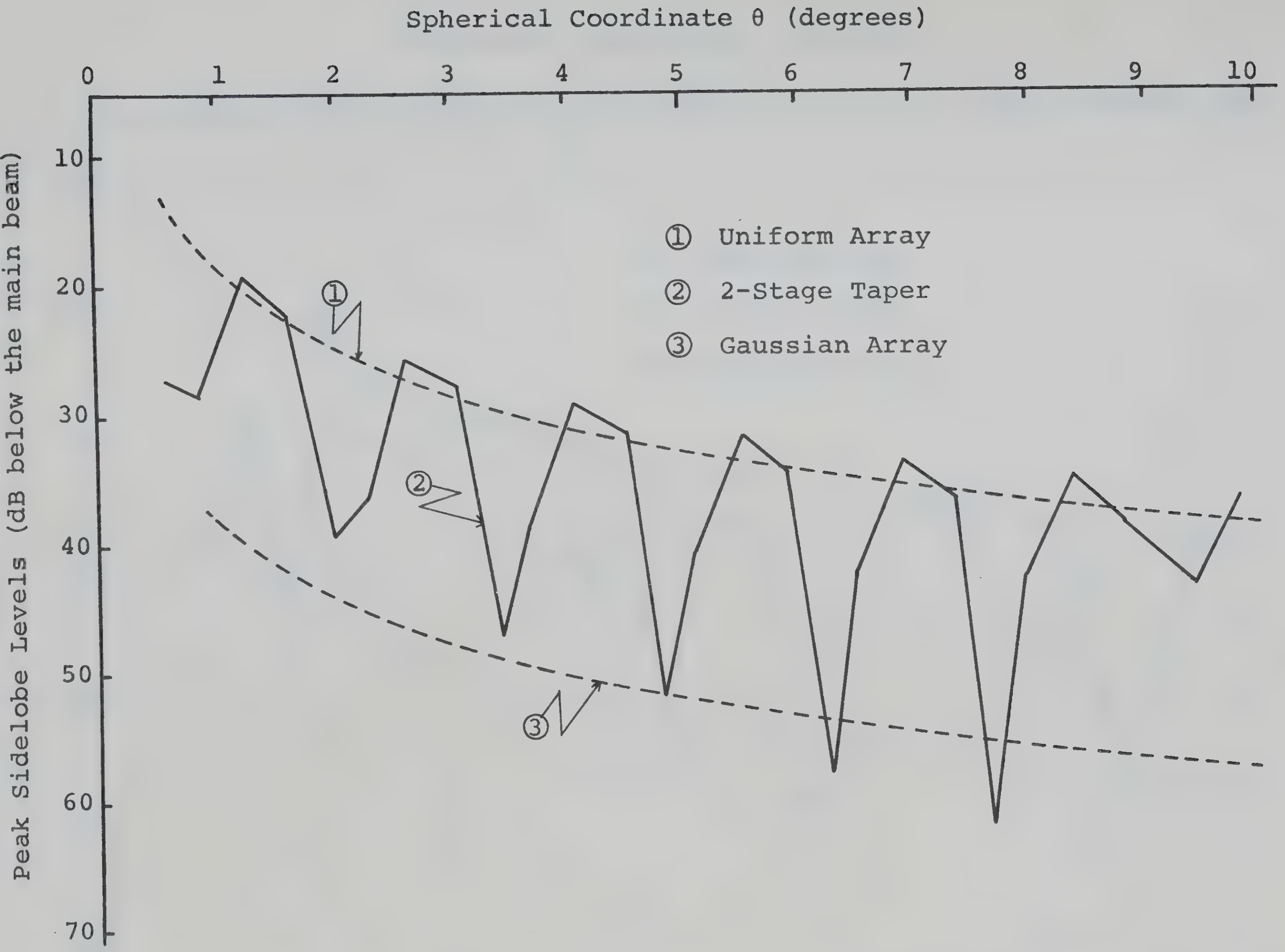

Figure 3.8a. Peak Sidelobe Levels near the Main Beam for the Array with 2 Stages of Tapering.

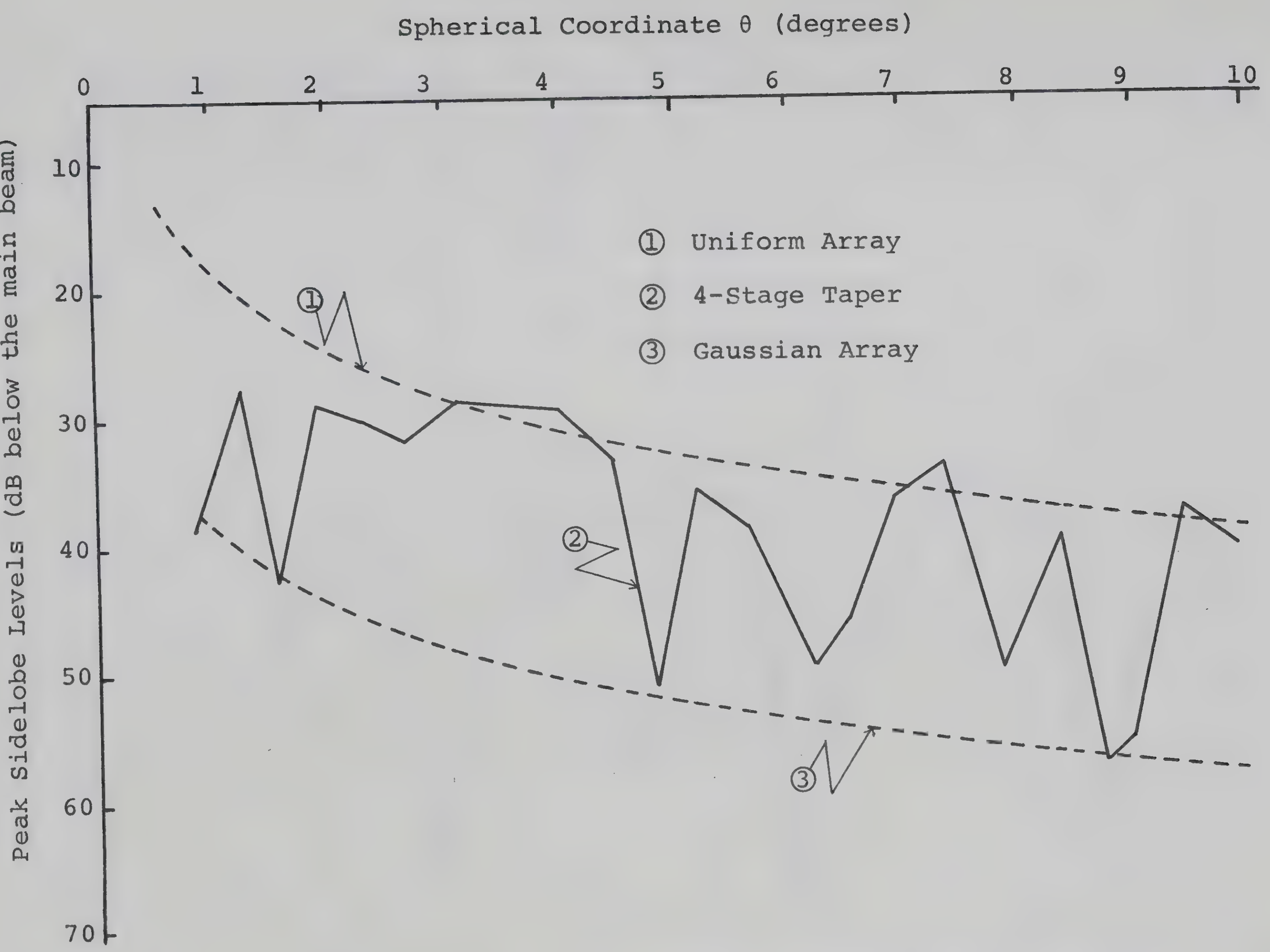

Figure 3.8b. Peak Sidelobe Levels near the Main Beam for the Array with 4 Stages of Tapering.

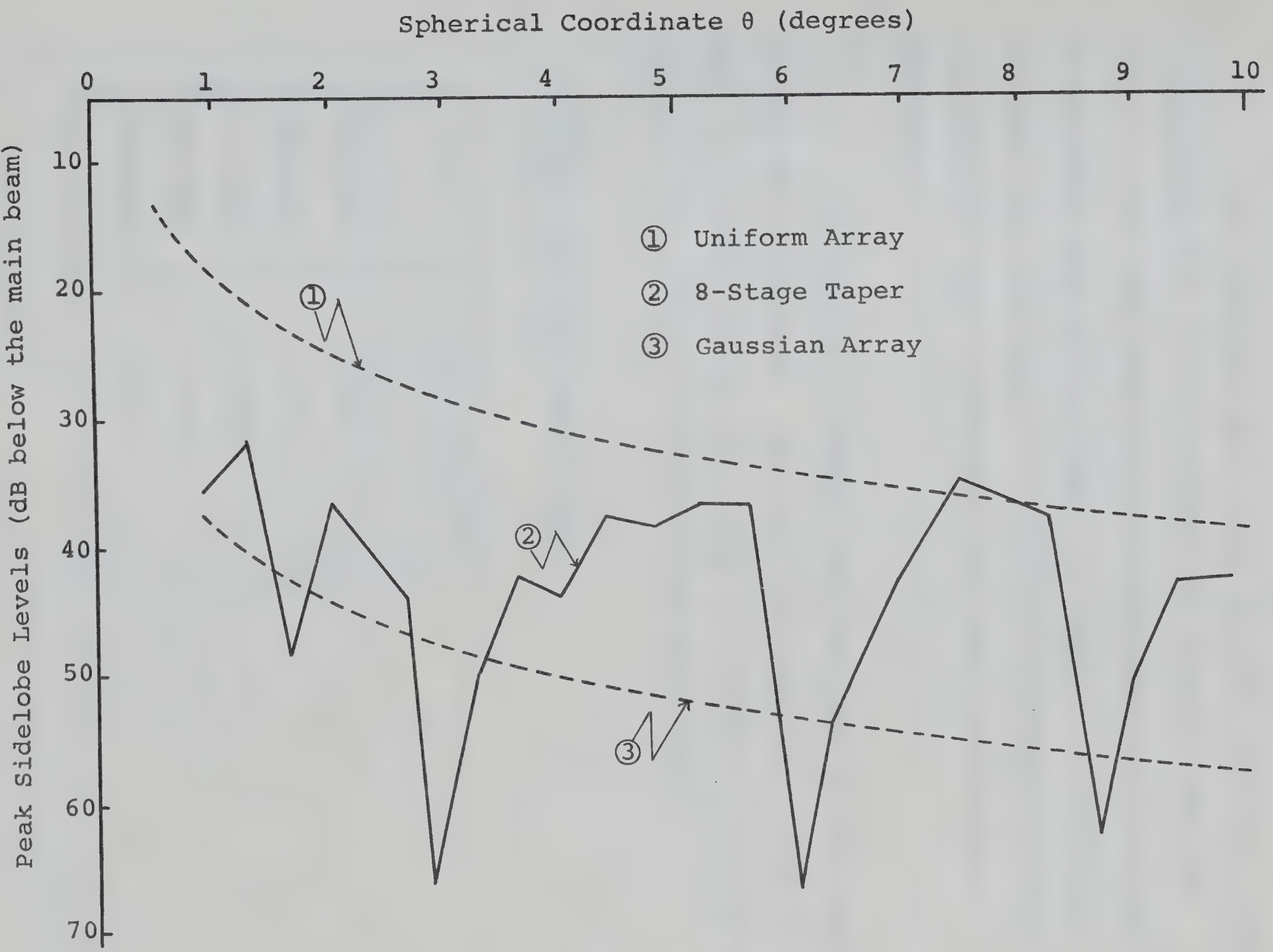

Figure 3.8c. Peak Sidelobe Levels near the Main Beam for the Array with 8 Stages of Tapering.

just touch the smooth curve through the peak sidelobe levels of the array with a uniform excitation distribution.

The frequency with which the peak sidelobe levels of the array with coarse tapering are greater than the levels of the array with uniform excitation were measured. It was found that as the number of stages of tapering was increased the frequency at which large sidelobes occurred was reduced. Hence, increasing the taper reduces more sidelobes.

The average sidelobe level for each of the array systems was calculated. The results, which are given in Table 3.2, show that as the number of stages of tapering is increased the average sidelobe level is reduced.

Table 3.2.
Average Sidelobe Levels close to the Main Beam.

Taper	Average Sidelobe Level (dB)
Uniform	-31.5
2-stage	-36.1
4-stage	-38.2
8-stage	-42.1
Gaussian	-51.4

CHAPTER 4

ANALYSIS OF TWO-DIMENSIONAL ARRAYS

4.1 Introduction

The array factors of several one-dimensional arrays were examined in Chapter 3. These also could be considered as two-dimensional arrays with constant array factors in their transverse planes. If a number of identical one-dimensional arrays are placed side by side to form a two-dimensional array then the resulting array factor will be the product of two orthogonal one-dimensional array factors as indicated in equation 2-52. If the one-dimensional arrays are not identical then the array must be broken up into sub-arrays where the one-dimensional arrays used in the sub-arrays are identical. The array factor for this type of array may be found by using equation 2-56.

The physical layout of the elements of all the arrays to be discussed in this chapter will follow either the arrangment of an 8 element wide rectangular array shown in Figure 4.1a or of an 8 element wide array with four stages of physical tapering shown in Figure 4.1b. It should be noted that it is possible, by a suitable choice of the excitation distribution, to design several different array systems combining both physical and resistive tapering such that the array factors in the principle plane are identical for each system.

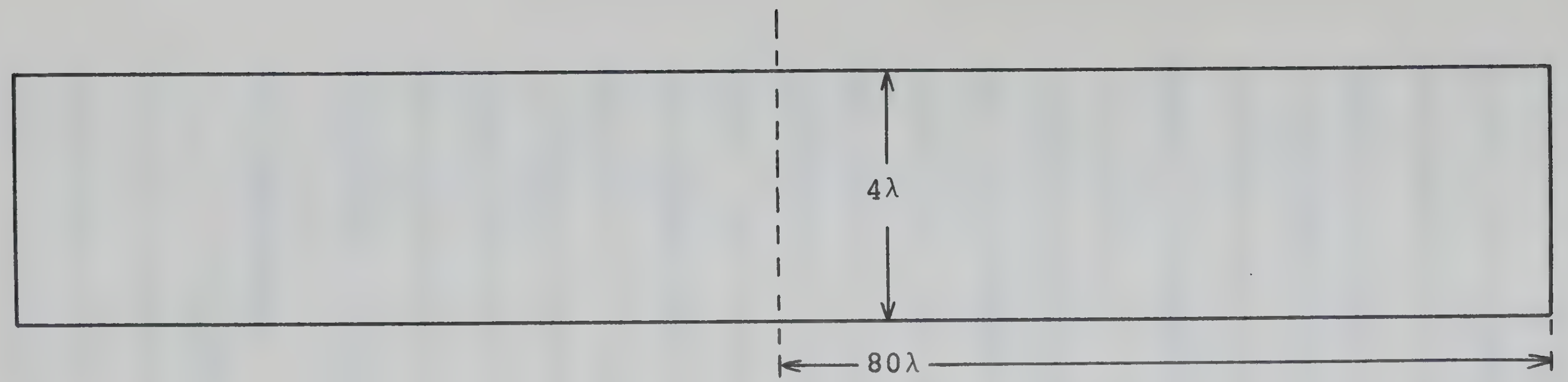

Figure 4.1a. Arrangement of the Elements in the Rectangular Arrays.

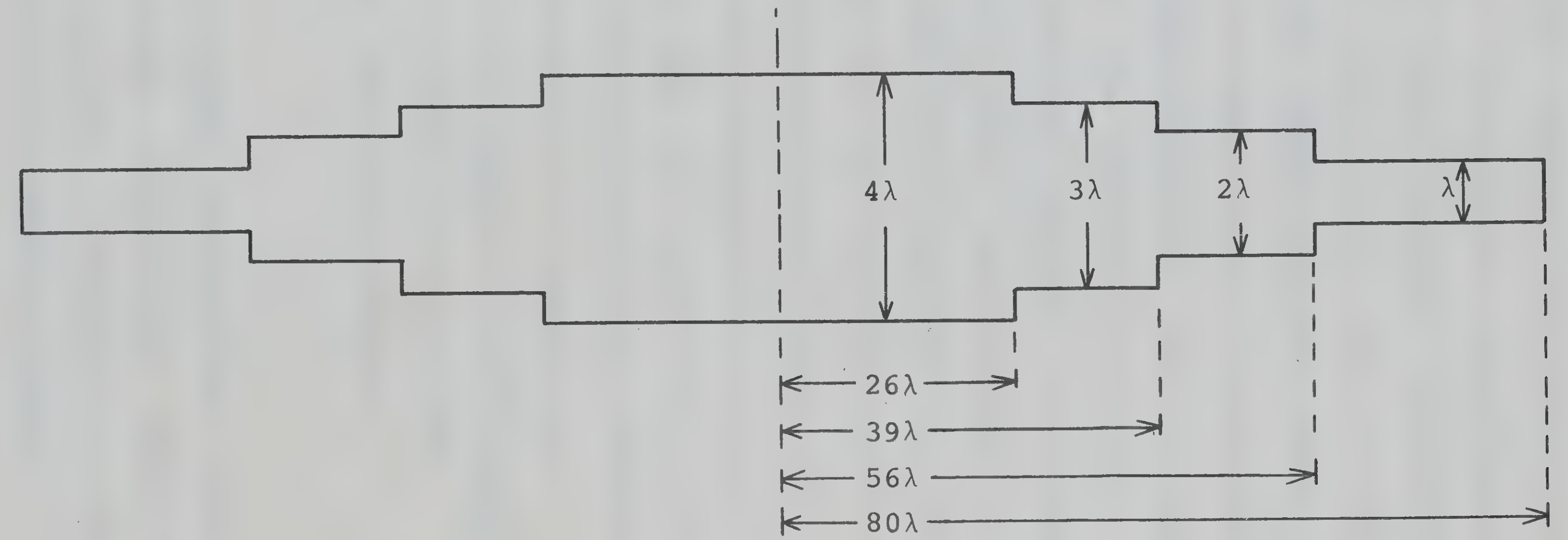

Figure 4.1b. Arrangement of the Elements in the Physically Tapered Arrays.

The arrangment of the elements and the excitation distribution of the arrays are symmetric about both X and Y so that it is only necessary to examine the array factor in one quadrant of K-space. In order to achieve a reasonable degree of resolution and to insure that no large sidelobes are missed, it is necessary to compute the array factor at approximately 10^6 points in K-space. A very considerable amount of computing is obviously required. The final output is arrived at in two stages. One quadrant of K-space, defined in the region $0 \leq K_x \leq 2\pi/\lambda$ and $0 \leq K_y \leq 2\pi/\lambda$, is divided up into 32 incriments along the K_x and K_y axes as shown in Figure 4.2. In turn this gives 1024 equal sections. The peak value of the array factor in each section, which also represents the peak sidelobe level in that section, is found. The section of K-space representing real space is now divided into 120 blocks along the θ and ϕ axes. For θ less than 30 degrees there are 60 of the latter blocks where each block represents a change in θ of 5 degrees and a change in ϕ of 10 degrees. For θ greater than 30 degrees there are also 60 blocks but in this case each block represents a change in both θ and ϕ of 10 degrees.

4.2 Excitation

The array factor of four two-dimensional arrays will be examined in this chapter. The physical layout and excitations of the arrays are shown in Figures 4.3a through 4.3d. For convenience they will be named as follows

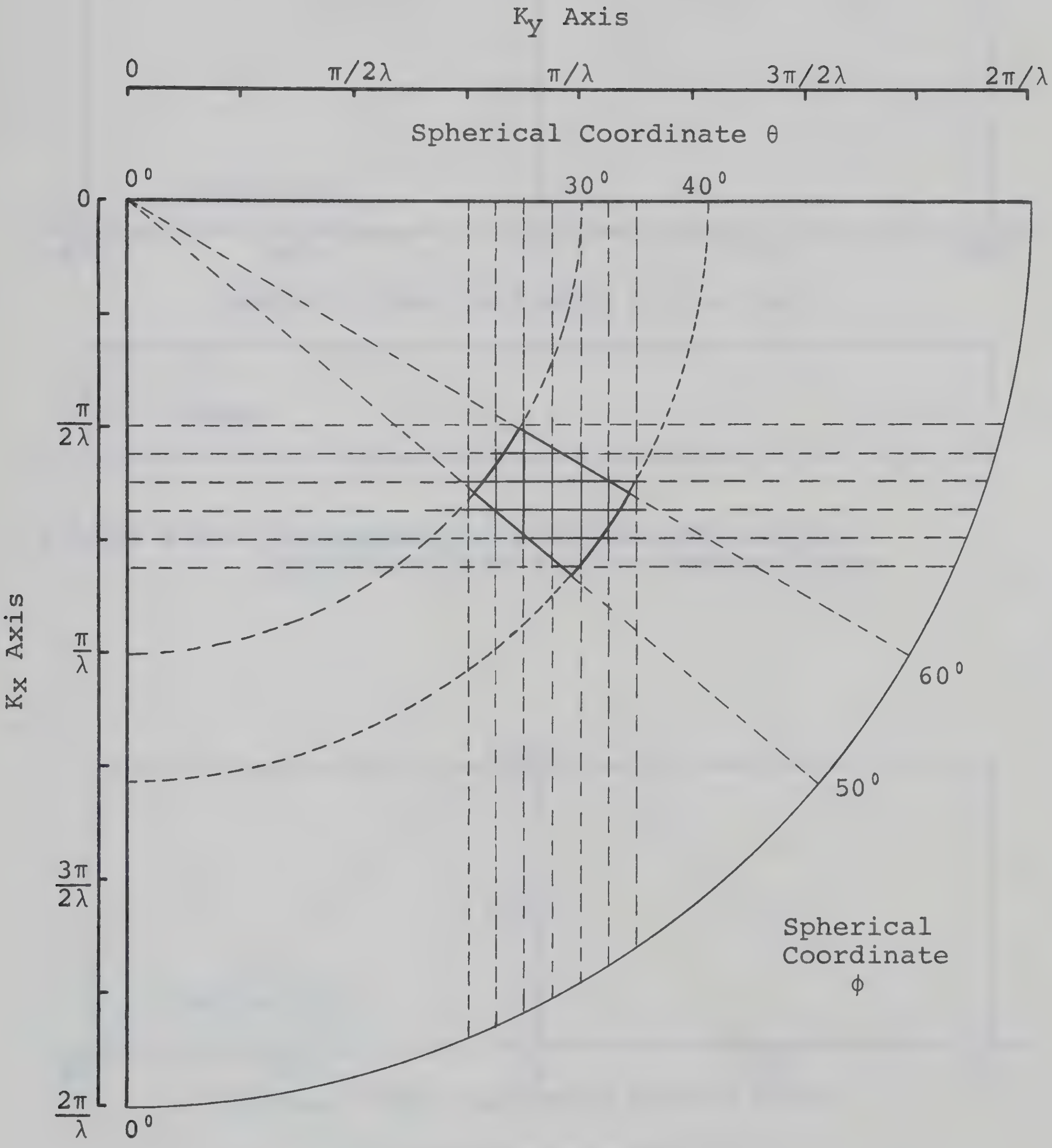

Figure 4.2 Block Representation of K-space.

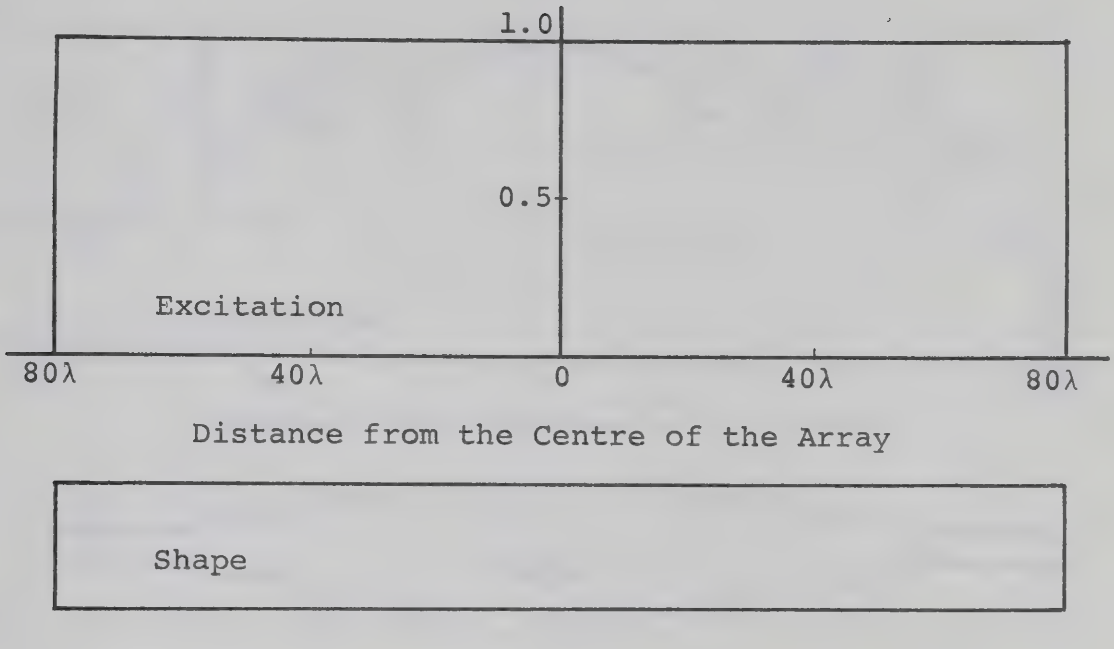

Figure 4.3a. Arrangement of the Elements and the Excitation Data for the Uniform Array.

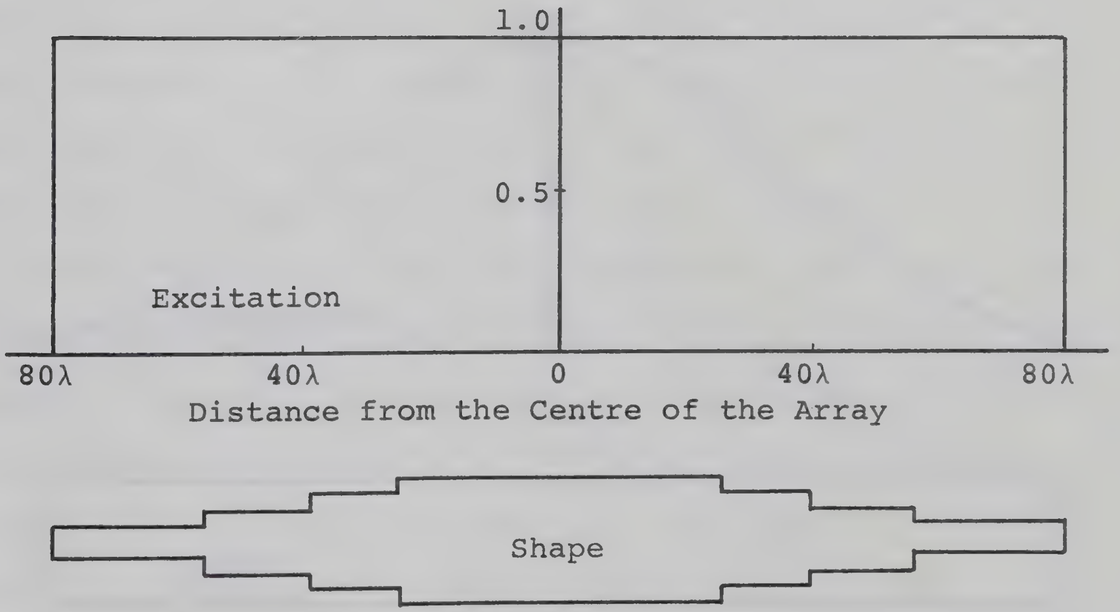

Figure 4.3b. Arrangement of the Elements and the Excitation Data for the Physically Tapered Array.

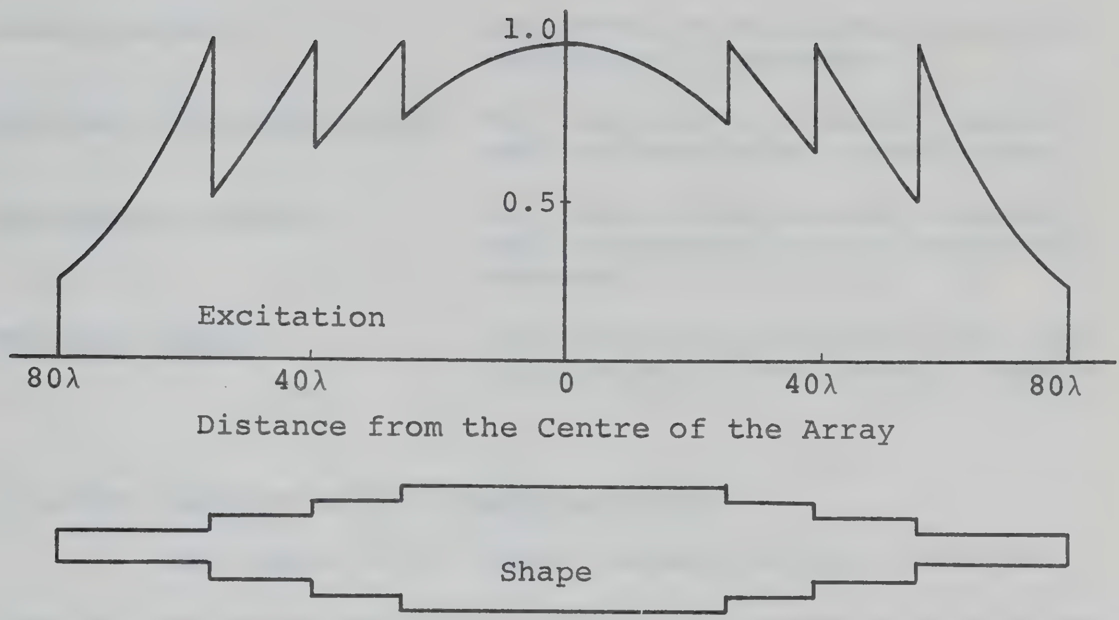

Figure 4.3c. Arrangement of the Elements and the Excitation Data for the Combination Array.

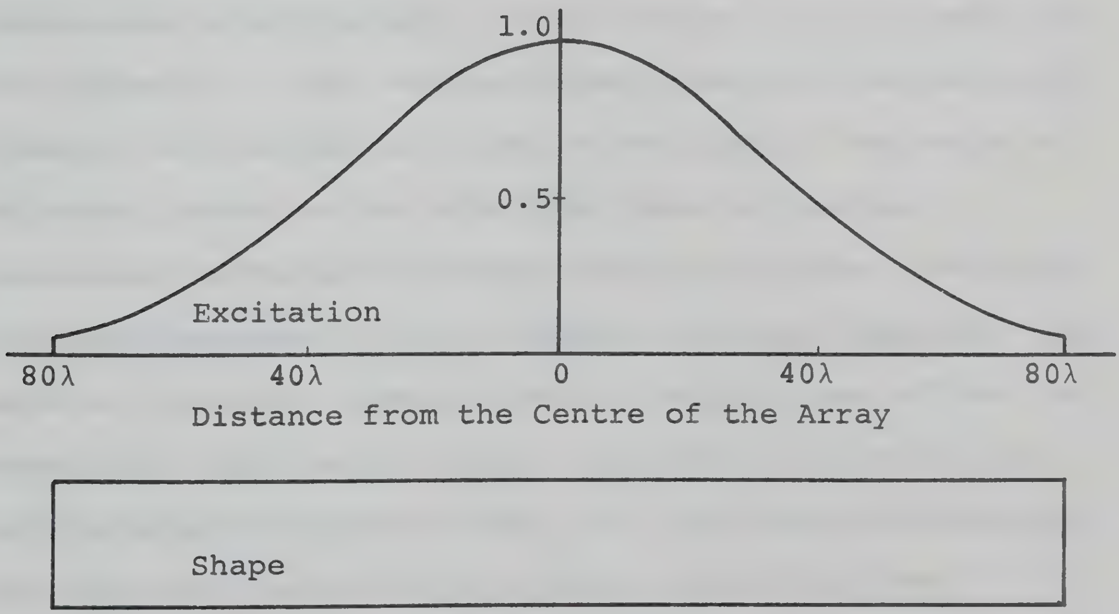

Figure 4.3d. Arrangement of the Elements and the Excitation Data for the Gaussian Array.

Uniform Array:	The shape is rectangular and the excitation is uniform.
Physically Tapered Array:	The shape is physically tapered and the excitation is uniform.
Combination Array:	The shape is physically tapered and the excitation is resistively tapered.
Gaussian Array:	The shape is rectangular and the excitation is resistively tapered

4.3 Array Factors in the Principle Plane

The shape of the array factors in the principle plane of the two-dimensicnal uniform and Gaussian arrays are respectively identical to those of the one-dimensional uniform and Gaussian arrays, as can be seen by setting P_x to zero in equation 2-52. The level of the two-dimensional array factors is 9 dB greater than the level of the one-dimensional array factors. This increase is the result of the increase, in the two-dimensional case, of the number of elements to 8 across the width of the array. The shape of the array factor in the principle plane of the two-dimensional physically tapered array is the same as that of the one-dimensional array with four stages of tapering. The shape of the array factor in the principle plane of the two-dimensional combination array is the same as that of the one-dimensional Gaussian array. In both cases the levels of the array factors of the physically tapered and the combination arrays are 9 dB higher than the levels of the corresponding one-dimensional arrays.

The shape of the array factor in the transverse plane depends on the amount of tapering that exists along the transverse axis. For a single line of dipoles the array factor in the transverse plane is constant. For a two-dimensional array made up of identical one-dimensional arrays placed side by side, such as the two-dimensional uniform and Gaussian arrays, the effective excitation along the transverse axis is constant as shown in Figure 4.4a. The array factor in the transverse plane for both of these arrays is shown in Figure 4.5a. The effective excitations shown in Figures 4.4a through 4.4c are found by summing C_{mn} over all n at each value of m.

The effective excitation along the transverse axis for the two-dimensional physically tapered and combination arrays are shown in Figures 4.4b and 4.4c respectively. The array factors in the transverse plane for these arrays are shown in Figures 4.5b and 4.5c respectively. They show a significant increase in the beamwidth and decrease in the sidelobe levels compared to those of the uniform or Gaussian arrays. The precise value of the decrease in the sidelobe level is not important. It will be shown in the next section that the sidelobes closest to the transverse plane for both the physically tapered and the combination arrays are not necessarily the greatest for arbitrary values of θ greater than 30 degrees, however, they are in general lower than the sidelobe levels of the uniform or Gaussian array in the same region.

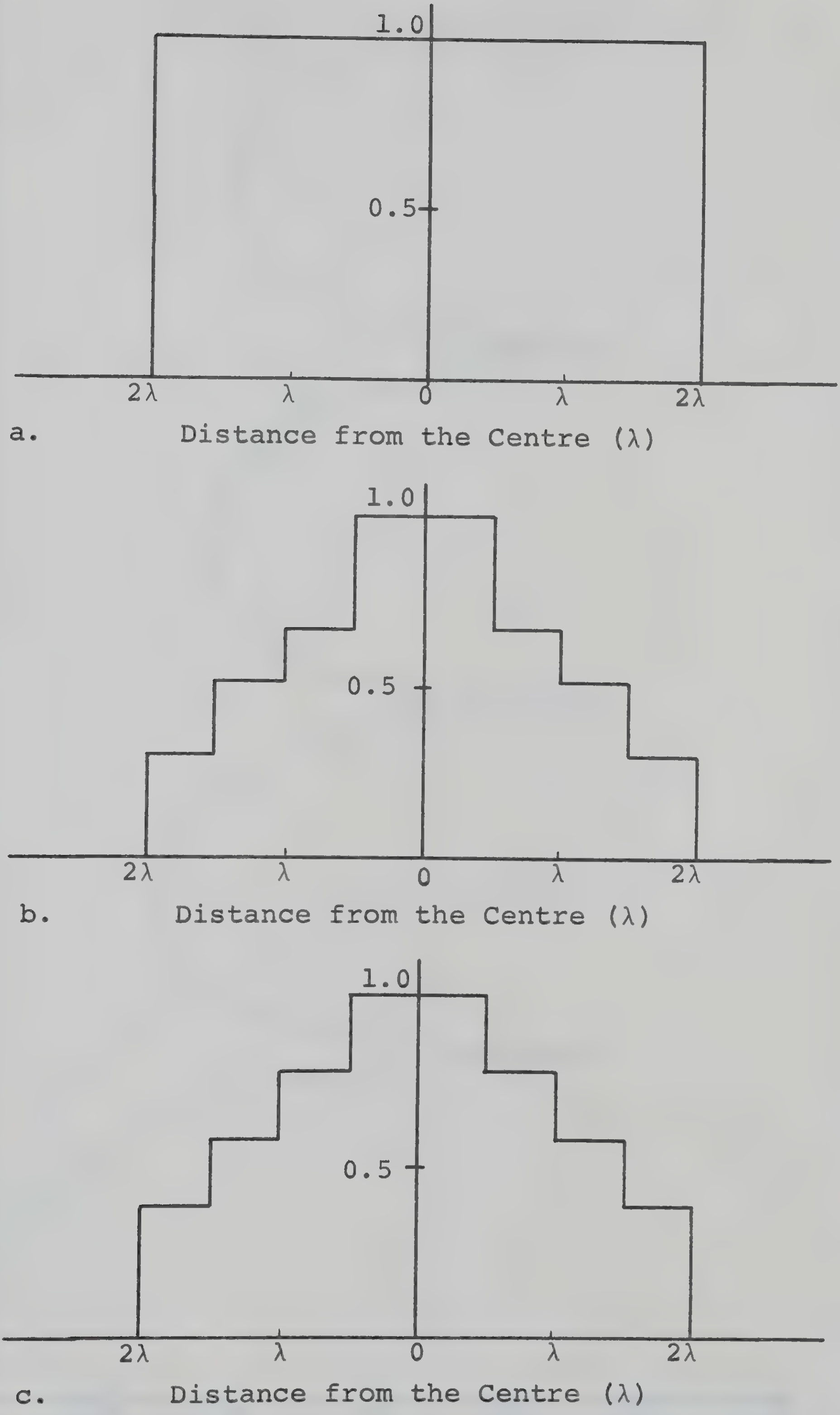

Figure 4.4. Effective Excitation in the Transverse Plane.
a) Uniform and Gaussian Arrays.
b) Physically Tapered Array.
c) Combination Array.

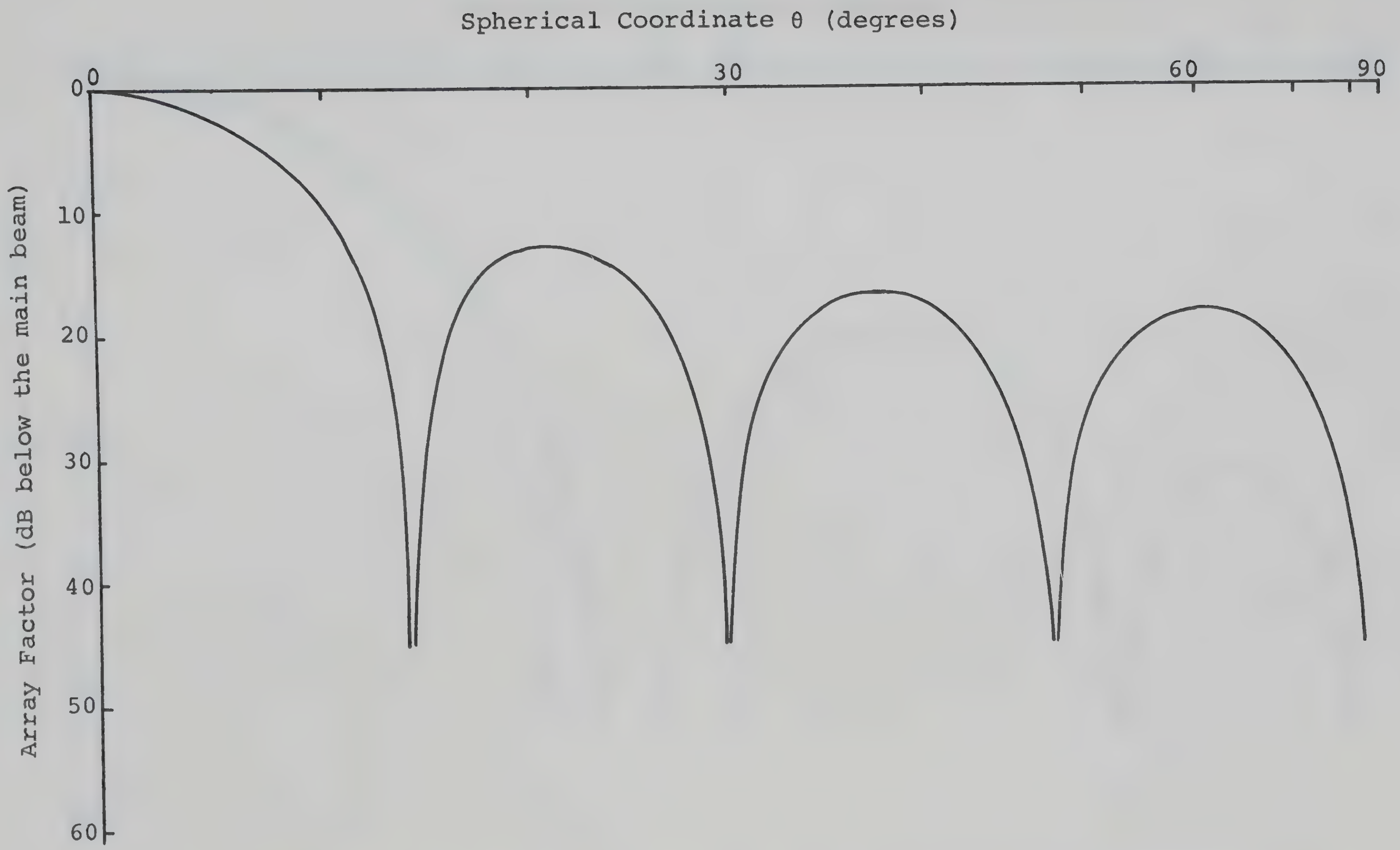

Figure 4.5a. Array Factor in the Transverse Plane for the Uniform and Gaussian Arrays.

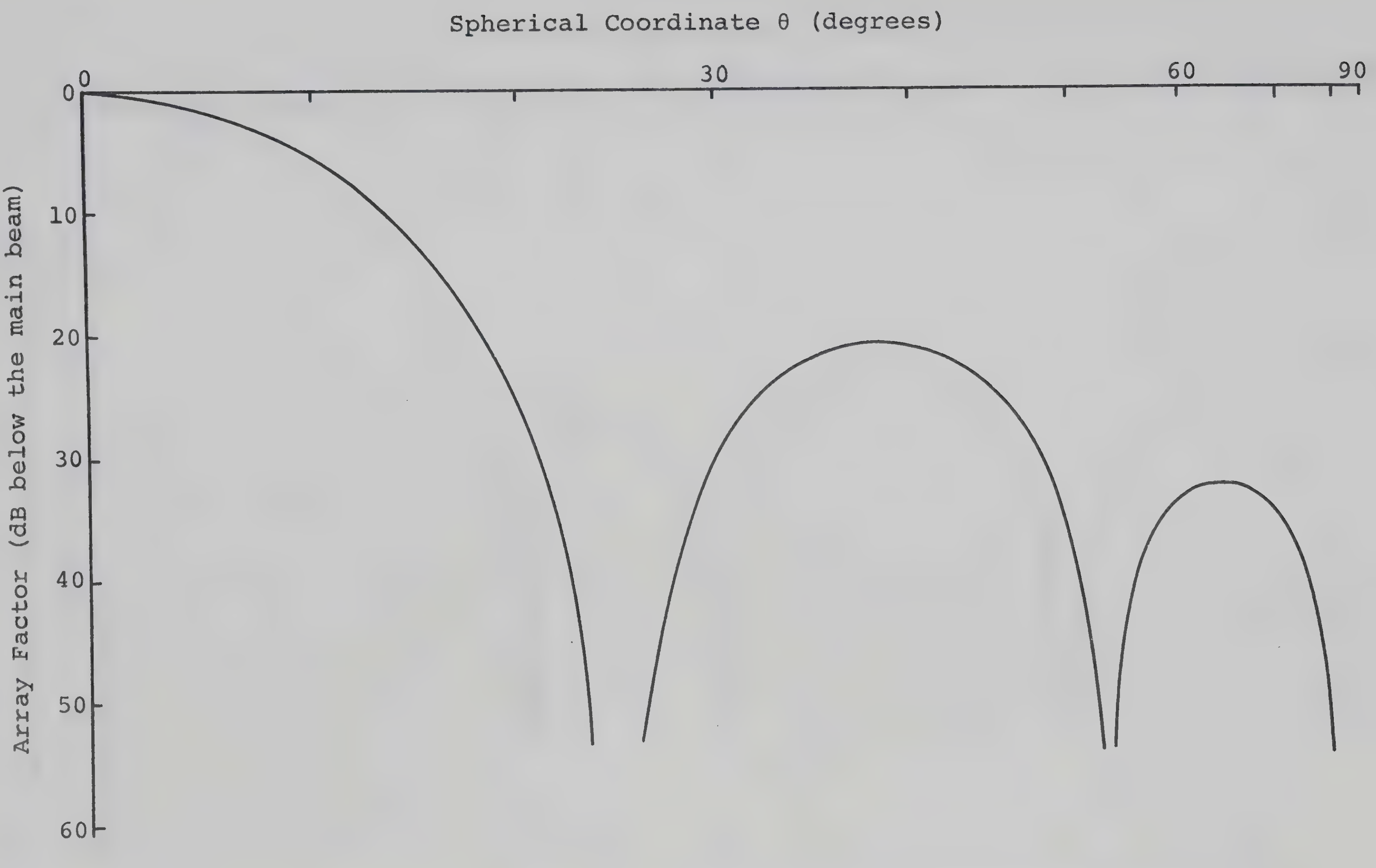

Figure 4.5b. Array Factor in the Transverse Plane for the Physically Tapered Array.

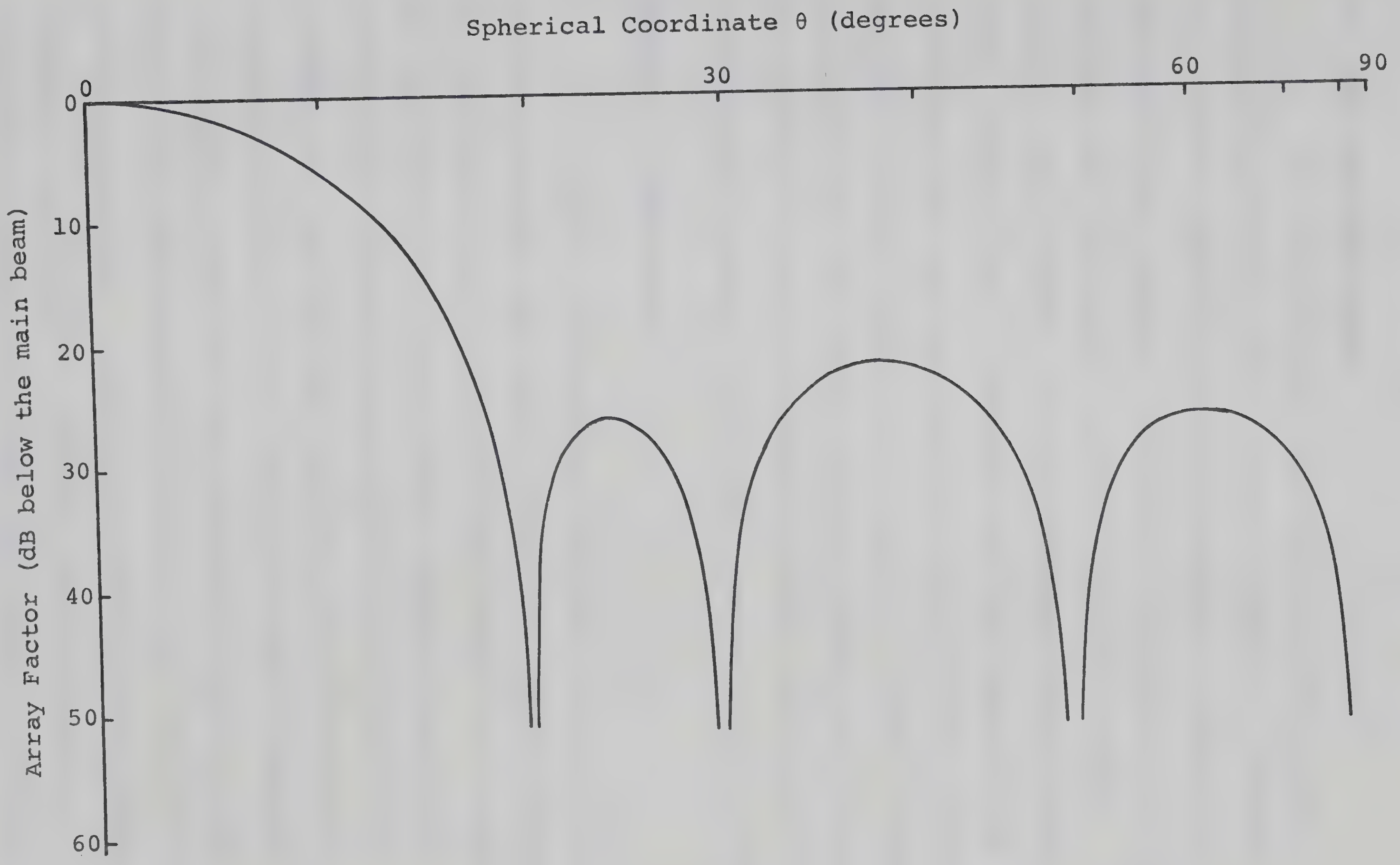

Figure 4.5c. Array Factor in the Transverse Plane for the Combination Array.

4.4 Peak Sidelobe Levels

The peak sidelobe levels for the four arrays described in Section 4.2 are given in Tables 4.1 through 4.4. For the purpose of making comparisons between the different array systems a quadrant of the sky will be divided into five regions as indicated in the tables. Region 1 ($\theta \leq 5$, $0 \leq \phi \leq 90$) represents the area close to main beam. Regions 2 and 3 represent the areas close to the principle plane and the transverse plane ($80 \leq \phi \leq 90$, $5 \leq \theta \leq 90$ and $\phi \leq 10$, $5 < \theta \leq 90$) respectively. Region 4 ($5 < \theta \leq 30$, $10 < \phi < 80$) represents the area off the principle planes for θ less than 30 degrees and Region 5 ($30 < \theta \leq 90$, $10 < \phi < 80$) represents the area off the principle planes for θ greater than 30 degrees.

Region 1. Main Beam.

Region 1 contains the main beam. In the tables the main beam has been suppressed and the entries represent, for each array, the largest sidelobe found in the region. In the case of the uniform and the Gaussian arrays this sidelobe is the first sidelobe in the principle plane; however, for the physically tapered or the combination arrays the location of the largest sidelobe is unknown. The relationship between the array factors in the principle plane of the two-dimensional arrays and the array factors of the one-dimensional arrays was indicated in the previous section. The analysis of the main beams of the one-dimensional arrays with uniform and Gaussian excitation

Spherical Coordinate Ø (degrees)

Spherical Coordinate θ (degrees)	0–10	10–20	20–30	30–40	40–50	50–60	60–70	70–80	80–90
0–5	Maximum Sidelobe Level: 13.3 dB.								
5–10	2.1	28.6	26.8	25.6	31.3	30.6	34.0	36.4	33.7
10–15	10.3	31.2	36.8	37.6	40.0	38.2	38.9	38.2	39.5
15–20	13.0	43.4	48.4	53.1	46.0	44.7	44.0	42.1	41.9
20–25	12.8	43.2	48.9	52.5	56.5	49.3	47.6	45.3	44.4
25–30	17.1	44.6	51.0	53.6	55.8	59.1	51.6	46.6	45.9
30–40	16.4	50.2	57.7	57.1	56.6	58.7	57.1	49.3	47.2
40–50	17.4	52.6	57.2	60.9	63.8	60.1	60.9	52.4	48.8
50–60	17.9	56.5	63.6	62.2	63.6	61.8	61.9	53.3	49.6
60–70	17.9	55.9	61.6	65.0	64.7	66.0	62.4	56.4	50.0
70–80	21.0	58.2	61.6	65.3	65.5	65.7	62.8	56.5	50.1
80–90	26.4	62.9	63.1	66.1	66.7	65.9	62.8	64.7	50.3

Table 4.1. Peak Sidelobe Levels in dB Below the Main Beam. Uniform Array. No Errors.

Spherical Coordinate Ø (degrees)

Spherical Coordinate θ (degrees)	0–10	10–20	20–30	30–40	40–50	50–60	60–70	70–80	80–90
0–5	Maximum Sidelobe Level: 25.5 dB.								
5–10	1.3	29.9	30.2	29.6	30.4	29.6	34.4	33.7	33.5
10–15	5.7	29.7	33.9	36.9	37.3	35.5	38.2	37.5	39.2
15–20	11.0	30.4	38.1	39.8	40.5	43.2	42.5	41.5	40.7
20–25	12.9	31.5	37.9	39.8	42.3	43.2	46.1	44.3	42.5
25–30	15.8	32.4	39.2	42.8	42.3	45.2	46.9	43.4	42.7
30–40	18.2	34.5	42.8	43.4	44.9	47.6	47.4	47.9	46.8
40–50	20.3	37.3	42.5	45.7	46.3	48.4	47.7	49.7	46.3
50–60	23.1	40.3	43.7	46.7	47.9	48.0	49.8	49.7	46.0
60–70	24.1	40.6	43.7	47.3	49.2	49.3	49.7	50.0	46.8
70–80	28.4	45.5	44.7	47.1	49.7	49.8	49.9	50.3	48.8
80–90	33.8	48.4	47.9	51.4	50.5	50.3	50.5	51.7	49.0

Table 4.2. Peak Sidelobe Levels in dB Below the Main Beam. Physically Tapered Array. No Errors.

Spherical Coordinate Ø (degrees)

Spherical Coordinate θ (degrees)	0–10	10–20	20–30	30–40	40–50	50–60	60–70	70–80	80–90
0–5	Maximum Sidelobe Level: 34.9 dB.								
5–10	1.5	36.8	35.6	38.3	41.3	44.9	48.9	52.1	52.7
10–15	6.3	31.4	32.3	39.5	43.2	45.8	48.8	52.9	57.6
15–20	12.6	30.9	37.9	38.5	43.0	45.6	48.0	53.5	57.0
20–25	14.0	31.5	37.9	41.9	43.1	44.3	46.0	51.9	58.8
25–30	17.2	33.9	40.0	44.1	44.4	44.6	47.5	52.5	58.0
30–40	19.6	36.0	43.1	44.7	45.0	46.9	48.2	50.9	58.4
40–50	21.6	38.5	43.7	46.3	47.7	49.5	49.5	50.8	56.5
50–60	23.7	40.2	44.1	48.1	49.3	49.3	50.3	50.4	57.2
60–70	24.7	40.3	44.0	47.2	50.0	50.2	49.5	49.4	54.1
70–80	28.1	45.4	45.0	48.0	51.1	51.1	50.8	51.7	57.0
80–90	33.4	48.7	47.7	51.2	51.8	52.0	52.4	53.3	56.3

Table 4.3. Peak Sidelobe Levels in dB Below the Main Beam. Combination Array. No Errors.

Spherical Coordinate ø (degrees)

Spherical Coordinate θ (degrees)	0–10	10–20	20–30	30–40	40–50	50–60	60–70	70–80	80–90
0–5	Maximum Sidelobe Level: 40.8 dB.								
5–10	2.1	48.0	46.2	45.1	50.8	50.1	53.2	55.6	52.9
10–15	10.3	50.6	56.3	56.8	59.2	57.4	58.0	57.3	58.7
15–20	13.0	62.9	67.6	72.3	65.1	63.8	63.1	61.2	61.0
20–25	12.8	62.7	68.2	71.7	75.6	68.4	66.7	64.4	63.5
25–30	17.1	64.1	70.1	72.7	74.9	78.1	70.6	65.7	65.0
30–40	16.4	69.4	76.8	76.2	75.7	77.8	76.1	68.3	66.2
40–50	17.4	71.8	76.3	79.9	82.9	79.2	80.0	71.5	67.9
50–60	17.9	75.7	82.7	81.2	82.7	80.8	80.9	72.4	68.7
60–70	17.9	75.0	80.7	84.1	83.8	85.0	81.5	75.4	69.0
70–80	21.0	77.3	80.7	84.3	84.6	84.8	81.8	75.6	69.1
80–90	26.4	82.0	82.2	85.2	85.8	85.0	81.9	83.8	69.4

Table 4.4. Peak Sidelobe Levels in dB Below the Main Beam. Gaussian Array. No Errors.

distributions and the array with four stages of tapering, considered in Section 3.3, is applicable to the arrays discussed in this chapter. For points off the principle planes but still close to the main beam equations 2-52 and 2-56 must be used to find the array factors. By examining the $F(P_x)$ terms in these equations it can be seen that for small values of P_x the dependence of the array factor on P_x is weak. It can be seen from Figures 4.5a through 4.5c that, for θ less than 5 degrees, the effects of P_x on the level of the main beam of the four two-dimensional arrays will differ by less than 1 dB. The Gaussian array has the lowest maximum sidelobe level in this region. The maximum sidelobe level of the combination array is 6 dB higher close to the transverse plane. No further analysis of this region will be made.

Region 2. Principle Plane.

In the region close to the principle plane the Gaussian array has the best sidelobe level performance. The peak sidelobe levels decrease from -52.9 dB for θ close to 5 degrees to -69.4 dB for θ close to 90 degrees. The performance of the combination array is not as good. There is little difference for small values of θ; however, for θ close to 90 degrees the peak sidelobe level is -56.3 dB. This represents an increase of 13.1 dB over the level of the Gaussian array. The performance of the uniform and the physically tapered arrays are simular to each other. The sidelobe levels go from -33.5 dB for small values of θ to

-50.3 dB for large values of θ. This represents a serious loss in the performance compared to the Gaussian or the combination arrays. For small values of θ the sidelobe levels of the uniform or the physically tapered arrays are about 20 dB higher than those of either the Gaussian or the combination arrays. For large values of θ the increase in sidelobe level is about 19 dB compared to the Gaussian array and about 6 dB compared to the combination array.

The physically tapered array has sidelobe levels up to 3.6 dB higher than those of the uniform array. As pointed out in Section 3.4 these sidelobe levels only appear higher than those of the uniform array because of the way in which the respective array factors were normalized.

Region 3. Transverse Plane.

The peak sidelobe level characteristics near the transverse plane for the two-dimensional arrays fall into two catagories. For arrays with no physical tapering, such as the uniform or the Gaussian array, the peak levels are almost identical. They also follow closely the array factor in the transverse plane, Figure 4.5a. This result may be anticipated since the array factors for these arrays may be expressed as the product of two orthogonal array factors which both show a progressive decrease in the sidelobe levels for increasing θ. The peak levels decrease from -2.1 dB for small values of θ to -26.4 dB for large values of θ.

For the arrays with physical tapering, such as the physically tapered array or the combination array, the peak sidelobe levels, for θ greater than about 20 degrees, are greater than the values of the array factor plotted in the transverse plane, Figures 4.5b and 4.5c, over the corresponding ranges of θ. This result indicates that for the physically tapered arrays the largest sidelobes in region 3 do not occur in the transverse plane. In general their locations are not easily predictable. Tables 4.2 and 4.3 for these arrays indicate that there is a general decrease in the peak sidelobe levels from -1.3 dB for small values of θ to -33.4 dB for large values of θ.

For θ less than 20 degrees the peak sidelobe levels of the combination array are higher than those of the Gaussian or the uniform arrays. This result is due to the increase in beamwidth in the transverse plane that accompanies physical tapering. The maximum difference of 4.0 dB occurs for θ between 10 and 15 degrees. For θ greater than 20 degrees the combination array produces the most rapid decrease in the peak sidelobe levels. The peak sidelobe levels of the combination array, for large values of θ, are about 7.0 dB lower than those of the Gaussian array.

Region 4. Near Sidelobe Levels off the Principle Planes.

In this region the Gaussian array has the lowest sidelobe levels. They vary from -45.1 dB to -72.3 dB. The

average level of the peaks is about -57.5 dB. For the combination array the peak sidelobe levels vary from -30.9 dB to -53.5 dB with the average peak level at -42.5 dB. The sidelobe levels of the combination array decrease steadily for increasing ϕ. The Gaussian array displays a similar decrease in the sidelobe levels but in addition the first zero of the array factor in the transverse plane introduces a large drop in the levels near θ equal to 20 degrees and ϕ equal to 35 degrees.

The peak sidelobe levels of the physically tapered and the uniform arrays are higher than those of the Gaussian or the combination arrays. For ϕ between 10 and 20 degrees there is little difference between the uniform or the physically tapered array and the combination array. For ϕ close to 80 degrees the peak sidelobe levels of the uniform or the physically tapered arrays are about 15.0 dB higher than those of the combination array.

Region 5. Far Sidelobe Levels off the Principle Planes.

In this region the Gaussian array has the lowest sidelobe levels. Over most of the region they are about 20 dB lower than those of the uniform array and about 30 dB lower than those of either the physically tapered or the combination arrays. They vary from -62.7 dB to -85.8 dB.

4.5 Discussion

Considering the main beam, the array factors in the principle planes and the peak sidelobe levels the

Gaussian array has the most satisfactory power pattern characteristics. The highest sidelobes that may be expected will be about 38 dB lower than the main beam. The performance of the combination array in the main beam area is almost identical to that of the Gaussian array. In the area close to the main beam the highest sidelobe levels that may be expected for the combination array are about 6 dB higher than those of the Gaussian array. Both the uniform and the physically tapered arrays have sidelobes between 15 and 25 dB higher than those of the Gaussian array. In the regions far from the main beam the Gaussian array has sidelobe levels 30 dB below the peak sidelobe levels of the combination or the physically tapered arrays and 20 dB lower than for the uniform array. It is in this region that random errors in the excitation of the elements are expected to have the greatest effects. This will be examined in the next chapter.

CHAPTER 5

EFFECTS OF RANDOM ERRORS

5.1 Introduction

The analysis of the one and two-dimensional arrays performed in the earlier chapters assumed that there would be no deviation in the construction or operation of the arrays from ideal arrays of identical elements equally spaced and having specified excitations. This situation will not occur in practice. The effects of the mutual impedances on the excitation and the gain of the elements will not be considered in this thesis. There are, however, several other sources of errors which can easily be accounted for in the calculation of the array factors.

An important source of errors is related to the construction and tuning of the arrays. The elements of the arrays may not be absolutely identical. There may be errors in the location of the elements or in the lengths of the cables joining them to the receiver. Location or cable length errors of a fraction of a percent will introduce phase errors of 1 degree or more in the excitation of the element. The processing equipment may introduce errors in the signals from the elements before they are correlated. It may be possible to compensate for or to correct some of these errors during the tuning of the array. However, the accuracy of the tuning will depend on the specifications of the equipment used.

Another source of errors is related to the physical enviroment in which the array and the processing equipment are placed. In the Northern Hemisphere ambient temperatures may vary from a low of -50 °F in the Winter to a high of about 100 °F in the Summer. In general an array would also be subjected to coatings of dust, water, snow and ice, all of which may affect its performance. Obviously, without a high degree of stability these enviromental extremes can produce significant errors in the excitation of an array.

If the errors arising from the construction, tuning or stability of the array systems are completely random they can be accounted for when computing the array factor by introducing equivalent random errors in the magnitude and phase of the excitation of the elements. It will be assumed for the analysis of the arrays in this chapter that the combined effect of all the errors can be accounted for by introducing magnitude errors in the excitation of the elements which will not exceed 0.5 dB and phase errors which will not exceed 5 degrees. The choice of these limits is based on the fact that such tolerances on the array system could be achieved in practice with careful design and construction. If the performance of the arrays is degraded to an unacceptable level by errors of these magnitudes it will be necessary to examine carefully the source of the errors and to attempt to reduce them. For a given system it would be possible to find the expected

errors by analysing the construction and tuning techniques and the specifications of the equipment used in the system or for tuning.

5.2 Generation of the Random Errors

The term in equation 2-38 representing the excitation of the elements is C_{mn}. To account for the errors C_{mn} may be redefined as follows

$$C_{mn} = Amn(1+\varepsilon_{mn})\,\mathrm{Exp}\{j\psi_{mn}\} \tag{5-1}$$

where ε_{mn} and ψ_{mn} are random variables within the limits defined by equations 5-2a and 5-2b.

$$-0.060 \leq \varepsilon_{mn} \leq 0.060 \tag{5-2a}$$

$$-0.087 \leq \psi_{mn} \leq 0.087 \tag{5-2b}$$

The calculation of the array factor will be performed on an IBM 360 so ε_{mn} and ψ_{mn} can most conveniently be generated by using the subroutine RANDU in the IBM Scientific Subroutine Package [16]. In order to see more clearly the effects of the errors, the magnitude and phase errors were applied separately. The analysis showed that magnitude errors of 0.5 dB degrades the performance of the system to almost the same extent as phase errors of 5 degrees. The effects of both of these errors on the average sidelobe levels and the peak sidelobe levels are so nearly the same that only the results of the analysis with the phase errors will be presented here.

The array factors were recomputed using four different sets of random variables. There were some large gaps between the peak sidelobe levels for any one set of random errors so that it was difficult to predict the maximum levels that may be expected in these regions. By using four sets of random errors it was found that there were sufficient data points available to predict the peak sidelobe levels in all regions of K-space. It was also possible with the additional data to assure that there were no trends in the random errors.

5.3 Effects of Errors on the One-dimensional Arrays

The five one-dimensional arrays discussed in Chapter 3 are considered here with random phase errors of 5 degrees in the excitation of the elements. The gain, beamwidth, the location of the first minimums and the peak sidelobe levels for the arrays with no excitation errors were found in Chapter 3 and will now be compared to those obtained when excitation errors are taken into account.

For all the systems the effect of the errors on the gain was less than 0.1% and the changes in beamwidth were not detectable. The only sections of the main beams to be affected by the errors were those close to the first zero where the levels were more than 40 dB lower than the level of the main beam.

To examine the effect of errors on the peak sidelobe levels it is necessary to consider the area close

to the main beam separately. Figure 5.1a shows the first 10 degrees of the array factors for the uniform and the Gaussian arrays. The solid lines represent the peak sidelobe levels found when errors were introduced into the excitation of the elements. The broken lines which represent the peak sidelobe levels for the arrays without errors are included for reference. It is apparent that the effect of the errors on both systems has been to increase the sidelobe levels. In the case of the uniform array the difference is small for θ less than 4 degrees and increaes slowly beyond this point. In the case of the Gaussian array the increase starts at about 2 degrees and is much more pronounced. However, for the latter system the sidelobe levels are much lower to start with and it is to be expected that the effect of the errors is greater.

The peak sidelobe levels in the first 10 degrees of the array factors for the one-dimensional arrays with 2, 4 and 8 stages of tapering and with errors of 5 degrees in the phase of the excitations are shown in Figures 5.1b through 5.1d. For reference, the corresponding peak sidelobe levels for the arrays with no excitation errors are shown in each figure and the peak sidelobe levels for the uniform and the Gaussian arrays having no excitation errors are shown in all the figures. The effects of the errors on these arrays is the same as the effect of the errors on the uniform and the Gaussian arrays. The sidelobe levels have increased and the increase is greatest at points furthest

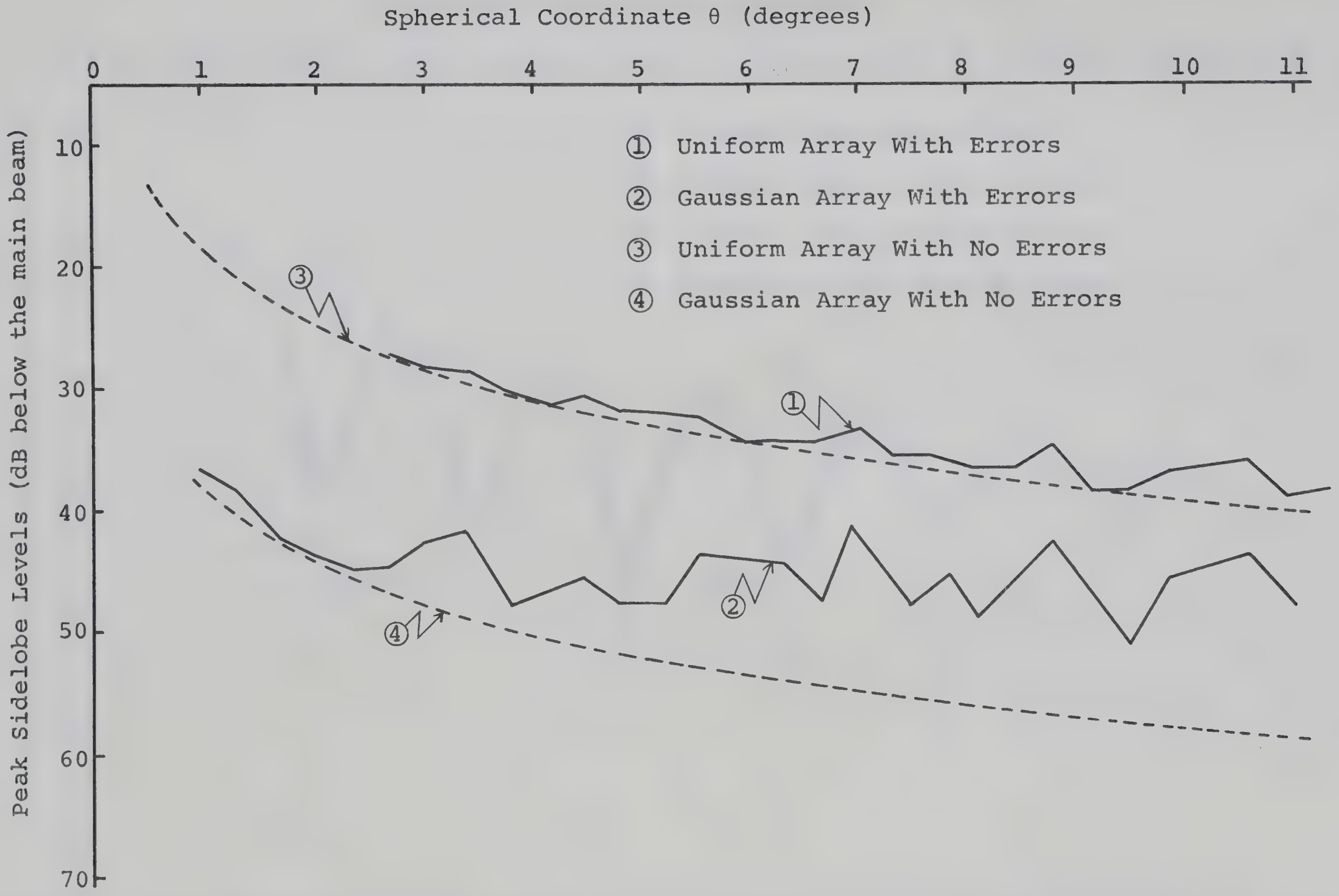

Figure 5.1a. Effects of Errors on the Array Factor of the Uniform and Gaussian Arrays.

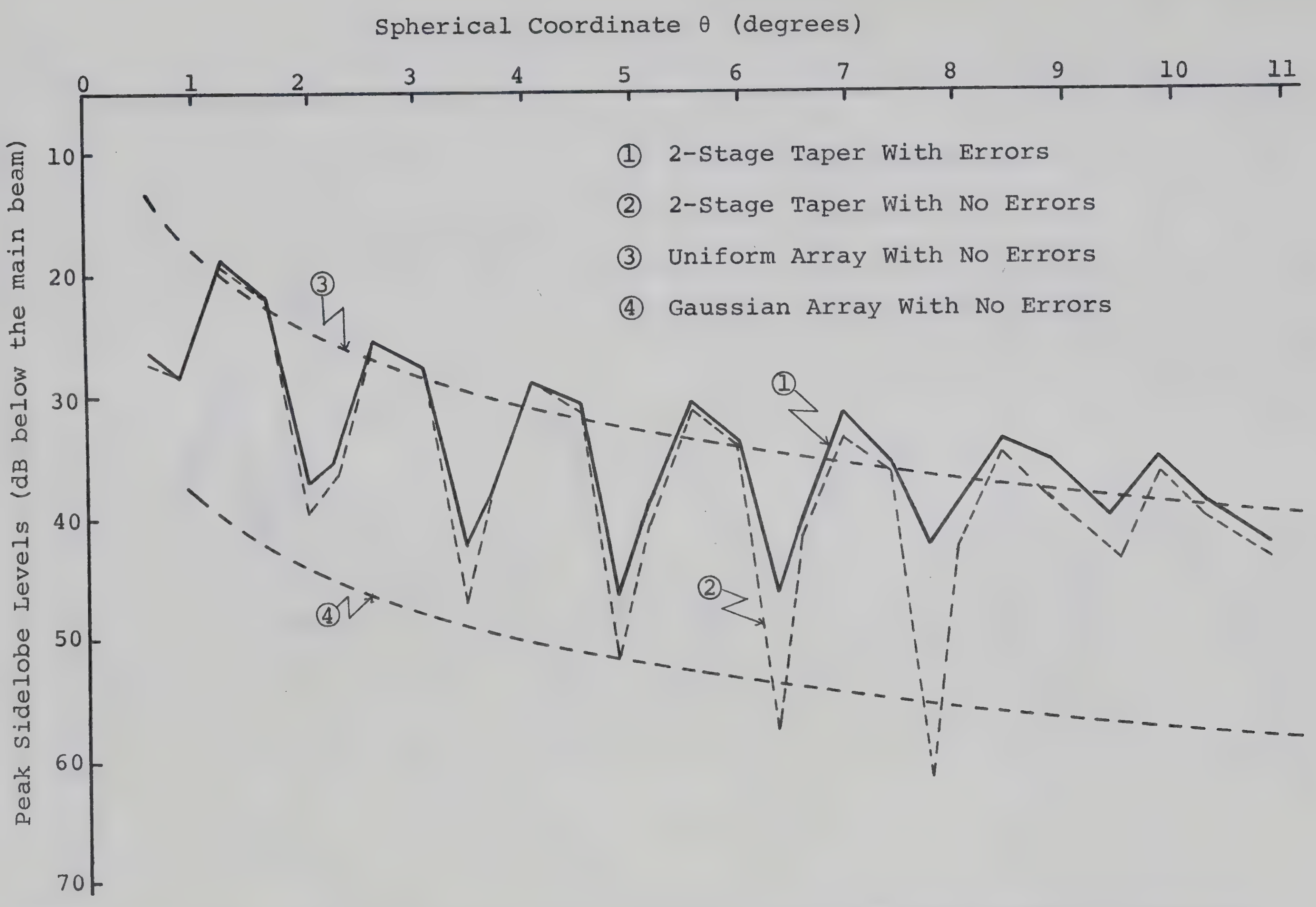

Figure 5.1b. Effects of Errors on the Array Factor Near the Main Beam of the Array with 2 Stages of Tapering.

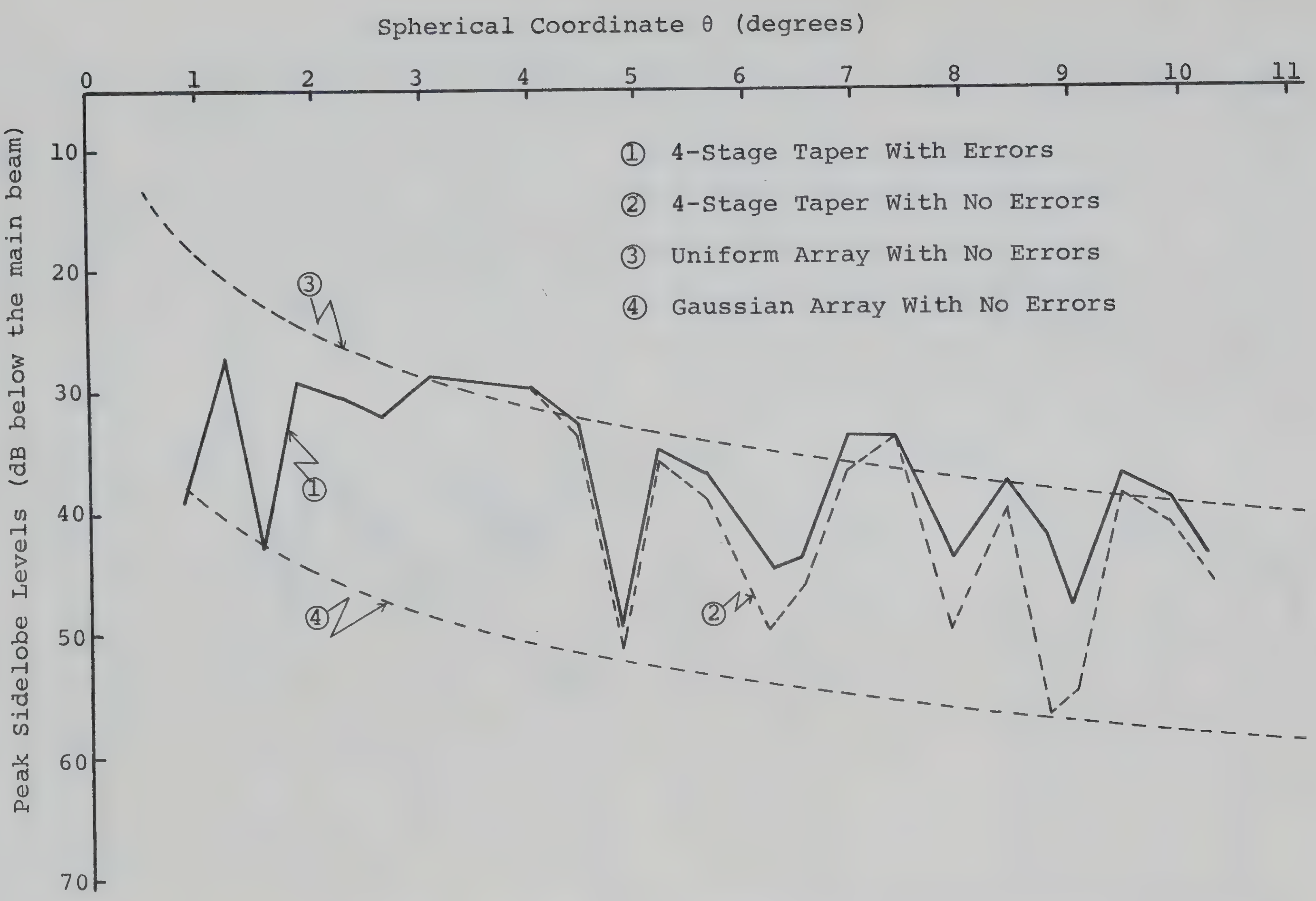

Figure 5.1c. Effects of Errors on the Array Factor Near the Main Beam of the Array with 4 Stages of Tapering.

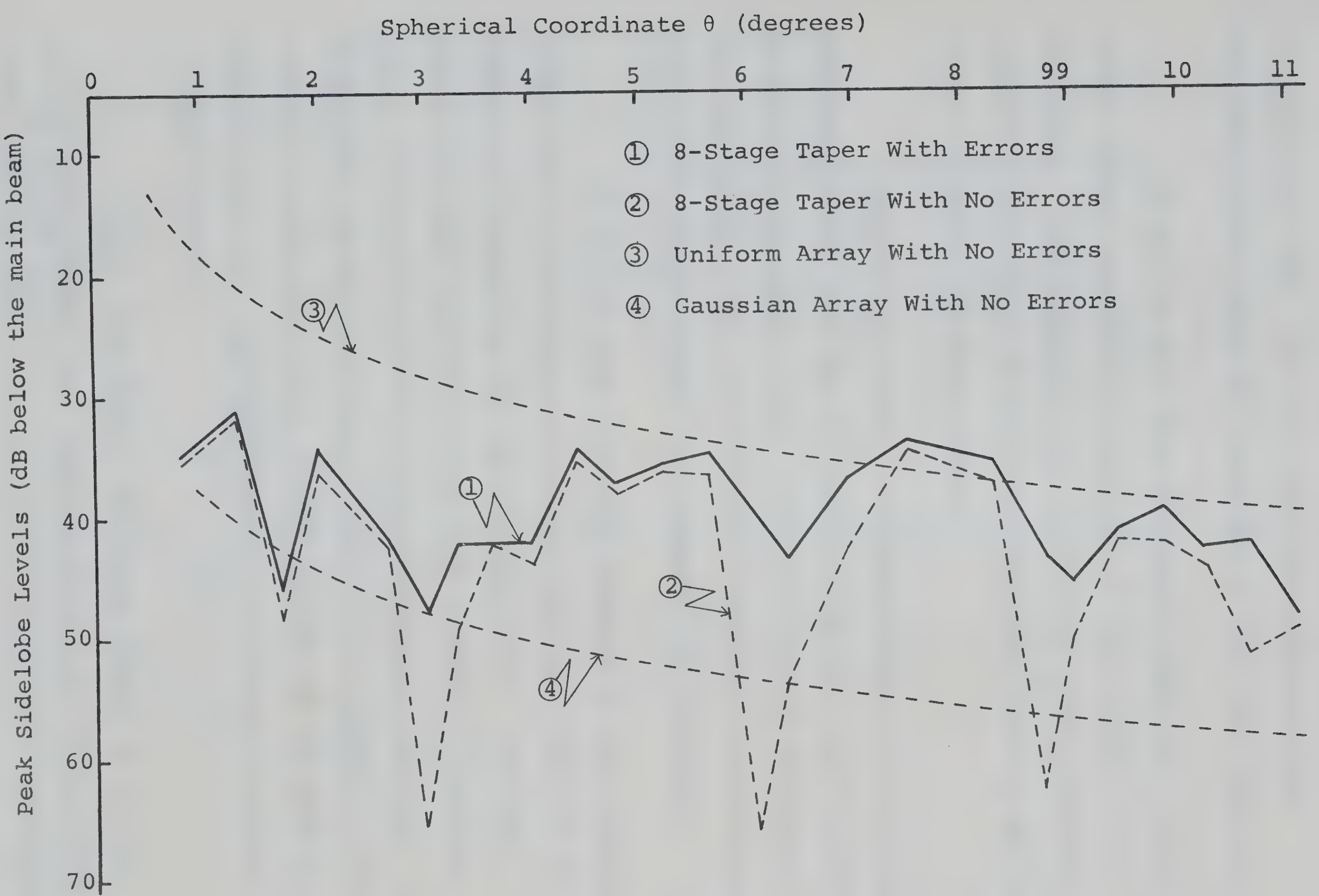

Figure 5.1d. Effects of Errors on the Array Factor Near the Main Beam on the Array with 8 Stages of Tapering.

from the main beam. In all cases the sidelobes most affected by the errors are those which were low initially.

It can be seen that the errors have very little effect on the magnitude or location of the largest sidelobes. The magnitude and location of these sidelobes depends on the sizes of the steps used for tapering and the points at which the steps occur.

Figure 5.2a shows, for large values of θ, the peak sidelobe levels that may be expected for the one-dimensional uniform and Gaussian arrays when errors in the excitation are introduced. The peak sidelobe levels of the same arrays with no excitation errors are included for reference.

It can be seen that the increase in the sidelobe levels due to the excitation error which was observed in Figure 5.1a continues for large values of θ. For both arrays the peak sidelobe levels fall towards a limiting value. The limit is -41 dB for the Gaussian array and 1 dB higher for the uniform array. When θ is 8 degrees in the case of the Gaussian array and 30 degrees in the case of the uniform array the sidelobe levels have fallen to within 1 dB of their limits.

Figure 5.2b shows, for large values of θ, the region within which peak sidelobe levels can be expected to occur for the arrays with 2, 4 and 8 stages of tapering when errors in the excitation are considered. The peak sidelobe

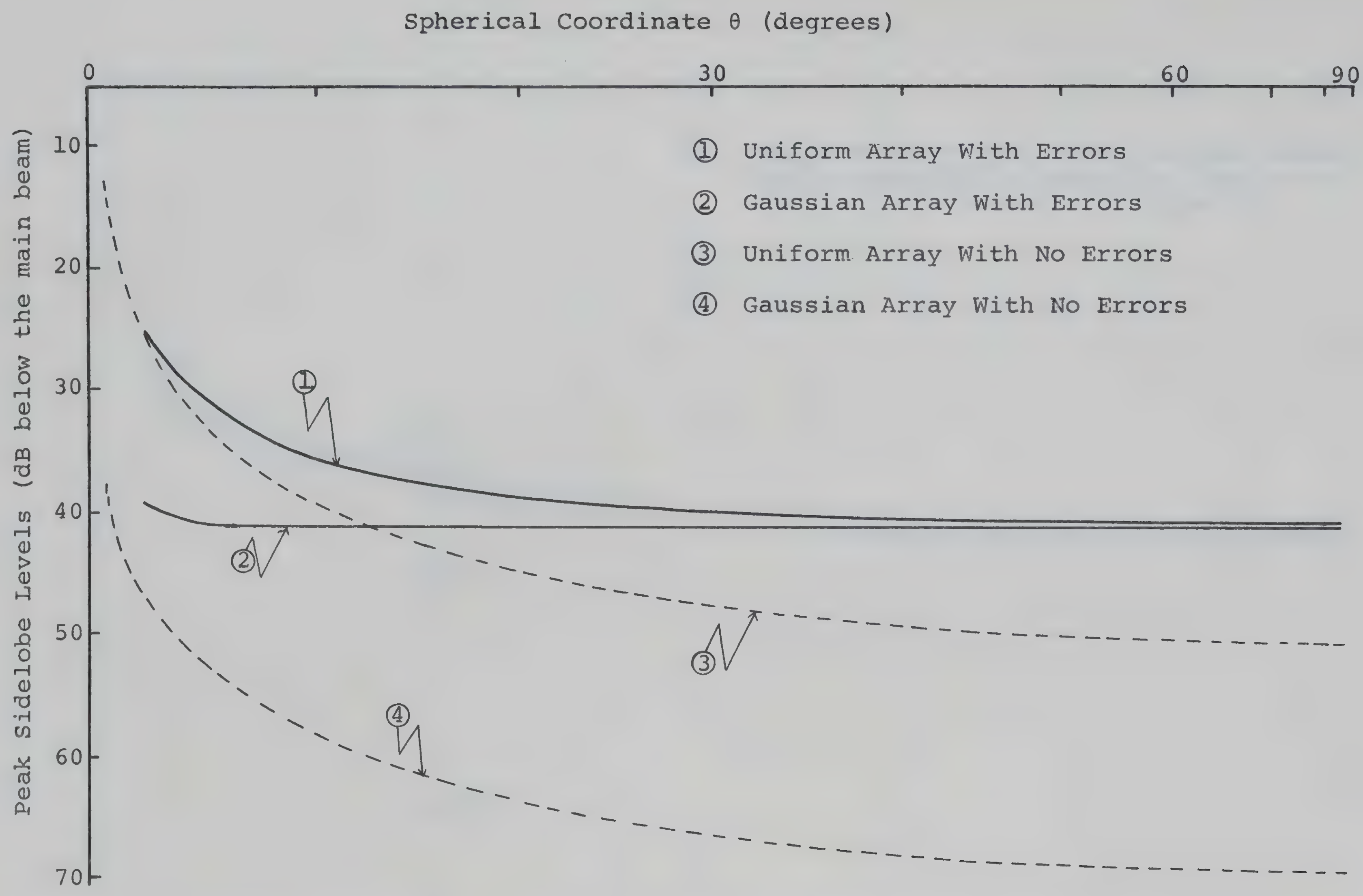

Figure 5.2a Effects of Errors on the Peak Sidelobe Levels of the Uniform and Gaussian Arrays.

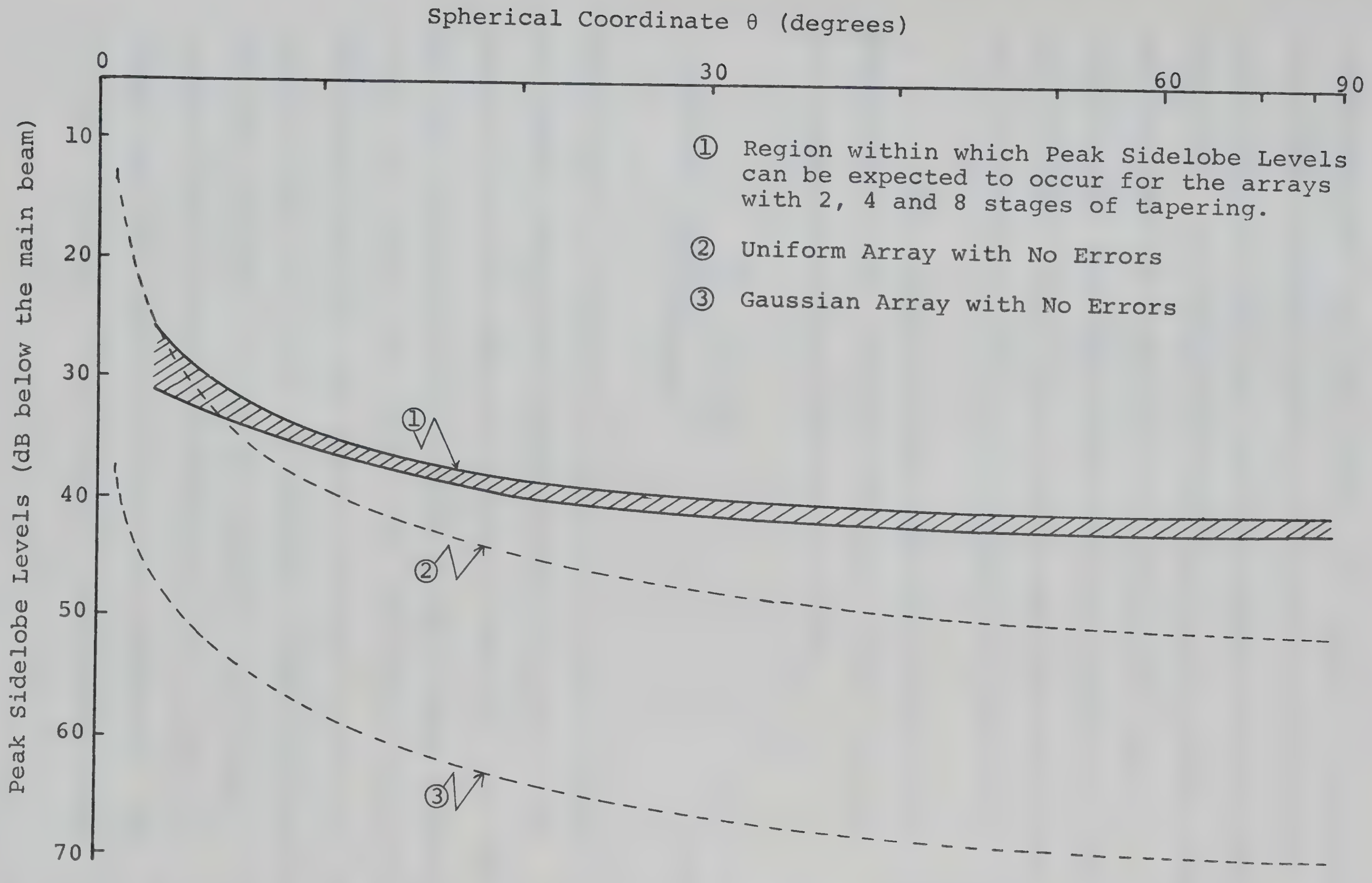

Figure 5.2b. Effects of Errors on the Peak Sidelobe Levels of the Arrays with 2, 4 and 8 Stages of Tapering.

levels expected for these systems are simular. For any one system some sidelobes should be at least as high as the lower solid line and none should be greater than the upper solid line. It can be seen that these limits follow closely the peak sidelobe levels that may be expected for the uniform array when excitation errors are considered. The peak sidelobe levels for the uniform and Gaussian arrays with no excitation errors are included for reference.

The average sidelobe level for the five one-dimensional arrays, without excitation errors and with excitation errors, were computed as follows

$$\mathrm{AF(avg)} = \frac{\int_{\theta(\mathrm{min1})}^{\pi/2} \mathrm{AF}(\theta)\,d\theta}{\pi/2 - \theta(\mathrm{min1})} \qquad (5\text{-}3)$$

where θ(min1) is the first minimum of the array factor. The results, which were normalized with respect to the levels of the main beams, are given in Table 5.1. It can be seen that the effect of the errors on the average sidelobe level is to increase the level. The increase is small for the uniform array (1.4 dB) and the increase is large for the Gaussian array (11.1 dB). An important result which can be seen from the table is that the spread in the average sidelobe levels between the different array systems is reduced when the excitation errors are considered. The array most affected by the errors is the Gaussian array.

Table 5.1.
Average Sidelobe Levels
Over all Sidelobes.

Taper	No Errors (dB)	Errors (dB)
Uniform	-45.8	-44.4
2-stage	-48.3	-45.9
4-stage	-50.7	-47.0
8-stage	-56.1	-48.4
Gaussian	-61.2	-50.3

5.4 Effects of Error on the Two-Dimensional Arrays

The effect of excitation errors on the performance of the two-dimensional arrays discussed in Chapter 4 will now be considered. As in Chapter 4 only the peak sidelobe levels will be examined. The sky will also be divided into the same five principle regions. The results of this analysis for errors of 5 degrees in the phase of the excitations are given in Tables 5.2 through 5.5.

Region 1. Main Beam.

It was indicated in the last section that excitation errors had very little effect on characteristics of the main beam of one-dimensional arrays. It is clear from that discussion and the discussion of the main beam area in Section 4.4 that for the two-dimensional array the effects of excitation errors on the main beams are small. The maximum sidelobe levels of the Gaussian, the combination

Spherical Coordinate Ø (degrees)

Spherical Coordinate θ (degrees)	0–10	10–20	20–30	30–40	40–50	50–60	60–70	70–80	80–90
0–5	Maximum Sidelobe Level: 12.9 dB.								
5–10	2.1	28.1	26.3	25.1	31.0	30.3	32.7	34.5	32.4
10–15	10.3	30.7	36.5	36.3	38.1	36.3	35.2	34.5	34.9
15–20	13.0	43.1	47.1	51.2	41.3	40.1	38.3	36.7	36.2
20–25	12.8	42.9	47.1	47.9	50.8	42.7	41.3	38.7	37.6
25–30	17.1	44.3	47.2	49.0	49.2	52.4	44.0	38.5	37.8
30–40	16.4	48.9	53.1	50.5	50.4	49.8	47.2	38.9	36.9
40–50	17.4	50.7	52.6	54.0	56.6	49.7	50.3	41.4	37.5
50–60	17.9	52.8	57.0	54.0	53.3	50.5	51.2	42.6	39.0
60–70	17.9	52.2	55.4	54.3	53.9	55.2	51.8	45.3	38.9
70–80	21.0	53.5	55.4	57.7	54.8	55.2	52.8	46.5	38.9
80–90	26.4	57.2	55.5	55.4	56.4	55.2	51.7	54.6	39.2

Table 5.2. Peak Sidelobe Levels in dB Below the Main Beam. Uniform Array. 5° Phase Errors

Spherical Coordinate Ø (degrees)

Spherical Coordinate θ (degrees)	0–10	10–20	20–30	30–40	40–50	50–60	60–70	70–80	80–90
0–5	Maximum Sidelobe Level: 22.1 dB.								
5–10	1.3	29.5	29.4	28.8	29.4	28.6	33.3	32.6	32.4
10–15	5.7	29.5	33.7	35.8	36.0	34.4	36.7	36.0	37.6
15–20	11.0	30.1	37.3	38.7	39.6	41.9	40.3	39.4	38.7
20–25	12.9	31.1	37.3	39.2	42.2	42.6	42.5	40.5	39.7
25–30	15.7	32.1	38.9	42.4	42.3	44.0	44.5	40.4	39.9
30–40	18.2	34.4	42.5	43.0	43.7	45.5	45.9	42.0	41.0
40–50	20.3	37.2	41.8	45.1	46.0	46.4	46.1	43.6	41.0
50–60	23.0	40.0	43.1	46.0	46.3	46.6	45.1	42.4	39.4
60–70	24.1	40.3	43.1	46.8	48.4	47.3	46.0	46.3	44.2
70–80	28.3	44.8	44.0	46.3	48.6	47.9	48.4	47.0	40.4
80–90	33.8	48.2	46.7	50.7	49.5	48.2	48.5	49.4	40.6

Table 5.3. Peak Sidelobe Levels in dB Below the Main Beam. Physically Tapered Array. 5° Phase Errors.

Spherical Coordinate Ø (degrees)

Spherical Coordinate θ (degrees)

θ \ Ø	0–10	10–20	20–30	30–40	40–50	50–60	60–70	70–80	80–90
0–5	Maximum Sidelobe Level: 31.2 dB.								
5–10	1.5	35.9	35.1	37.5	40.5	41.8	44.2	44.2	43.0
10–15	6.3	31.1	32.0	38.9	41.6	43.4	43.5	43.1	44.4
15–20	12.6	30.7	37.6	38.0	42.1	44.1	43.3	43.6	43.4
20–25	13.9	31.2	37.6	41.2	41.8	43.1	45.0	42.2	41.6
25–30	17.1	33.6	39.7	42.8	43.4	43.4	46.0	43.9	42.3
30–40	19.6	35.8	42.9	43.9	43.8	46.0	46.1	42.8	41.3
40–50	21.6	38.4	43.1	45.9	47.5	47.7	48.0	46.0	42.5
50–60	23.7	39.9	43.5	47.4	47.7	48.0	45.5	42.6	39.9
60–70	24.7	39.9	43.4	46.6	49.3	48.5	46.3	47.0	43.9
70–80	28.0	44.7	44.4	47.0	50.1	49.1	48.8	47.1	42.6
80–90	33.3	48.3	46.7	50.4	50.7	49.4	50.1	50.0	42.9

Table 5.4. Peak Sidelobe Levels in dB Below the Main Beam. Combination Array. 5^{0} Phase Errors.

Spherical Coordinate Ø (degrees)

Spherical Coordinate θ (degrees)	0–10	10–20	20–30	30–40	40–50	50–60	60–70	70–80	80–90
0–5	Maximum Sidelobe Level: 36.4 dB.								
5–10	2.1	39.4	37.6	36.4	36.9	36.2	37.1	38.0	35.6
10–15	10.3	42.0	42.4	40.8	41.6	37.7	36.5	35.8	38.0
15–20	13.0	49.0	51.5	52.5	44.5	42.9	35.2	34.0	33.1
20–25	12.8	48.8	48.4	49.6	47.7	39.6	39.5	37.4	36.5
25–30	17.1	50.2	48.5	45.9	46.1	51.1	41.8	37.5	35.4
30–40	16.4	52.0	52.0	47.4	48.3	48.2	46.8	38.6	36.5
40–50	17.4	52.0	49.5	51.8	54.5	49.3	48.0	37.3	33.4
50–60	17.9	54.1	53.9	51.8	52.9	47.7	46.2	40.7	36.1
60–70	17.9	51.0	53.5	53.9	49.9	50.3	48.9	41.7	35.3
70–80	21.0	51.8	53.3	55.9	49.9	53.3	48.1	42.7	36.3
80–90	26.4	54.1	53.3	55.0	53.4	53.3	49.0	50.9	36.7

Table 5.5. Peak Sidelobe Levels in dB Below the Main Beam. Gaussian Array. 5° Phase Errors.

and the physically tapered arrays have increased by about 3 dB.

Region 2. Principle Plane.

In the region close to the principle plane the combination array has the lowest sidelobe levels, which vary from -39.9 dB to -43.9 dB. The sidelobe levels of the physically tapered array are about 4 dB higher than those of the combination array over most of this region, hovever, for θ less than 10 degrees they are 10.6 dB higher. The peak sidelobe levels of the Gaussian array vary from -33.1 dB to -38.0 dB which indicates that the errors have introduced a serious degradation in the performance of this array.

Region 3. Transverse Plane.

The effect of the errors on the sidelobe levels close to the transverse plane for all the two-dimensional arrays is less than 0.1 dB.

Region 4. Near Sidelobes off the Principle Planes.

Over most of this region the performance of the Gaussian and combination arrays are similar. The largest sidelobe for the Gaussian array are at -34.0 dB and for the combination array are at -30.7 dB. The peak sidelobe levels of both the physically tapered array and the uniform array are larger than those of either the Gaussian array or the combination array. This is most clearly evident close to the main beam.

Region 5. Far Sidelobes off the Principle Planes.

In this region the peak sidelobe levels of both the Gaussian array and the uniform array vary from about -31 dB to about -51 dB while those of both the physically tapered array and the combination array vary from about -37 dB to about -57 dB. For θ close to 30 degrees the Gaussian array has the lowest sidelobe levels.

5.5 Discussion

The analysis of the effects of excitation error on the one-dimensional arrays showed that they are small close to the main beam but that they increase for large values of θ. For θ close to 90 degrees the peak sidelobe level approaches a limiting value. It can be seen that the same trend is apparent for the two-dimensional arrays; however, since the array factor in the transverse plane is not affected by the errors, the first zero of these array factors influence the sidelobe levels over much of K-space. This situation accounts for the lowest sidelobe levels in Tables 5.2 through 5.5.

Considering the overall performance of the two-dimensional arrays the Gaussian array is best in the vicinity of the main beam. The combination array has sidelobes about 6 dB higher close to the main beam. However, close to the principle plane and for θ greater than 5 degrees the performance of this array actually becomes better than the Gaussian array. This statement is also true

for the region off the principle planes and where θ is less than 30 degrees. Both the uniform array and the physically tapered array have large sidelobes close to the main beam (at least 15 dB higher than the Gaussian array). The uniform array has the highest sidelobes in all regions where θ is less than 30 degrees. The physically tapered array has the highest sidelobes in the regions off the principle planes and far from the main beam.

CHAPTER 6

SUMMARY AND CONCLUSIONS

In this thesis it was shown that the power pattern of an antenna array can be considered as the product of an array factor and a reference or element pattern. The array factor accounts for the arrangment and excitation of the elements in the array. The reference pattern depends on the shape of the elements used in the array and the position of the reflecting screen.

A technique was developed for computing the array factor of one and two-dimensional arrays which is based on the use of the fast Fourier transform. Because the number of steps involved in the calculations using this type of algorithm is small it is faster and more accurate than the usual summing techniques.

The technique was applied to the analysis of one-dimensional arrays without excitation errors. The first array to be examined had a uniform excitation distribution. Arrays with tapering in 2, 4 and 8 stages were considered. These represent coarse approximations to a Gaussian distribution. Finally, an array with a Gaussian excitation was examined. As the excitation distribution was changed from uniform through progressively better approximations to a Gaussian, the following changes in the array factor were observed.

1. the gain decreased.
2. the beamwidth increased.
3. the average sidelobe level decreased.
4. the peak sidelobe levels decreased.
5. The arrays with 2, 4 and 8 stages of tapering had sidelobe levels as much as 3 dB greater than those of the uniform array, however, the frequency with which these occurred decreased as the taper became more Gaussian.

Extension of the analysis to a two-dimensional uniform array and three progressively better approximation to a two-dimensional Gaussian array showed very little change in the array factors in the principle plane. The sidelobe levels in the transverse plane of both the physically tapered array and the combination array decreased compared to those of both the uniform and Gaussian arrays. This decrease in the sidelobe levels is due to the fact that the introduction of physical tapering in two-dimensional arrays introduces a taper along the transverse axis.

In the area close to the main beam the sidelobe performance of the Gaussian array is best. The peak sidelobe level of this array is at least 6 dB lower than that of the combination array and at least 15 dB lower than that of both the uniform and physically tapered arrays.

In the area far from the main beam the sidelobe level performance of the combination array is best. The

principle contribution to the power from this region comes from the area close to the transverse plane where the peak sidelobe levels of the combination array are lower than those of the Gaussian array by 3 dB when θ is 30 degrees and by 6 dB when θ is 90 degrees.

The effects of introducing magnitude and phase errors in the excitation of the elements were examined. In the case of the one-dimensional arrays it was found that magnitude errors of 0.5 dB and phase errors of 5 degrees produced comparable degradation in the performance of each system. The principle effect of the errors was to increase the average sidelobe level and the peak sidelobe levels. The effects of the errors on the main beam and the areas close to the main beam were small. The array most affected by the errors was the Gaussian array which initially had the lowest sidelobes levels. The most significient result to be obtained from the analysis was the reduction in the spread in the average sidelobe levels between the systems from 25.4 dB to 6 dB by the effects of the errors.

The introduction of excitation errors in the two-dimensional arrays produced severe degradation in the performance of all the arrays. As was the case for the one-dimensional arrays the effect of the errors in the area close to the main beam was small. In this region the Gaussian array is still the best. When the regions far from the main beam were examined it was found that the most

significient contribution to the power came from the area close to the transverse plane where the performance of the combination array is up to 6 dB better than that of the Gaussian array. The sidelobe level performance of both the Gaussian array and the combination array was found to be very much better than that of the uniform array or the physically tapered array.

On the basis of these results it is concluded that the performance of an array combining both physical and resistive tapering is comparable to that of an array with only resistive tapering. The performance of an array with only physical tapering would not be satisfactory due to the large sidelobes close to the main beam which would be introduced by such a taper.

If the arrays discussed in this thesis are to be used as part of a T-interferometer it would be necessary to consider the combined operation of both arms of the T. The sidelobes of the T cannot be obtained directly from the results presented in Chapter 5 as only the peak sidelobe levels were considered. If any further investigation of these types of arrays is to be conducted it would be useful to compute the average sidelobe level for the arrays in addition to the peak sidelobe levels.

BIBLIOGRAPHY

1. A Large 10 MHz Array for Radio Astronomy.
   J. A. Galt, C. R. Purton, and P. A. G. Scheur.
   Publ. Dominion Obs., Vol 25, No 10, pp295-304, 1967.

2. A Large 22MHz Array for Radio Astronomy.
   Carman H. Costain, J. David Lacey, snd Robert S. Roger.
   Trans IEEE, Antennas and Propogation Vol ap-17, No 2,
   March 1969 pp45-55.

3. T-shaped Radio Telescope with Electrical Beam Scanning
   in the 10-25 MHz Band.
   Yu. M. Bruk, et al.,
   Radio Physics and Quantum Electronics. Vov 10, No 5,
   pp608-619, 1967.

4. Experimental Study of the Multielement Antenna Array
   of the UTR-1 Radio Telescope.
   Yu. M. Bruk, et al.,
   Radio Physics and Quantum Electronics. Vol 10 No 5,
   pp28-43, 1968.

5. A Proposal for an Electronic System for the Clark
   Lake Teepee Tee. November 1970. Astronomy Programme
   University of Maryland, College Park, Maryland.

6. A High Resolution Radio Telescope for use at 3.5 MHz
   B. Y. Mills, A. G. Little, K. V. Sheriden, O. B. Slee.
   Proc IRE Vol 46, pp 67-84, 1958.

7. The 19 MHz Mills Cross and Absorbtion in Interstellar
   Gas. M. M. Komesaroff.
   Proc IRE Vol 20, pp141-147, February 1963.

8. A High Resolution Radio Telescope of a New Type.
   B. Y. Mills, A. G. Little,
   Aust. J. Phys., Vol 6, pp272-278, September 1953.

9. Site Testing for a Proposed 12 MHz Radio Telescope in
   Alberta. F. S. Chute, C. G. Englefield,
   P. J. R. Harding, C. R. James, and D. Routledge.
   Journal of the Royal Astronomical Society of Canada,
   Vol 65, NO 2.

10. Array Antennas: A New Application of an Old Technique.
    John L. Allen. IEEE Spectrum, November 1964.

11. Private Communication. Carman H. Costain.
    Dominion Radio Astrophysical Oobservatory,
    White Lake, Penticton, BC.

12. A Guided Tour of the fast Fourier Transform.
    G. D. Bergland. IEEE Spectrum, July 1969.

13. IBM System/360 Operating System: Introduction.
    Form C28-6534.

14. Time Harmonic Electromagnetic Fields.
    R. N. Harrington. McGraw-Hill Book Co. 1961.

15. The Finite Fourier Transform.
    J. W. Cooley, P. A. W. Lewis, P. D. Welch.
    IEEE Trans Vol AU-17, pp77-85, June 1969.

16. IBM System/360 Scientific Subroutine Package,
    (360a-cm-03x) Version III, Programmers Manual.

17. Antennas. John D. Kraus.
    McGraw-Hill Book Co. 1950.

APPENDIX A

Referring to figure 2.1 the expression for $|\vec{r}-\vec{r}'|$ is obtained as follows

$$X = r\mathrm{Sin}\theta\mathrm{Cos}\phi$$

$$Y = r\mathrm{Sin}\theta\mathrm{Sin}\phi$$

$$Z = r\mathrm{Cos}\theta$$

$$|\vec{r}'|^2 = (X')^2 + (Y')^2$$

$$\begin{aligned}|\vec{r}-\vec{r}'|^2 &= (X' - r\mathrm{Sin}\theta\mathrm{Cos}\phi)^2 + (Y' - r\mathrm{Sin}\theta\mathrm{Sin}\phi)^2 + r^2\mathrm{Cos}^2\theta \\ &= X'^2 + Y'^2 - 2r\mathrm{Sin}\theta(X'\mathrm{Cos}\phi + Y'\mathrm{Sin}\phi) \\ &\quad + r^2\mathrm{Sin}^2\theta(\mathrm{Cos}^2\phi + \mathrm{Sin}^2\phi) + r^2\mathrm{Cos}^2\theta \\ &= r^2 - 2r\mathrm{Sin}\theta(X'\mathrm{Cos}\phi + Y'\mathrm{Sin}\phi) + r'^2 \\ &= r^2\left\{1 - \frac{2\mathrm{Sin}\theta}{r}(X'\mathrm{Cos}\phi + Y'\mathrm{Sin}\phi) + \left(\frac{r'}{r}\right)^2\right\}\end{aligned}$$

In the far field

$$\left(\frac{r'}{r}\right)^2 << 1 - \frac{2\mathrm{Sin}\theta}{r}(X'\mathrm{Cos}\phi + Y'\mathrm{Sin}\phi)$$

$$|\vec{r}-\vec{r}'|^2 = r^2\left\{1 - \frac{2\mathrm{Sin}\theta}{r}(X'\mathrm{Cos}\phi + Y'\mathrm{Sin}\phi)\right\}$$

And

$$|\vec{r}-\vec{r}'| = r\left\{1 - \frac{\mathrm{Sin}\theta}{r}(X'\mathrm{Cos}\phi + Y'\mathrm{Sin}\phi)\right\}$$

APPENDIX B

Equation 2-18 is evaluated as follows

$$A_{mn}(K_x,K_y) = \int_{-\infty}^{\infty}\int_{-\infty}^{\infty}\int_{-\infty}^{\infty} [I_o C_{mn}\delta(X'-X'_m)\overline{U}(Y'-Y'_n)\delta(Z')\,\mathrm{Sin}(kY'')$$
$$\mathrm{Exp}\{jK_x X'+jK_y Y'\}]dX'dY'dZ'$$

where

$$Y'' = L/2-|Y'-Y'_n|$$

and

$$\overline{U}(Y'-Y'_n) = u(Y'-Y'_n-L/2) - u(Y'-Y'_n+L/2)$$

Integrating with respect to X' and Z' gives

$$A_{mn}(K_x,K_y) = I_o C_{mn}\mathrm{Exp}\{jK_x X'_m\}F$$

where

$$F = \int_{-\infty}^{\infty} \overline{U}(Y'-Y'_n)\,\mathrm{Sin}\{k(L/2-|Y'-Y'_n|)\}\,\mathrm{Exp}\{jK_y Y'\}dY'$$

Let $W' = Y'-Y'_n$

then $dW' = dY'$

$$F = \int_{-\infty}^{\infty} \{u(W'-L/2)-u(W'+L/2)\}\,\mathrm{Sin}\{k(L/2-|W'|)\}$$
$$\mathrm{Exp}\{jK_y(W'+Y'_n\}dW'$$

$$= \mathrm{Exp}\{jK_y Y'_n\}G(L)$$

where

$$G(L) = \int_{-L/2}^{L/2} \mathrm{Sin}\{k(L/2-|W'|)\}\,\mathrm{Exp}\{jK_y W'\}dW'$$

This is a standard integral evaluated in most elementry

texts on antenna theory [17]. Noting that

$$K_y = k\mathrm{Sin}\theta\mathrm{Cos}\phi$$

G(L) is given as

$$G(L) = 2\frac{[\mathrm{Cos}\{(kL/2)\mathrm{Sin}\theta\mathrm{Sin}\phi\} - \mathrm{Cos}\{kL/2\}]}{1 - \mathrm{Sin}^2\theta\ \mathrm{Sin}^2\phi}$$

$A_{mn}(K_x,K_y)$ now becomes

$$A_{mn}(K_x,K_y) = I_oC_{mn}\mathrm{Exp}\{jK_xX_m'+jK_yY_n'\}G(L)$$

$$= C_{mn}\mathrm{Exp}\{jK_xX_m'+jK_yY_n'\}A_{yr}(K_x,K_y)$$

where

$$A_{yr}(K_x,K_y) = 2I_o\frac{[\mathrm{Cos}\{(kL/2)\mathrm{Sin}\theta\mathrm{Sin}\phi\} - \mathrm{Cos}\{kL/2\}]}{1 - \mathrm{Sin}^2\theta\ \mathrm{Sin}^2\phi}$$

APPENDIX C

COMPUTER PROGRAMMS

The following is a brief description of the computer programmes used to calculate the array factors of the arrays described in this thesis. A listing of the programmes is contained at the end of the Appendix. Subroutines which use standard techniques have not been listed.

MAIN PROGRAMME 1

This programme was used to perform the calculations involved in the analysis of the one-dimensional arrays. The input for the programme is

1. IC	control parameter.
2. ERRORM	maximum magnitude error.
3. ERROR	Maximum phase error
4. L	the points at which course tapering occurs.

The first of the programme up to and including the section for applying the B(K) correction was used to generate the tables of transforms required for the analysis of the two-dimensional arrays.

MAIN PROGRAMME 2

This programme was used to compute the array

factors and the peak sidelobe levels of the two-dimensional arrays. The input for the programme is

1. Tables of transforms from the first main programme.
2. Tables of COS functions.

MAIN PROGRAMME 3

This programme was used to find the peak sidelobe levels of the array factors as described in Section 4.1.

AFACTS This package is an assembler subroutine used to compute the array factors and the peak sidelobe levels for the two-dimensional arrays. This portion was found to be the most time consuming part of all the calculations. By writing the programme in assembler language the total number of machine steps required for the calculation is reduced to the minimum.

CSL This subroutine is used to generate the tables for the SIN and COS of large angles which occur in the evaluation of equations 2-51 and 2-54.

GENARY This subroutine generates the excitation data for the arrays.

HARM This is the fast Fourier transform programme available in the IBM Scientific Subroutine Library. It is used in the evaluation of equations 2-51 and 2-54.

INTR1 This subroutine is used to perform the integrations needed for evaluating the average sidelobe levels described by equation 5-3. The trapezoidal rule is used.

INTR2 This subroutine performs the same calculation as INTR1 except that the integration is performed over the peaks of the sidelobe levels. It is less accurate but faster than INTR1.

LOG10 This subroutine converts the array factor, which is normalized with respect to the peak level, from the magnitude form to the dB form.

MAG1 This subroutine converts the array factor from the real and imaginary number form to the magnitude and phase form.

MAX This subroutine is used to find the maximum value of the array factor.

MINA1 This subroutine finds the location of the first minimum of an array factor.

LOCMAX This subroutine finds the location and magnitude of the all the sidelobes of an array factor.

PITAB This subroutine generates a table of equally spaced numbers in the range -2π to 2π.

RNUM This subroutine generates a table of random numbers with a uniform distribution.

RANM This subroutine is used to apply random errors to the phase of the excitation of the elements of an array as described by equation 5-1b.

RANM This subroutine is used to apply random errors to the magnitude ofthe excitation of the elements of an array as described in section 5.2.

ROTATE This subroutine is used to apply a correction to the phase of an array factor calculated using the subroutine HARM.

SCALE This subroutine is used to normalize an array factor with respect to the maximum value found by LOCMAX.

SETA This subroutine is used to expand the size of an array so that the resolution of the array factor is increased.

ZERO This subroutine is used to zero parts of storage between programme steps.

MAIN PROGRAMME 1

```
      DIMENSION A1(4096),A2(4096),A3(4096),A4(4096),
     1          A5(4096),AREF(320),AR(320),THETAT(1025),
     2          PIP(2048),COSPF(2048),SINPF(2048),
     3          M(3),INV(512),S(512),L(8),
     4          B1(400),B2(400),B3(400),B4(400),B5(400),
     5          L1(400),L2(400),L3(400),L4(400),L5(400)
      EQUIVALENCE (B1(1),L1(1)),(B2(1),L2(1)),(B3(1),L3(1)),
     1            (B4(1),L4(1)),(B5(1),L5(1))
      DATA N,NAI,NAR/2048,4096,320/,NL/8/,M/11,0,0/,
     1     PI,TAPER,D/3.1415927,-12.0,0.5/
C ***
C *** PROGRAMME TO EXAMINE THE EFFECT OF RANDOM ERRORS IN
C *** THE PHASE OR MAGNITUDE OF THE EXCITATION OF THE
C *** ARRAY ELEMENTS.
C ***
C *** READ IN DATA
C ***
      READ(5,101) L
      READ(5,102) ERRORM
      READ(5,102) ERRORP
      READ(5,101) IC
C ***
C *** GENERATE TABLES AND CONSTANTS.
C ***
      EM = ERRORM/100.0
      EP = ERRORP
      PI2 = 2.0*PI
      Q = 180.0/PI
      R = 1.0/1024.0
      CALL PITAB(PIP,PI,N)
      CALL CSL(PIP,COSPF,SINPF,N)
      DO 1 I=1,1025
    1 THETAT(I) = ARSIN(FLOAT(I-1)*R)
C ***
C *** GENERATE THE EXCITATION DATA FOR THE ARRAYS
C *** WITHOUT ERRORS IN THE MAGNITUDE OR THE PHASE.
C ***
      DO 99 IK=1,5
      CALL GENARY(AREF,NAR,L,NL,TAPER,IK)
      IC = 1
C ***
C *** ZERO THE ARRAYS.
C ***
    5 CALL ZERO(A1,NAI)
      CALL ZERO(A2,NAI)
      CALL ZERO(A3,NAI)
      CALL ZERO(A4,NAI)
      CALL ZERO(A5,NAI)
C ***
C *** EXPAND INTO A LARGER VECTOR TO INCREASE THE
```

```
C *** RESOLUTION
C ***
      CALL SETA(A1,AREF,NAI,NAR)
      CALL SETA(A2,AREF,NAI,NAR)
      CALL SETA(A3,AREF,NAI,NAR)
      CALL SETA(A4,AREF,NAI,NAR)
      CALL SETA(A5,AREF,NAI,NAR)
C ***
C *** DETERMINE WHICH TYPE OF ERROR IS TO BE EXAMINED.
C ***     MAGNITUDE IF IC=1
C ***     PHASE IF     IC=2
C ***     NO ERRORS IF IC=3
C ***
      GO TO (10,20,30), IC
C ***
C *** GENERATE A RANDOM ERROR IN THE MAGNITUDE.
C ***
   10 IX1 = 1111
      DK = EM
      CALL RNUM(AR,1.0,DK,IX1,NAR)
      CALL RANM(A2,AR,NAI,NAR)
      CALL RNUM(AR,1.0,DK,IX1,NAR)
      CALL RANM(A3,AR,NAI,NAR)
      CALL RNUM(AR,1.0,DK,IX1,NAR)
      CALL RANM(A4,AR,NAI,NAR)
      CALL RNUM(AR,1.0,DK,IX1,NAR)
      CALL RANM(A5,AR,NAI,NAR)
      WRITE(6,103) ERRORM
      GO TO 30
C ***
C *** GENERATE A RANDOM ERROR IN THE PHASE.
C ***
   20 IX1 = 1111
      DK = EP*PI/180.0
      CALL RNUM(AR,0.0,DK,IX1,NAR)
      CALL RANP(A2,AR,NAI,NAR)
      CALL RNUM(AR,0.0,DK,IX1,NAR)
      CALL RANP(A3,AR,NAI,NAR)
      CALL RNUM(AR,0.0,DK,IX1,NAR)
      CALL RANP(A4,AR,NAI,NAR)
      CALL RNUM(AR,0.0,DK,IX1,NAR)
      CALL RANP(A5,AR,NAI,NAR)
      WRITE(6,104) ERRORP
C ***
C *** PRINT OUT THE EXCITATION CF THE ARRAY ELEMENTS.
C ***
   30 WRITE(6,107)
      DO 60 I=864,1185
      N2 = 2*I
      N1 = N2-1
   60 WRITE(6,108) I,N1,N2,
     1             A1(N1),A1(N2),A2(N1),A2(N2),A3(N1),
     2             A3(N2),A4(N1),A4(N2),A5(N1),A5(N2)
```

```
C ***
C *** FIND THE ARRAY FACTOR BY FOURIER TRANSFORMING THE
C *** EXCITATIONS.
C ***
      CALL HARM(A1,M,INV,S,1,IFERR)
      CALL HARM(A2,M,INV,S,1,IFERR)
      CALL HARM(A3,M,INV,S,1,IFERR)
      CALL HARM(A4,M,INV,S,1,IFERR)
      CALL HARM(A5,M,INV,S,1,IFERR)
C ***
C *** APPLY THE B(K) CORRECTION.
C ***
      CALL ROTATE(A1,COSPF,SINPF,-1,NAI,N)
      CALL ROTATE(A2,COSPF,SINPF,-1,NAI,N)
      CALL ROTATE(A3,COSPF,SINPF,-1,NAI,N)
      CALL ROTATE(A4,COSPF,SINPF,-1,NAI,N)
      CALL ROTATE(A5,COSPF,SINPF,-1,NAI,N)
C ***
C *** FIND THE MAGNITUDE AND PHASE OF THE ARRAY FACTOR.
C ***
      CALL MAG1(A1,NAI)
      CALL MAG1(A2,NAI)
      CALL MAG1(A3,NAI)
      CALL MAG1(A4,NAI)
      CALL MAG1(A5,NAI)
C ***
C *** FIND THE MAXIMUM VALUE OF THE ARRAY FACTOR.
C ***
      CALL MAX(A1,NAI,A1MAX,LA1MAX,2)
      CALL MAX(A2,NAI,A2MAX,LA2MAX,2)
      CALL MAX(A3,NAI,A3MAX,LA3MAX,2)
      CALL MAX(A4,NAI,A4MAX,LA4MAX,2)
      CALL MAX(A5,NAI,A5MAX,LA5MAX,2)
C ***
C *** NORMALISE THE ARRAY FACTOE.
C ***
      CALL SCALE(A1,NAI,A1MAX,2)
      CALL SCALE(A2,NAI,A2MAX,2)
      CALL SCALE(A3,NAI,A3MAX,2)
      CALL SCALE(A4,NAI,A4MAX,2)
      CALL SCALE(A5,NAI,A5MAX,2)
C ***
C *** FIND THE FIRST MINIMUMS OF THE ARRAY FACTOR.
C ***
      CALL MINA1(A1,LA1MAX,LA1MIN,2,N)
      CALL MINA1(A2,LA2MAX,LA2MIN,2,N)
      CALL MINA1(A3,LA3MAX,LA3MIN,2,N)
      CALL MINA1(A4,LA4MAX,LA4MIN,2,N)
      CALL MINA1(A5,LA5MAX,LA5MIN,2,N)
C ***
C *** FIND THE PEAK SIDELOBE LEVELS.
C ***
      CALL LOCMAX(A1,B1,B1,400,NEBL1,LA1MIN,N,2)
      CALL LOCMAX(A2,B2,B2,400,NEBL2,LA2MIN,N,2)
```

```
      CALL LOCMAX(A3,B3,B3,400,NEBL3,LA3MIN,N,2)
      CALL LOCMAX(A4,B4,B4,400,NEBL4,LA4MIN,N,2)
      CALL LOCMAX(A5,B5,B5,400,NEBL5,LA5MIN,N,2)
C ***
C *** FIND THE AVERAGE SIDELOBE LEVEL AS A FUNCTION OF
C *** THETA.
C ***
      CALL INTTR3(A1,LA1MIN,THETAT,1025,SAT1)
      CALL INTTR3(A2,LA2MIN,THETAT,1025,SAT2)
      CALL INTTR3(A3,LA3MIN,THETAT,1025,SAT3)
      CALL INTTR3(A4,LA4MIN,THETAT,1025,SAT4)
      CALL INTTR3(A5,LA5MIN,THETAT,1025,SAT5)
      SAT1 = SAT1/(THETAT(1025)-THETAT(LA1MIN/2+1))
      SAT2 = SAT2/(THETAT(1025)-THETAT(LA2MIN/2+1))
      SAT3 = SAT3/(THETAT(1025)-THETAT(LA3MIN/2+1))
      SAT4 = SAT4/(THETAT(1025)-THETAT(LA4MIN/2+1))
      SAT5 = SAT5/(THETAT(1025)-THETAT(LA5MIN/2+1))
C ***
C *** FIND THE AVERAGE OF THE PEAK SIDELOBE LEVELS AS A
C *** FUNCTION OF THETE.
C ***
      CALL INTTR4(B1,B1,THETAT,SBT1,NEBL1)
      CALL INTTR4(B2,B2,THETAT,SBT2,NEBL2)
      CALL INTTR4(B3,B3,THETAT,SBT3,NEBL3)
      CALL INTTR4(B4,B4,THETAT,SBT4,NEBL4)
      CALL INTTR4(B5,B5,THETAT,SBT5,NEBL5)
      SBT1 = SBT1/(THETAT(L1(NEBL1-1))-THETAT(L1(1)))
      SBT2 = SBT2/(THETAT(L2(NEBL2-1))-THETAT(L2(1)))
      SBT3 = SBT3/(THETAT(L3(NEBL3-1))-THETAT(L3(1)))
      SBT4 = SBT4/(THETAT(L4(NEBL4-1))-THETAT(L4(1)))
      SBT5 = SBT5/(THETAT(L5(NEBL5-1))-THETAT(L5(1)))
C ***
C *** FOR EACH ARRAY PRINT OUT:
C ***     THE LOCATION OF THE MAXIMUM LEVEL,
C ***     THE VALUE OF THE MAXIMUM LEVEL,
C ***     THE LOCATION OF THE FIRST MINIMUM,
C ***     FIND THE AVERAGE OF THE PEAK SIDELOBE LEVELS AS A
C ***     FUNCTION OF THETA.
C ***     THE AVERAGE SIDELOBE LEVEL AS A FUNCTION OF THETA.
C ***
      WRITE(6,110)
      WRITE(6,111) LA1MAX,A1MAX,LA1MIN,SAT1,SBT1
      WRITE(6,111) LA2MAX,A2MAX,LA2MIN,SAT2,SBT2
      WRITE(6,111) LA3MAX,A3MAX,LA3MIN,SAT3,SBT3
      WRITE(6,111) LA4MAX,A4MAX,LA4MIN,SAT4,SBT4
      WRITE(6,111) LA5MAX,A5MAX,LA5MIN,SAT5,SBT5
C ***
C *** WRITE OUT THE PEAK VALUES OF THE SIDELOBES.
C ***
      WRITE(6,120)
      DO 85 I=1,400,2
      J = I+1
   85 WRITE(6,121) B1(I),B1(J),B2(I),B2(J),B3(I),B3(J),
     1             B4(I),B4(J),B5(I),B5(J)
```

```
C ***
C *** CONVERT THE OUTPUT TO DB.
C ***
      CALL LOG10(A1,NAI)
      CALL LOG10(A2,NAI)
      CALL LOG10(A3,NAI)
      CALL LOG10(A4,NAI)
      CALL LOG10(A5,NAI)
C ***
C *** FIND THE PEAK SIDELOBE LEVELS IN DB.
C ***
      CALL LOCMAX(A1,B1,B1,400,NEBL1,LA1MIN,N,2)
      CALL LOCMAX(A2,B2,B2,400,NEBL2,LA2MIN,N,2)
      CALL LOCMAX(A3,B3,B3,400,NEBL3,LA3MIN,N,2)
      CALL LOCMAX(A4,B4,B4,400,NEBL4,LA4MIN,N,2)
      CALL LOCMAX(A5,B5,B5,400,NEBL5,LA5MIN,N,2)
C ***
C *** FOR EACH ARRAY PRINT OUT:
C ***     THE LOCATION OF THE MAXIMUM LEVEL,
C ***     THE VALUE OF THE MAXIMUM LEVEL,
C ***     THE LOCATION OF THE FIRST MINIMUM,
C ***
      WRITE(6,110)
      WRITE(6,111) LA1MAX,A1MAX,LA1MIN
      WRITE(6,111) LA2MAX,A2MAX,LA2MIN
      WRITE(6,111) LA3MAX,A3MAX,LA3MIN
      WRITE(6,111) LA4MAX,A4MAX,LA4MIN
      WRITE(6,111) LA5MAX,A5MAX,LA5MIN
C ***
C *** WRITE OUT THE ARRAY FACTOR IN DB.
C ***
      WRITE(6,112)
      DO 90 I=1025,1250
      T = FLOAT(I-1025)
      J = IABS(I-1025)
      V = FLOAT(J)
      J = J+1
      IF(I.LE.1024) J = I+1024
      AK = PI2*T*R
      THETAJ = ARSIN(V*R)*Q
      N2 = 2*J
      N1 = N2-1
   90 WRITE(6,113) I,J,AK,THETAJ,
     1             A1(N1),A1(N2),A2(N1),A2(N2),A3(N1),
     2             A3(N2),A4(N1),A4(N2),A5(N1),A5(N2)
C ***
C *** WRITE OUT THE PEAK VALUES OF THE SIDELOBES IN DB.
C ***
      WRITE(6,122)
      DO 95 I=1,400,2
      J = I+1
   95 WRITE(6,121) B1(I),B1(J),B2(I),B2(J),B3(I),B3(J),
     1             B5(I),B5(J)
      IF(IC.EQ.2) GO TO 99
```

```
      IC = 2
      GO TO 5
   99 CONTINUE
      WRITE(6,114)
      STOP
C ***
C *** FORMAT STATEMENTS.
C ***
  101 FORMAT(8I10)
  102 FORMAT(F10.6)
  103 FORMAT('1EXAMINING THE EFFECT OF RANDOM MAGNITUDE',
     1       ' ERRORS OF',F6.1, 'PERCENT.')
  104 FORMAT('1EXAMINING THE EFFECT OF RANDOM PHASE ERRORS',
     '       ' OF',F5,1,' DEGREES.')
  107 FORMAT('1EXCITATION DATA FOR THE ARRAYS.',
     1        //,T12,'LOCATION',T28,'TYPE 1 ARRAY',T50,
     2       'TYPE 2 ARRAY',T72,'TYPE 3 ARRAY',T94,'TYPE 4',
     3       ' ARRAY',T116,
     4       'TYPE 5 ARRAY',//,' ELEMENT   REAL IMAG',T27,
     5       'REAL      IMAG',T49,'REAL      IMAG',T71,
     6       'REAL      IMAG',
     7       T93,'REAL      IMAG',T115,'REAL      IMAG',//)
  108 FORMAT(I6,I9,I5,5(F12.6,F10.6))
  110 FORMAT('1ARRAY FACTOR DATA.',////' LAMAX',T12,'AMAX',
     1       T26,'LAMIN',T41,'A(MEAN)',T61,'AP(MEAN)',
     2       T81,'A(MEAN)',T101,'AP(MEAN)',//)
  111 FORMAT(I7,F14.7,I10,4F20.10,/)
  112 FORMAT('1ARRAY FACTORS FOR THE ARRAYS.',
     1       //,T32,'TYPE 1 ARRAY',T53,'TYPE 2 ARRAY',T74,
     2       'TYPE 3 ARRAY',T95,'TYPE 4 ARRAY',T116,'TYPE ',
     3       '5 ARRAY',//,T5,'I',T10,'J',T14,'K',T19,
     4       'THETA,
     5       T30,'MAGNITUDE  PHASE',T51,'MAGNITUDE  PHASE',
     6       T72,'MAGNITUDE  PHASE',T93,'MAGNITUDE  PHASE',
     7         T114,'MAGNITUDE  PHASE',//)
  113 FORMAT(2I5,2F7.3,5(F12.3,F9.3))
  114 FORMAT('1')
  115 FORMAT(2I5,2F7.3,5(F13.7,F8.3))
  120 FORMAT('1PEAK SIDELOBE LEVELS',//)
  121 FORMAT(5(I10,F12.7))
  122 FORMAT('1PEAK SIDELOBE LEVELS IN DB.',//)
  123 FORMAT(5(I10,F13.3))
      END
```

MAIN PROGRAMME 2

```
      DIMENSION A(9216),C4096),AF(2048),AMAX(64)
C ***
C *** PROGRAMME TO COMPUTE THE ARRAY FACTOR OF TWO-
C *** DIMENSIONAL ARRAYS.
C ***
C *** A    TRANSFORM TABLES.
C *** C    COS TABLES.
C *** AF   ARRAY FACTOR.
C *** AMAX PEAK LEVELS OF AF.
C ***
      EXTERNAL GETFD
      INTEGER*2 LEN
      INTEGER*4 FDUB,ADROF,FSIZE,BLOCK
      REAL*8 FNAME
      DATA NEB,NB/32,32/,LEN/8192/
C ***
C *** READ IN THE TABLES OF DATA.
C ***
      READ(4) A
      READ(4) C
      READ(5,101) FNAME,FSIZE
C ***
C *** CREATE THE OUTPUT FILES.
C ***
      CALL GFILES(FNAME,FSIZE,FDUB,1,&501,&502)
C ***
C *** COMPUTE THE ARRAY FACTOR.
C ***
      READ(5,102) KSTART
      READ(5,102) NBLKS
      CM = C(1)*A(2)+C(2)*A(4)+C(3)*A(6)+C(4)*A(8)
      CP = C(1)*A(3)+C(2)*A(5)+C(3)*A(7)+C(4)*A(9)
      CNORM = 1.0/SQRT(CM*CM+CP*CP)
      K = KSTART
    1 CALL ZERO(AMAX,64)
      BLOCK = (K-1)/32+1
      WRITE(10,112)
      DO 50 I=1,32
      KC = 4*K-3
      CALL AFACTS(A,AF,AMAX,C(KC),NEB,NB,CNORM)
   50 K = K+1
      WRITE(9,111) AMAX
      DO 60 I=1,64,2
      IB = (I+1)/2
      I1 = I+1
   60 WRITE(10,113) BLOCK,IB,AMAX(I),AMAX(I1)
      NBLKS = NBLKS-1
      IF(NBLKS.GT.0) GO TO 1
      STOP
```

```
  501 WRITE(6,601)
      STOP 64
  502 WRITE(6,602)
      STOP 68
C ***
C *** FORMAT STATEMENTS
C ***
  101 FORMAT(A8,I8)
  102 FORMAT(10I10)
  103 FORMAT('1',T5,'B',T10,'K',T27,'WRITE POINTER',/,'0',/)
  104 FORMAT(2I5,I20)
  111 FORMAT(8X,8Z8)
  112 FORMAT('1   B   IB     ARMAX       APMAX',/,'0',/)
  113 FORMAT(2I5,2F12.7)
  602 FORMAT(' RCALL FAILURE:')
  601 FORMAT(' CREATE FAILURE:')
      END
```

MAIN PROGRAMME 3

```
      DIMENSION AB(2048),A1(512),A2(512),B1(512),B2(512)
      READ(5,101) AB
      IAB = 1
      I1 = 1
      IL = 32
      DO 30 J=1,32
      DO 20 I=I1,IL,2
      A1(IAB) = AB(I)
      B1(IAB) = AB(I+1)
      A2(IAB) = AB(I+32)
      B2(IAB) = AB(I+33)
   20 IAB = IAB+1
      I1 = I1+64
   30 IL = IL+64
      WRITE(7,103) A1
      WRITE(7,103) A2
      WRITE(7,103) B1
      WRITE(7,103) B2
      CALL LOG10(AB,2048)
      IAB = 1
      I1 = 1
      IL = 32
      DO 50 J=1,32
      DO 40 I=I1,IL,2
      A1(IAB) = -AB(I)
      B1(IAB) = -AB(I+1)
      A2(IAB) = -AB(I+32)
      B2(IAB) = -AB(I+33)
   40 IAB = IAB+1
      I1 = I1+64
   50 IL = IL+64
      WRITE(7,102) A1
      WRITE(7,102) A2
      WRITE(7,102) B1
      WRITE(7,102) B2
      STOP
  101 FORMAT(8X,8Z8)
  102 FORMAT('1',/,' ',16F5.1,(/,'0',/,' ',16F5.1))
  103 FORMAT('1',16F8.5,(//,'0',16F8.5))
      END
```

SUBROUTINE AFACTS

```
AFACTS   CSECT
*
*     CALL AFACTS(A,AF,AMAX,C,NEB,NB,CNORM)
*
         STM   14,12,12(13)
         BALR  12,0
         USING *,12
         ST    13,SGR13
         LA    13,SAVEAREA
         LA    2,36                F'36'
         L     5,16(1)             ADROF NEB
         L     5,0(5)              NEB
         S     5,=F'1'             NEB-1
         MR    4,2                 36*(NEB-1)
         LR    3,5                 36*(NEB-1)
         LA    4,8                 F'8'
         L     5,20(1)             ADROF NB
         L     5,0(5)              NB
         S     5,=F'1'             NB-1
         SLL   5,3                 8*(NB-1)
         L     6,0(1)              ADROF A
         AR    3,6                 ADROF A + 36*(NEB-1)
         L     7,8(1)              ADROF AMAX
         AR    5,7                 ADROF AMAX + 8*(NB-1)
         L     8,12(1)             ADROF C
         L     9,4(1)              ADROF AF
         L     10,24(1)            ADROF CNORM
LOOP     LE    0,0(6)              AM
         ME    0,0(8)              AM*COS8
         LPER  0,0                 AFRTM
         STE   0,0(9)              AFRTM
         CE    0,0(7)
         BNH   *+8
         STE   0,0(7)
         LE    0,4(6)              A8RE
         LE    2,8(6)              A8IM
         ME    0,0(8)              A8RE*COS8
         ME    2,0(8)              A8IM*COS8
         LE    4,12(6)             A6RE
         LE    6,16(6)             A6IM
         ME    4,4(8)              A6RE*COS6
         ME    6,4(8)              A6IM*COS6
         AER   0,4
         AER   2,6
         LE    4,20(6)             A4RE
         LE    6,24(6)             A4IM
         ME    4,8(6)              A4RE*COS4
         ME    6,8(6)              A4IM*COS4
         AER   0,4
         AER   2,6
```

```
         LE    4,28(6)              A2RE
         LE    6,32(6)              A2IM
         ME    4,12(8)              A2RE*COS2
         ME    6,12(8)              A2IM*COS2
         AER   0,4
         AER   2,6
         MER   0,0
         MER   2,2
         AER   0,2
         STE   0,ARG
         LA    1,PARLSQRT           LOAD PARLIST FOR SQRT
         L     15,ESQRT             LOAD ENTRY PT FOR SQRT
         BALR  14,15                BRANCH TO SQRT
         DE    0,0(10)
         STE   0,4(9)
         C     0,4(7)
         BNH   *+8
         STE   2,4(7)
         BXLE  6,2,LOOP
         LA    3,1152
         LA    7,8(7)
         BXLE  7,4,LOOP
         L     13,SGR13
         LM    14,12,12(13)
         BR    14
SGR13    DS    F
SAVEAREA DS    18F
PARLSQRT DC    X'80'
         DC    AL3(ARG)
ESQRT    DC    V(SQRT)
ARG      DS    F
         END
```

```
      SUBROUTINE GENARY(A,NA,L,NL,TAPER,TYPE)
      INTEGER*4 TYPE
      DIMENSION A(NA),L(NL)
      GO TO (10,20,30,40,50), TYPE
   10 INCJ = 8
      GO TO 60
   20 INCJ = 4
      GO TO 60
   30 INCJ = 2
      GO TO 60
   40 INCJ = 1
      GO TO 60
   50 C = (-ALOG(10.0**(TAPER/10.0)))
      C = C/(157.0*157.0)
      DO 51 I=2,160
      A(160+I) = EXP(-C*(I-1)*(I-1))
   51 A(161-I) = A(160+I)
      A(160) = 1.0
      A(161) = 1.0
      RETURN
   60 NI1 = 1
      DO 80 J=1,8,INCJ
      NIL = L(J+INCJ-1)
      C = 1.0-0.125*FLOAT(J-1)
      DO 70 I=NI1,NIL
      A(160+I) = C
   70 A(161-I) = C
   80 NI1 = NIL+1
      RETURN
      END
```

```
      SUBROUTINE CSL(A,COSL,SINL,N)
      DIMENSION A(N),COSL(N),SINL(N)
      C = 1.0
      DO 10 I=1,N
      COSL(I) =  C*COS(A(I))
      SINL(I) = -C*SIN(A(I))
   10 C = -C
      RETURN
      END
```

```
      SUBROUTINE ROTATE(A,COSPF,SINPF,IC,N,NCS)
      DIMENSION A(N),COSPF(NCS),SINPF(NCS)
      IF(IC.EQ.-1) GO TO 20
      DO 10 I=1,NCS
      X = A(2*I-1)*COSPF(I)  - A(2*I)*SINPF(I)
      Y = A(2*I)*COSPF(I)    + A(2*I-1)*SINPF(I)
      A(2*I-1) = X
   10 A(2*I) = Y
      RETURN
   20 DO 30 I=1,NCS
      X = A(2*I-1)*COSPF(I)  + A(2*I)*SINPF(I)
      Y = A(2*I)*COSPF(I)    - A(2*I-1)*SINPF(I)
      A(2*I-1) = X
   30 A(2*I) = Y
      RETURN
      END
```

```
      SUBROUTINE RNUM(A,C,D,IX,N)
      DIMENSION A(N)
      DO 10 I=1,N
      CALL RANDU(IX,IY,YFL)
      A(I) = (YFL-0.5)*2.0*D+C
   10 IX = IY
      RETURN
      END
```

```
      SUBROUTINE RANM(A,R,NA,NR)
      DIMENSION A(NA),R(NR)
      N1 = NA/2-NR+1
      DO 10 I=1,NR
      A(N1) = A(N1)*R(I)
   10 N1 = N1+2
      RETURN
      END
```

```
      SUBROUTINE RANP(A,R,NA,NR)
      DIMENSION A(NA),R(NR)
      N1 = NA/2-NR+1
      N2 = N1+1
      DO 10 I=1,NR
      C = COS(R(I))
      S = SIN(R(I))
      X = A(N1)*C-A(N2)*S
      Y = A(N1)*S+A(N2)*C
      A(N1) = X
      A(N2) = Y
      N1 = N1+2
   10 N2 = N2+2
      RETURN
      END
```

B30070